AN ABSTRACT OF THE THESIS OF

Nelson R. Silva-Sandoval for the degree of Master of Science

in Oceanography presented on August 4, 1977

Title: WATER MASS STRUCTURE AND CIRCULATION OFF SOUTHERN CHILE

Redacted for privacy

Abstract Approved:

Dr. Steve Neshyba

Redacted for privacy

Dr. Louis I. Gordon

A detailed analysis of the water mass structure and geostrophic circulation off Southern Chile (43° - 63° S, 91° W to the Chilean Coast; (hereafter called study area) was performed. It was found that:

1. Potential temperature-salinity relations indicate four distinct structure types north of the Polar Front Zone in the study area, involving seven identifiable water masses. These water masses are: Subantarctic Water (SAAW), Antarctic Water (AAW), Equatorial Subsurface Water (ESSW), Western Pacific Subsurface Water (WPSSW) (a new regional water mass identified in this study), Antarctic Intermediate Water (AAIW), Pacific Deep Water (PDW), and Antarctic Bottom Water (AABW).

2. A scattergram of dissolved oxygen-salinity maximum pairs identifies two distinct subsurface salinity maxima. The subsurface salinity maximum associated with dissolved oxygen minimum, establishes the presence of the ESSW as a wedge that penetrates to at least 40° S. The other subsurface salinity maximum which is non-associated with dis-

solved oxygen minimum, is traced from at least 162° W to as close to the Chilean Coast as 80° W at 43° S. In this study, this water mass is called the Western Pacific Subsurface Water (WPSSW).

3. Acceleration potential on the 26.84 sigma-θ surface relative to 3000 db, combined with the analysis of θ-S structures distribution and vertical sections of geostrophic velocity relative to 3000 db, show that the Peru-Chile Undercurrent extends as far south as 48° S.

4. Significant linear correlation between surface phosphate or nitrate vs. salinity for the study area where the salinity ranges between 33 - 34 °/₀₀, show that the relatively low nutrient content of the coastal waters (<300 km) mainly results from mixing oceanic waters with waters of the Archipelago system of Southern Chile. Two point mixing explains only 60 - 70% of the nutrient variability; thus, biological and/or chemical processes may also be important causes of the relatively low nutrient concentrations of the coastal waters.

Water Mass Structure and Circulation off Southern Chile

by

Nelson R. Silva-Sandoval

A THESIS

submitted to

Oregon State University

in partial fulfillment of
the requirements for the
degree of

Master of Science

Completed August 4, 1977

Commencement June 1978

APPROVED:

Redacted for privacy

Redacted for privacy

Professors of Oceanography
in Charge of Major

Redacted for privacy

Acting Dean of School of Oceanography

Redacted for privacy

Dean of Graduate School

Date thesis is presented August 4, 1977

Typed by Cheryl M. Schurg for Nelson R. Silva-Sandoval

ACKNOWLEDGEMENTS

Help and care are more appreciated if they are offered in a foreign country. Dr. Steve Neshyba was always rich in them, willing to be with me during my good as well as my bad moments. His advice and comments on my work were cheerfully given to me. His office was my office, his home was my home. There is no doubt that I am in debt to him forever and I want here to give him my acknowledgement "desde el fondo de mi corazon."

Several other professors from the School of Oceanography were always willing to help me during my attendance at Oregon State University. I want to thank Dr. Wayne Burt, Dr. Louis Gordon, Dr. Victor Neal, and Dr. Robert Smith.

I want my acknowledgement to be extended to my sponsor, Organization of American States, without whose help my studies at Oregon State University would not have become a reality. I also want to acknowledge the Universidad Catolica de Valparaiso-Chile which allowed me to take a leave of absence, making possible my attendance at Oregon State University.

Finally, I want to thank Mrs. Cheryl Schurg for her care in typing my thesis. She was the hero of the last minute rush.

To my wife Rosi

To my son Marcelo and my daughter Erika

To my country "Chile Lindo"

TABLE OF CONTENTS

TABLE OF CONTENTS (Continued)

LIST OF TABLES

LIST OF FIGURES

LIST OF FIGURES (Continued)

LIST OF FIGURES (Continued)

LIST OF FIGURES (Continued)

LIST OF FIGURES (Continued)

WATER MASS STRUCTURE AND CIRCULATION OFF SOUTHERN CHILE

I. INTRODUCTION

The details of water mass structure and circulation of the southernmost extreme of the Eastern Pacific Ocean are poorly known. This area, off Chile, between 35° S and 55° S and east of 90° W, has been included in several studies of circulation and water masses (Gunther, 1936; Reid, 1961; Reid and Arthur, 1975; Warren, 1970, and Wyrtki, 1975). Only the gross characteristics of the regional waters were described because of the large scale geographic ranges of these papers. More specifically, little attention has been paid to a unique feature of this region, namely, that it is the only southern hemisphere coastline where the West Wind Drift (WWD) reaches a solid continental barrier. There is a clear need for improvement of our knowledge of the region.

If an inventory of oceanographic expeditions in the area is performed, a striking reality becomes apparent: even though several cruises have sampled the region there is a great variety in depth of maximum sampling, variables measured and degree of synopticity. Only two major oceanographic cruises have produced a good coverage of the area in the sense of a dense sampling grid. These are the PIQUERO Leg III 1969 (S.I.O., 1974) and the R/V Professor DERYUGIN 1968 (Mamayev, 1973). Neither of these cover the total area off southern Chile, and only PIQUERO Leg III has stations closer than 200 nautical miles to the coast and complete water column sampling. A composite data base of these PIQUERO data plus the 1967 SCORPIO Expedition (S.I.O., 1969)

covering from 43° to 63° S and from the coast to 91° W, hereafter called the study area, form the basis for the analysis and results presented in this study.

The present study examines the water mass structure present in the water column off southern Chile. It also analyzes the horizontal distribution of physical and chemical characteristics of the Subantarctic Water, Antarctic Water, Equatorial Subsurface Water, Western Pacific Subsurface Water, and Antarctic Intermediate Water. The Western Pacific Subsurface Water is presented as a water mass carried eastward into the area of study by advective processes.

This study also treats the geostrophic velocity patterns of this extreme Southeastern Pacific area on vertical and horizontal sections. The southernmost extension of the Peru-Chile Undercurrent is established from a chart of acceleration potential on the 26.84 isopycnal, combined with the analysis of the θ-S structure distribution and vertical sections of geostrophic velocity relative to 3000 db.

II. BACKGROUND

2.1 Water masses and water mass structure

The water masses present in the study area have been described in general by authors such as Sverdrup et al. (1942) and Defant (1961). A more detailed study of the distribution of the water mass characteristics in the Southern Hemisphere has been done by Taft (1963). He described the distribution of properties using isentropic analysis on the isanosteres of 125, 100, 80 and 60 cl/ton. Detailed studies of water mass distributions and their characteristics off the Chilean Coast have been prepared by Gunther (1936), Wyrtki (1966; 1967), Brandhorst (1971), Robles et al. (1974), Sievers and Silva (1975), and Silva and Konow (1975). Nevertheless, none of these papers covered the area south of 43° S.

Reid (1965) performed an analysis of the Antarctic Intermediate Water distribution in the Pacific Ocean. He also made use of isentropic analysis showing the intermediate water mass distribution and its geostrophic flow on the 80 cl/ton isanostere.

The distribution of properties of the Pacific Deep Water (Common Water) in the Southern Hemisphere south of 40° S was studied by Callahan (1972). He also used isentropic analysis, selecting for this purpose the isanosteres of 50 and 30 cl/ton.

A detailed analysis of the vertical water mass structure in the Eastern South Pacific was done by Mamayev (1973). He discussed the different T-S structures present in the area and elaborated a rather complex classification. Mamayev (1973) described two T-S structure types, one subtype and two transient types for the area between 30° - 53° S and

80° W - 109° W. Based on his classification system, he presented a T-S structure distribution chart.

2.2 Geostrophic circulation

The geostrophic circulation of the southern part of the Eastern South Pacific Ocean (south of 35° S) has not been described in as much detail as has been done off Peru (Wooster and Gilmartin, 1961; Wyrtki, 1963; and Zuta and Guillen, 1970), or off northern Chile (Brandhorst, 1971; Robles et al., 1974; and Sievers and Silva, 1975). Nevertheless, this area has been included in several general circulation studies, for instance, by Reid (1961, 1965, 1967b), Wooster and Reid (1963), Warren (1970), Reid and Arthur (1975), and Wyrtki (1975).

2.2.1 West Wind Drift - Division at the Chilean Coast

One of the most outstanding features in the circulation pattern in this area, is the bifurcation of the WWD off southern Chile. The fact that the WWD impinges the South American Continent and divides into a northward and southward branch has been known for a long time. Perez-Rosales is cited by Gunther (1936) to have reported in 1857 some thermal observations relative to the characteristics of the Cape Horn Current and the Peru Coastal Current at their commencement off the coast of Chile. Gunther (1936) also cites the textbooks of Hoffmann in 1884 and Somerville in 1923 as describing the WWD division at 40° S into two branches in "the Cape Horn Current flowing to the south the Peru or Humboldt Current to the north."

Charts of Pacific Ocean Currents based on ship drift including the area where the WWD reaches the South American Continent have been pre-

sented by authors such as Sverdrup et al. (1942) and Defant (1961). These charts present the WWD approaching the coast from the W-SW and impinging at about 45° S. The geostrophic circulation of the sea surface relative to 1000 db prepared by Reid (1961), shows in a broad way the WWD impingement at ≈ 43° S but with a final approach to the coast (east of 90° W) from the W-NW. Wyrtki's (1975) sea surface mean annual dynamic topography relative to 1000 db showed a final W-NW flow direction in a fashion similar to that of Reid's (1961). Sandoval (1971) has prepared a chart of the sea surface dynamic topography relative to 500 db for the Eastern Pacific Ocean (0° - 47° S) where this W-NW direction can be observed also. Nevertheless, some geostrophic velocities inferred from his chart are doubtful (for example 168 cm/sec at 47° S and 78° W). Silva and Neshyba (1977) prepared a sea surface dynamic chart relative to 500 db using available austral summer data in the region 35° - 56° S, east of 91° W. They found that the WWD has a final approach from the W-NW reaching the coast off Chiloe Island (≈ 42° S). They also describe an apparent correlation between the dynamic flow and the bathymetry of the Chile Ridge.

2.2.2 Peru-Chile Undercurrent

The presence of a subsurface poleward flow close to the Chilean Coast was first described by Gunther (1936). He based his description on the temperature, salinity and oxygen distributions. Wooster and Gilmartin (1961) further describe the poleward subsurface flow between 6° S and 24° S using both vertical sections of geostrophic flow relative to 1000 db and a set of direct measurements by drogues. They further proposed that this flow, which they called the Peru-Chile Undercurrent,

should extend at least as far as 41° S, using as a basis a set of north-south (along coast) vertical sections of salinity and oxygen.

A dynamic topography chart on 200/1000 db was prepared by Wooster and Reid (1963) to analyze the poleward currents in the Eastern Pacific Ocean. This chart shows the extension of a poleward subsurface flow along the Chilean Coast as far south as 40° S. Brandhorst (1971), using isentropic analysis on the 150 and 140 cl/ton isanosteres, described the extension of the Peru-Chile Undercurrent as far as 42° S. He based his results on the distribution of properties of the Equatorial Subsurface Water, rather than geostrophic computations.

Vertical sections of geostrophic velocity relative to 1000 db at 24° S and 28° S off the coast of Chile prepared by Sievers and Silva (1975), also show the Peru-Chile Undercurrent. Flow magnitudes were 10 and 5 cm/sec, respectively, which are compatible with those of Wooster and Gilmartin (1961) off Peru.

2.2.3 Flow of intermediate, deep, and bottom levels

Dynamic topography charts at intermediate levels have also been prepared by Reid (1965) and by Johnson (1972). The first author described the Antarctic Intermediate Water flow along the 80 cl/ton isanostere (sigma-t = 27.29), while the second showed this flow along the 27.1 isopycnal. Johnson (1972) showed a general northward flow of the Antarctic Intermediate Water along the Chilean Coast. In Reid's (1965) chart, the situation is not very well defined due to the scarcity of data.

Relative to the deep water circulation, Callahan (1972) proposed a deep southward flow along the coast of Chile which carries oxygen poor

waters to the Antarctic. This low oxygen water joints the Antarctic Circumpolar Current west of the Drake Passage, flowing through it to the South Atlantic. The dynamic topography maps at 2000/3000 db and 2500/3500 db prepared by Reid and Arthur (1975) are in agreement with Callahan's (1972) proposed flow.

The bottom circulation in the Bellinghausen Basin was described by Gordon (1966) based on potential temperature, salinity and oxygen distributions. He pointed out that the flow velocity in the basin is probably moderate in the western (east of East Pacific Ridge) and northern (south of Chile Ridge) sections and weak in its eastern branch (along Southern Chile).

III. DATA AND METHODS

3.1 Cruises and data

The Leg III of PIQUERO Expedition took place off the southern coast of Chile during January 13 to February 16, 1969. The cruise occupied 51 oceanographic stations including the development of seven current meter arrays in the Drake Passage. Only 43 of these stations were considered in the present study; 8 coastal stations from 40 to 55° S were omitted because they lacked nutrient data. The 43 PIQUERO stations selected covered the area between 45 to 63° S, 91° W to the coast of Chile and they are shown in Figure 1. The current meter data have been analyzed by Reid and Nowlin (1971), and part of their results have been included in the interpretation of the geostrophic velocity profiles.

Eleven of the easternmost stations of the section along 43° S (deeper than 2000 m) of the SCORPIO Expedition (April 30 to May 8, 1967), were added to the PIQUERO Leg III station grid to obtain a better coverage to the north (Figure 1). This composite permits construction of smooth connections between the hydrosections of the two cruises when contours of the different variables are traced, even though the cruises are separated in time by two years and were taken in different seasons (austral summer for PIQUERO and austral autumn for SCORPIO). Additional SCORPIO stations toward the west along 43° S at 93°, 104°, 116°, 127°, 139°, 150°, 162° and 169° W, were used in the analysis of the Western Pacific Subsurface Water Mass.

The basic data from both cruises consist in observations of temperature, salinity, dissolved oxygen, and nutrients. Descriptions of the methods and data have been presented in data reports (S.I.O., 1969

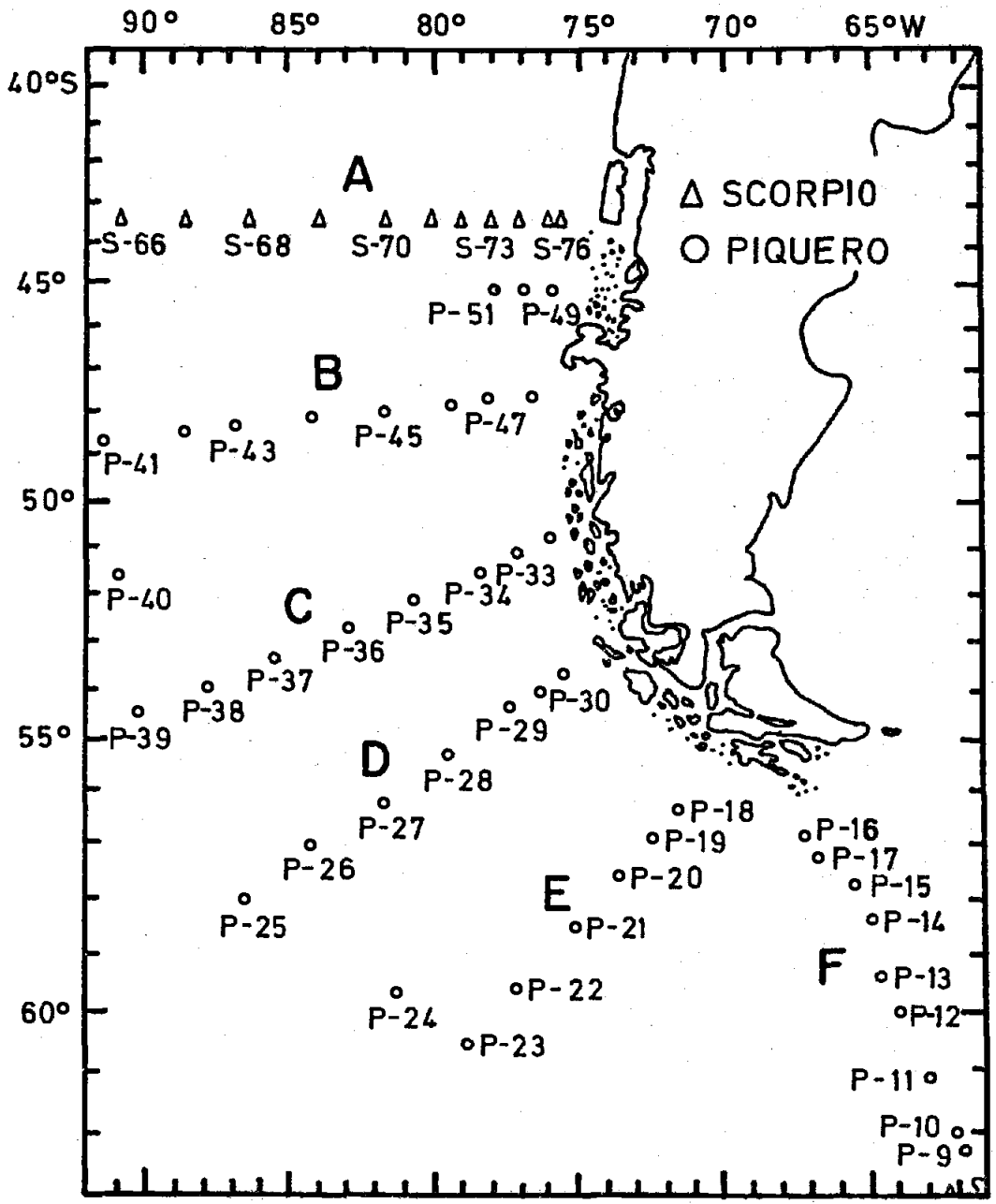

Figure 1. The study area, showing locations of SCORPIO (S) 1967 and PIQUERO (P) 1969 oceanographic stations. Letters A - F define vertical sections.

for SCORPIO and S.I.O., 1974 for PIQUERO).

To analyze relationships between horizontal surface mixing and nutrient distribution in coastal water off Chile, additional data were incorporated from the HUDSON 70 Expedition. These data consist mainly in observations of temperature, salinity, and dissolved oxygen in the Chilean Archipelago. Some HUDSON 70 oceanographic stations did have additional phosphate, nitrate, and silicate observations (CSS HUDSON, 1970).

3.2 Methods of data analysis

3.2.1 Water masses

Water masses were identified using diagrams of potential temperature (θ) versus salinity (S) (Helland-Hansen, 1916). The movement or distribution of water masses was studied using Wust's (1935) core method. An additional technique employed to discriminate between water masses used oxygen (O_2) versus S_{max} plots to correlate the specific values of O_2 with the S_{max} values at which they occurred. It will be shown later this technique provides the basis for identification of the Western Pacific Subsurface Water (WPSSW) in the study area. Linear regressions of phosphate and nitrate versus salinity were used to examine relationships between horizontal surface mixing and nutrient distribution.

3.2.2 Distribution of properties on sigma-θ surfaces

The distribution of water mass properties along surfaces of constant potential density is an established method of analyzing horizontal advection and mixing (Montgomery, 1937; and Sverdrup *et al.*, 1942).

The selection of specific isopycnal surfaces for this purpose involved calculating the averages of the density values associated with salinity maxima or minima, for the PIQUERO and SCORPIO stations within the study area. A mean sigma-θ value of 26.84 was obtained for Equatorial Subsurface Water (ESSW), while 27.12 defined Antarctic Intermediate Water (AAIW).

3.2.3 Geostrophic analysis

Geostrophic flow patterns at intermediate levels were inferred from distribution of acceleration potential along the isentropic surfaces described above. On the sea surface, where a specific isopycnal cannot be defined, the horizontal flow pattern was inferred from sea surface dynamic topography computed relative to 3000 db. Vertical sections of geostrophic velocity relative to 3000 db were prepared to complement the information given by horizontal charts of dynamic topography and acceleration potential.

3.2.4 Choice of level of no motion

The choice of the level of 3000 db level as a no motion for the computation of the geostrophic velocities is a key decision in this method. In strongly stratified waters, the level of no motion is found at a shallower depth than in more nearly stratified waters (Neumann, 1968). In high latitudes, such as found around the Antarctic Continent, the weakly stratified waters will show a very deep level of no motion. Gordon (1966), for example, indicated that a level of no motion does not exist for zonal flow in the northern and western Drake Passage. He also points out that the level of no motion in the Drake Passage slopes

steeply down toward the north, reaching the bottom about half way across the passage. Cabrera-Muro (1977), using the method of Defant (1961), did not find a level of no motion at high latitudes in the South Pacific due to the lack of stratification.

Johnson (1972) selected a depth of 2500 m as a level of no motion based on: "the Pacific Deep Water (PDW) considered to be moving generally south, and the AAIW moving north, would have a point of flow reversal (or level of no motion) between them." Reid (1961, 1965, 1973b), and Reid and Arthur (1975), have used 1000, 2000, 3000, 3500, or 4000 db, as a reference level depending upon the actual value of the feature which they are discussing.

Computations of the level of no motion at different latitudes using PIQUERO-SCORPIO data, also lead to similar conclusions to those of Gordon's (1966) and Cabrera-Muro's (1977). South of 55° S, Defant's (1961) method did not indicate the presence of a level of no motion in the water column. Since the study area includes stations where a level of no motion does not exist, or at least can not be defined with Defant's method, an arbitrary depth of 3000 m was selected as a reference level for dynamic computations. The choice of 3000 db was based on: (1) No one reference level satisfies the total area included; (2) Flow at greater depths is usually considered to be weaker than at shallower depths; (3) 3000 db is the deepest common standard depth for most of the stations used here; and (4) It is desirable to compare these results with those of Reid and Nowlin (1961) from the PIQUERO data across the Drake Passage. Stations P-9, 16, 31, 50, 51 and S-69 were not used in this analysis since depths were less than 3000 m.

IV. DESCRIPTION OF WATER MASSES IN THE STUDY AREA

4.1 General

An analysis of all the θ-S diagrams for the study area reveals the presence of seven distinct water masses at depths below the seasonal thermocline. These water masses are shown in Figure 2. They are the Subantarctic Water (SAAW), Antarctic Water (AAW), Equatorial Subsurface Water (ESSW), Western Pacific Subsurface Water (WPSSW), Antarctic Intermediate Water (AAIW), Pacific Deep Water (PDW), and Antarctic Bottom Water (AABW).

Descriptions of the temperature, salinity, dissolved oxygen and nutrient contents of these surface, subsurface, and intermediate waters are given below. The deep and bottom water masses, PDW and AABW, rexpectively, are not described in detail here because the characteristics of these deeper waters do not change appreciably over the study area and they already have been described by Gordon (1966), Reid and Lynn (1971), and Callahan (1972). The description of the Subantarctic Water includes a discussion of the influence of estuarine waters of the Chilean Coast. The Western Pacific Subsurface Water is discussed in detail because this is a new water mass designation for this region which has resulted from the water mass structure analysis presented in this study.

4.2 Subantarctic Water

The SAAW occupies the surface layer in the whole area of study, north of the Polar Front Zone. As a surface water, its temperature distribution (Figure 3) is dominated by the influence of seasonal varia-

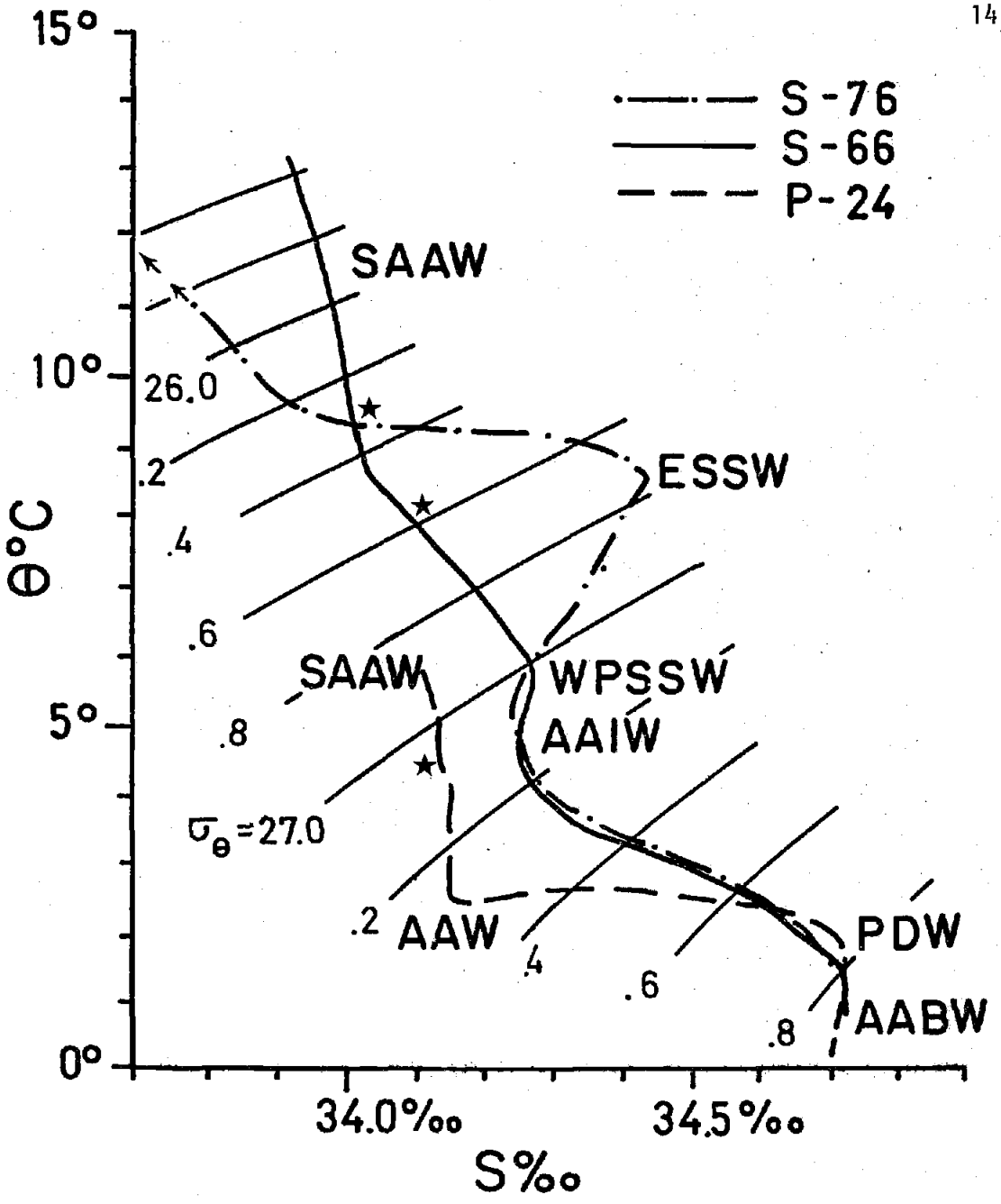

Figure 2. θ-S diagrams of representative stations showing the different water masses present in the study area. Depth of the base of seasonal thermocline is indicated by stars.

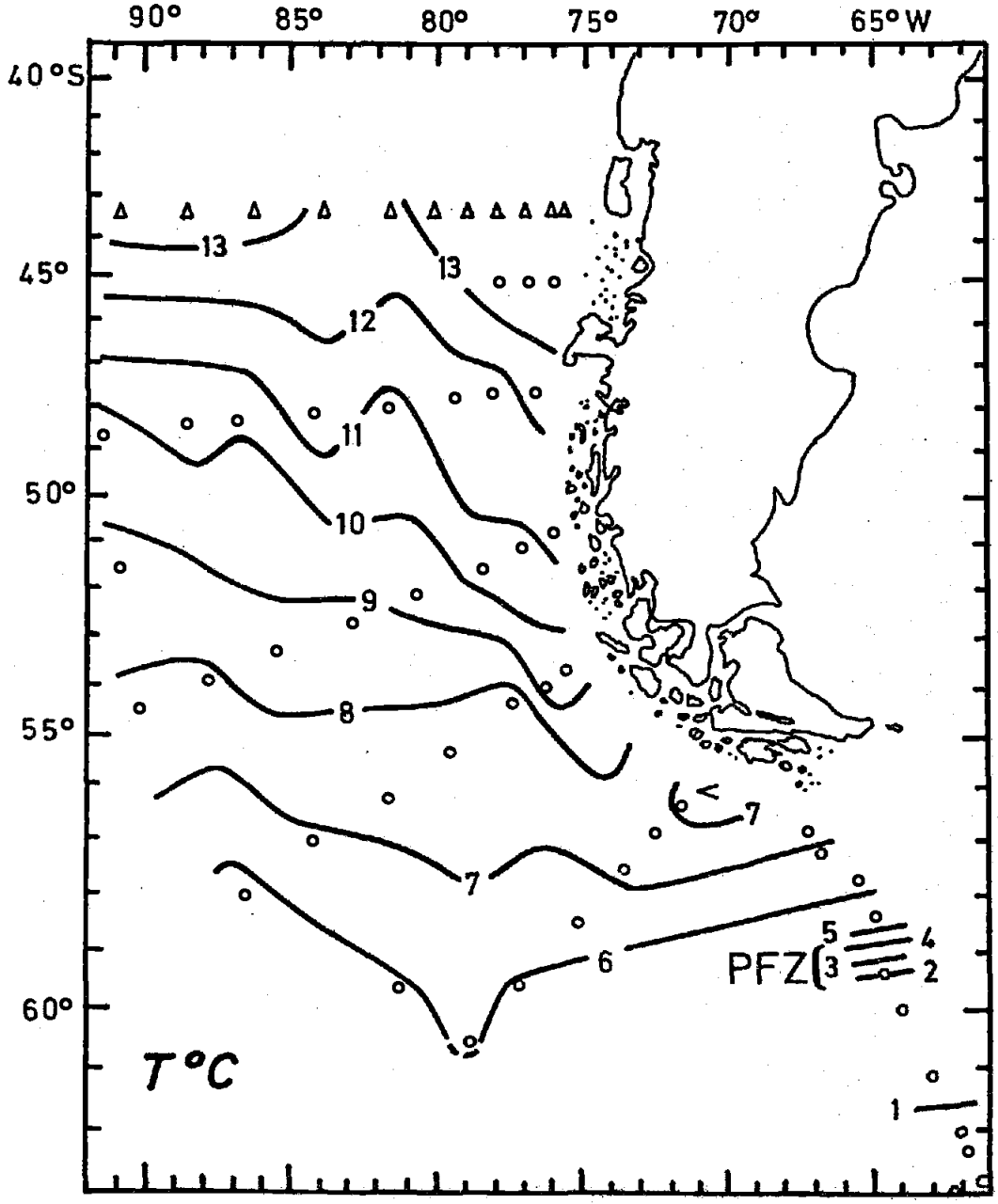

Figure 3. Temperature distribution on the sea surface, from the SCORPIO (Δ) 1967 and PIQUERO (∘) 1969 Expeditions; PFZ marks the Polar Front Zone.

tions of solar heating. Since the data was taken during summer and early fall, a seasonal thermocline was present in the thermal structure.

Close to the Chilean coast, relatively low surface salinities are present (Figure 4). Reid (1969) showed surface waters of salinity less than 34.0% extended as far as 100° W at 40° S. Figure 4 shows that the lowest values, less than 33.6%, are located along the coast; these apparently result from coastal runoff. Pickard (1971, 1973), using data from the HUDSON 70 Expedition, demonstrated increasing salinity trends from fresher inside waters of the Chilean fjord region to the oceanic waters offshore.

Since the SAAW is in the surface layer, its dissolved oxygen is high (Figure 5). The dissolved oxygen increases towards the Antarctic as a result of the increase in oxygen solubility with decreasing temperature, hence the direct correlation between the patterns of isotherm and iso-oxygen contours.

Surface phosphate and nitrate values decrease toward the coast, with the lowest values off the Chonos Archipelago (≈ 45° S) (Figures 6 and 7). These low values might be explanable as depletion of phoshate and nitrate from surface waters by phytoplankton and/or mixing of oceanic waters with comparatively lower nutrient estuarine waters. The first explanation implies that the lowering of phosphate and nitrate would be independent of salinity. The second, on the other hand, would require a covariation between salinity and nutrient content consistent with a two point mixing process. Phosphate and nitrate observations in some of the Chilean fjords and adjacent coastal waters were also made by the HUDSON 70 Expedition (CSS HUDSON, 1970). Even though the surface

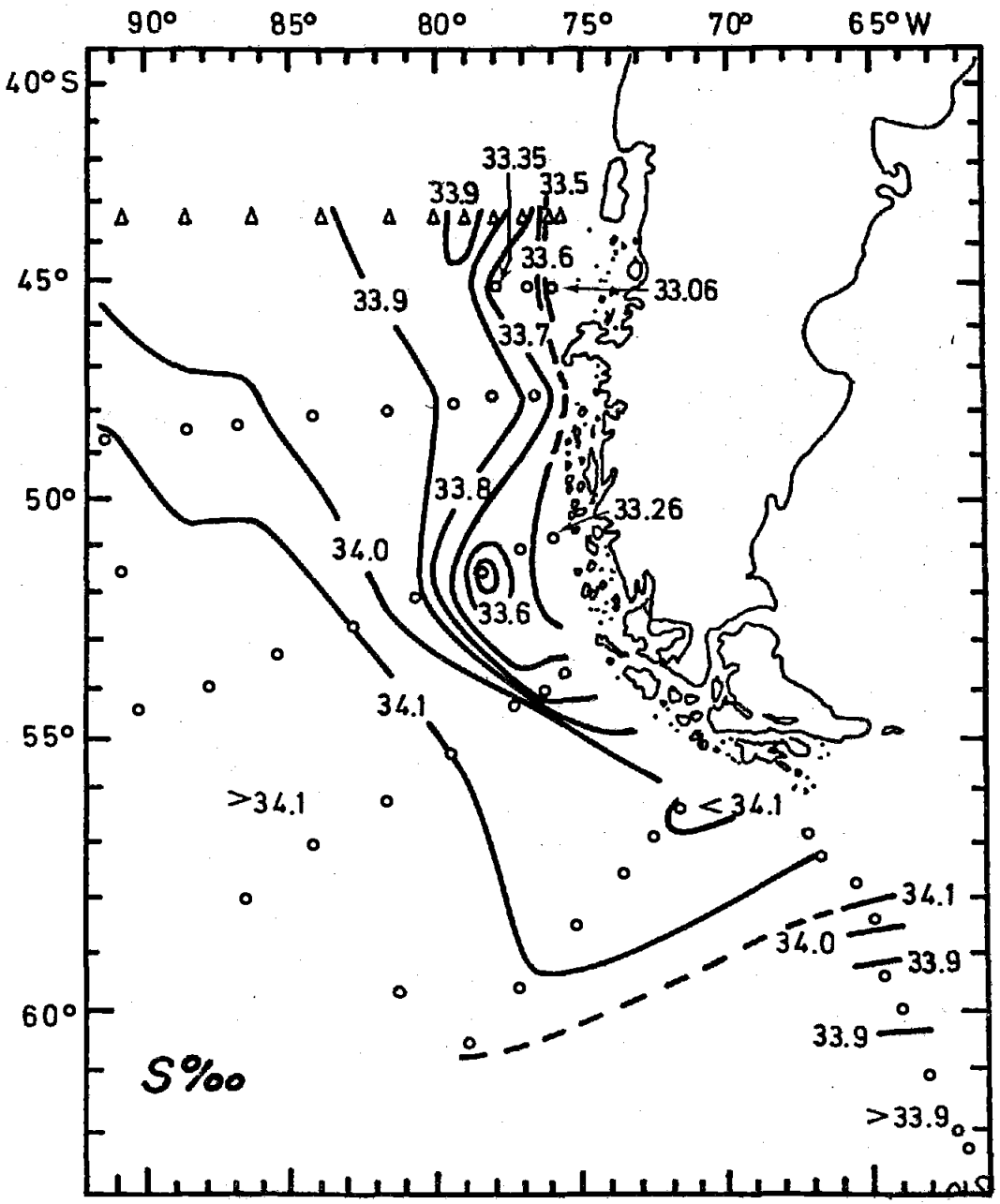

Figure 4. Salinity distribution on the sea surface, from the SCORPIO (Δ) 1967 and PIQUERO (∘) 1969 Expeditions.

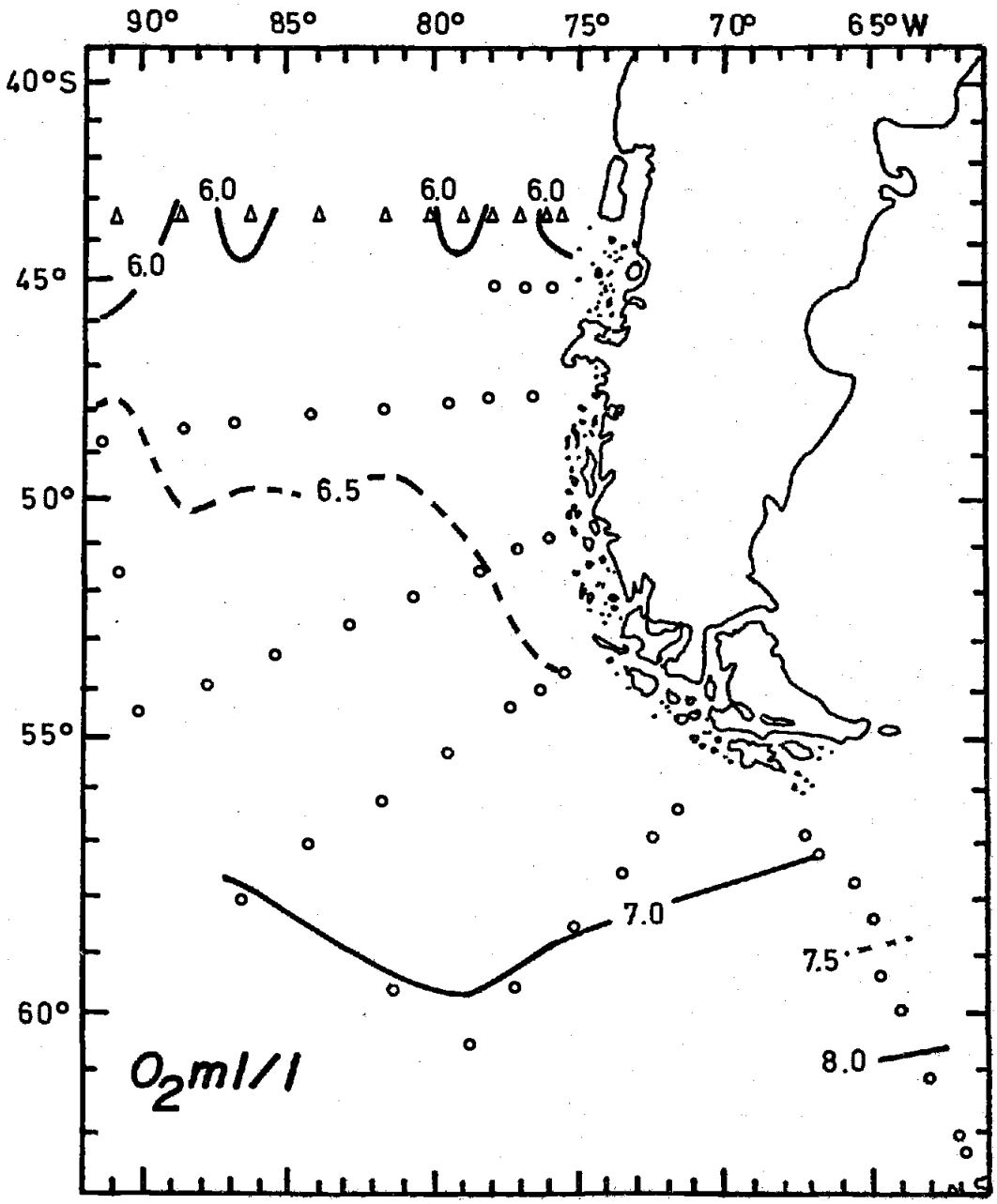

Figure 5. Dissolved oxygen distribution on the sea surface, from the SCORPIO (Δ) 1967 and PIQUERO (∘) 1969 Expeditions.

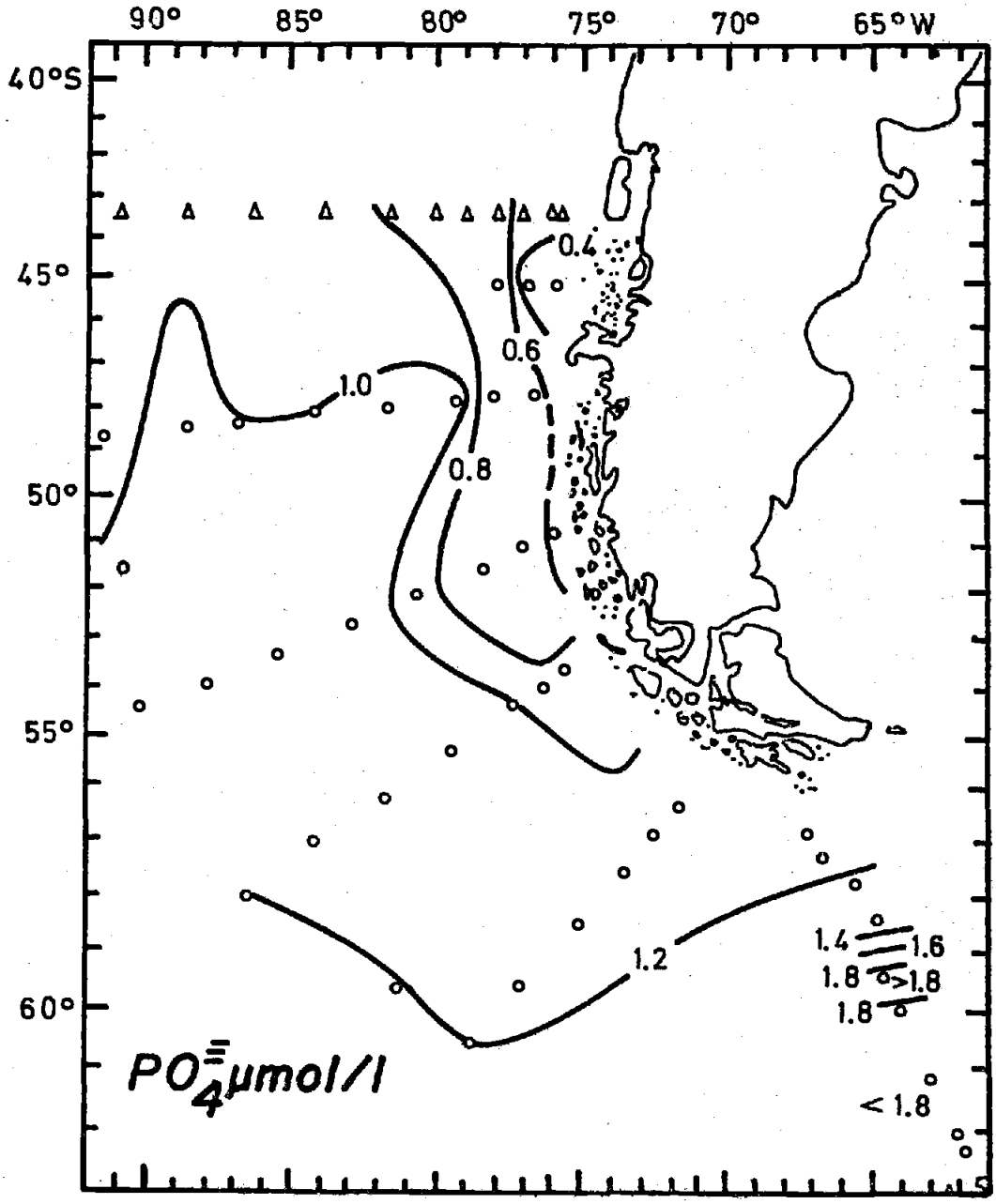

Figure 6. Phosphate distribution on the sea surface, from the SCORPIO (Δ) 1967 and PIQUERO (∘) 1969 Expeditions.

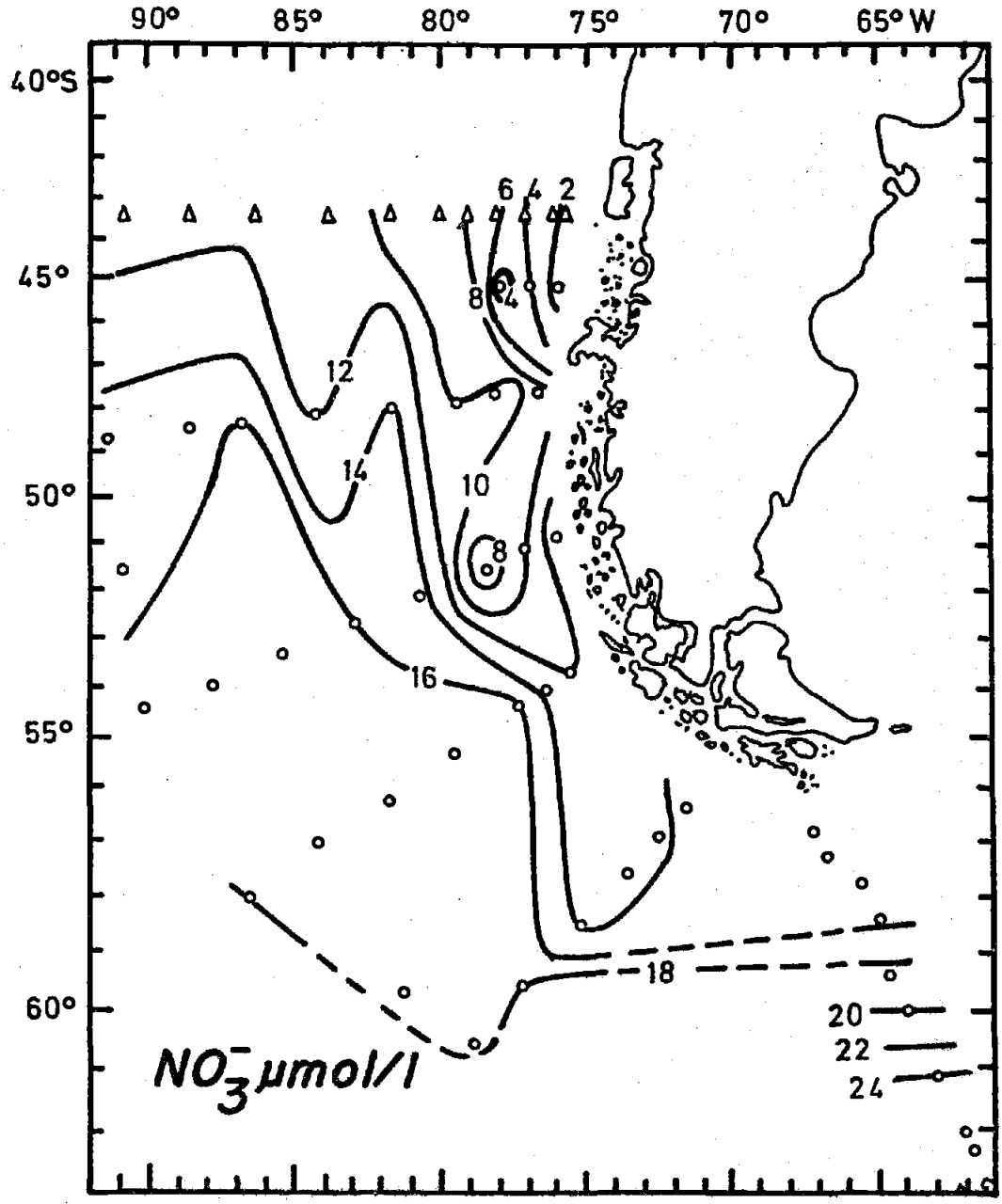

Figure 7. Nitrate distribution on the sea surface, from the SCORPIO (Δ) 1967 and PIQUERO (∘) 1969 Expeditions.

data is highly variable (≈ 0-1 - 1.3 µmol/l in phosphate, ≈ 0 - 14 µmol/l in nitrate), comparatively lower phosphate and nitrate contents are the general trend observed in the estuarine region relative to the adjacent coastal waters. Plots of surface phosphate and nitrate vs. salinity show a significant direct linear correlation at the 99% confidence level (Figure 8), for the study area where the salinity ranges between 33 - 34°/₀₀ (Figure 4). This dependency supports the second explanation, that is, the low phosphate and nitrate values close to the coast seem to be caused principally by a mixing process between oceanic and estuarine waters. Because of the r^2 values (Figure 8), only 71% of the phosphate and 65% of the nitrate variability can be explained by means of the respective linear regressions. Therefore, the biological and/or chemical processes could also account for an important fraction of the observed nutrient variability.

The surface silicate content of the SAAW in the study area is zero with some exception where the silicate reaches 1-2 µmol/l (Figure 9). Surface silicate measured by the HUDSON 70 Expedition in the fjord area shows highly variable silicate content (≈ 1 - 113 µmol/l). Nevertheless, it generally shows relatively high values at the heads of the fjords with decreasing values toward the ocean.

The above discussion of coastal surface nutrients is general because the data are limited. More work should be done on these coastal waters to answer some questions such as: How important are the phosphate and nitrate depletions by primary producers in this area? How is the high silicate estuarine water, generally present at the head of the estuary, depleted before it reaches the ocean? Biologically? Geo-

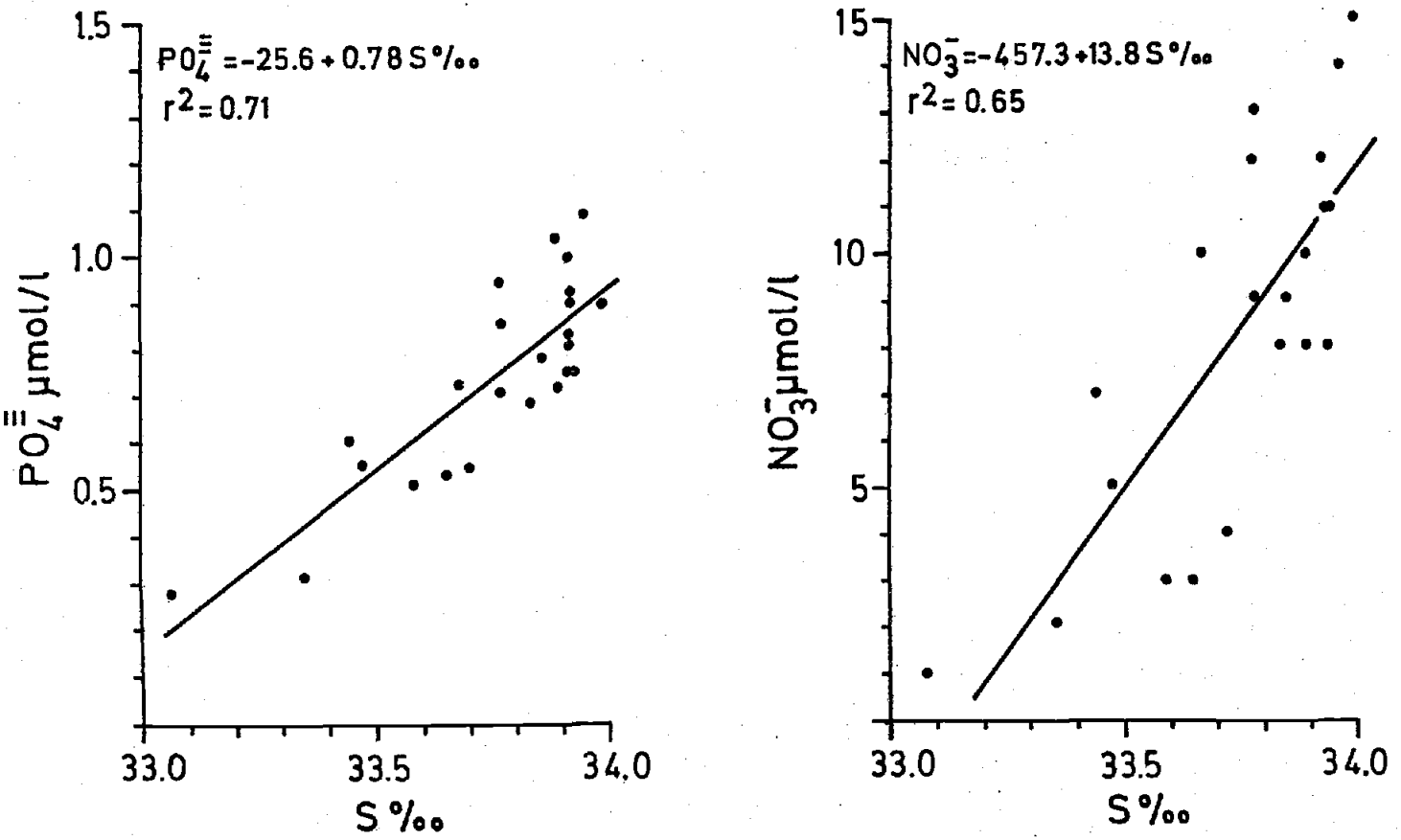

Figure 8. Regression of surface phosphate or nitrate with salinity for surface waters of salinity range 33 - 34°/₀₀, from the SCORPIO 1967 and PIQUERO 1969 Expeditions. Regression equation and correlation coefficient r^2 are given.

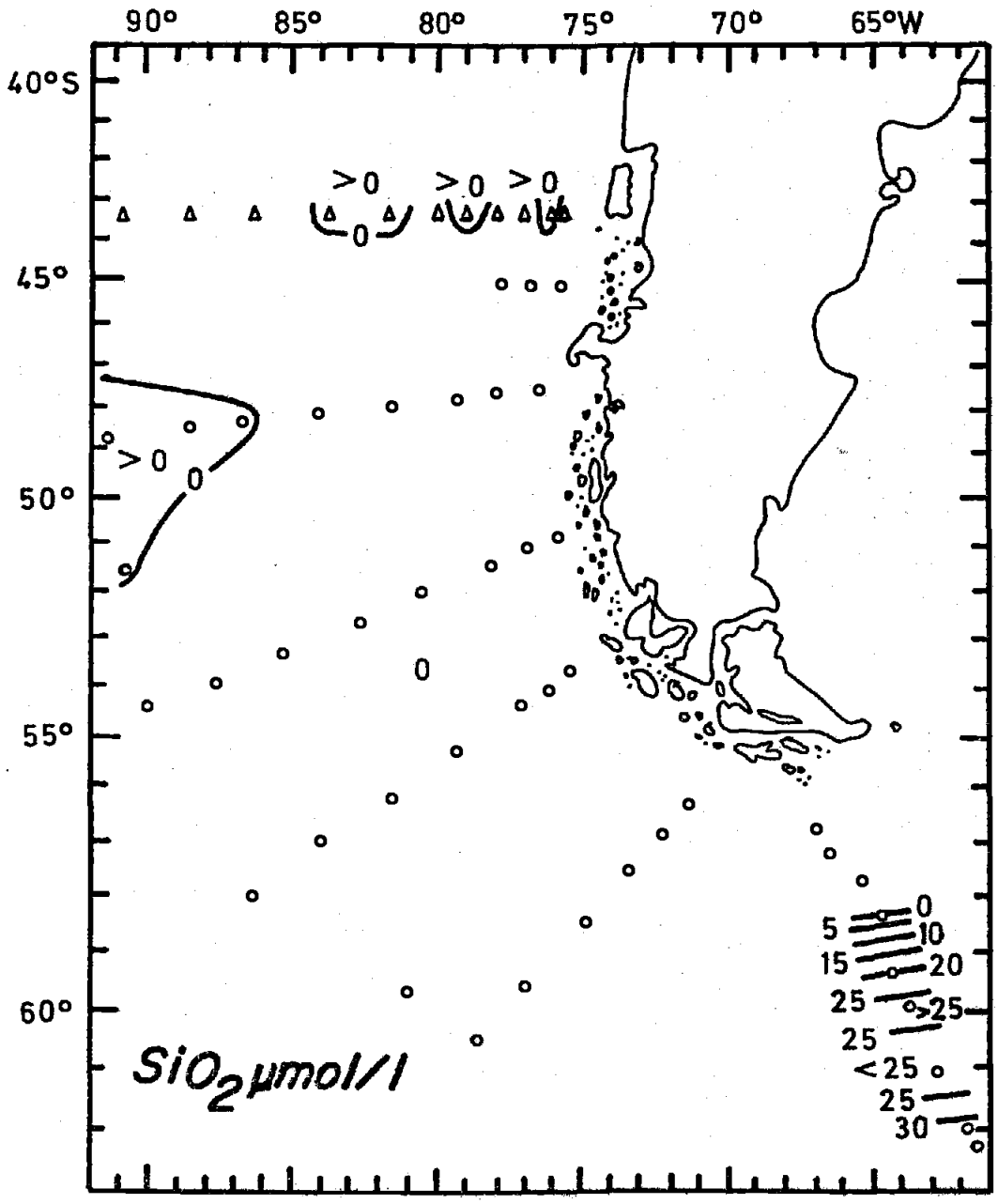

Figure 9. Silicate distribution on the sea surface, from the SCORPIO (Δ) 1967 and PIQUERO (∘) 1969 Expeditions.

chemically? Both?

4.3 Antarctic Water

Because of the Polar Front Zone location and the station distribution, only five stations are situated within the Antarctic zone (P-9 to P-13). The vertical temperature structure of the AAW is characterized by a temperature minimum localized at 100 - 150 m, which reaches its lowest value of -1.13° C at station P-10. The Antarctic surface salinity is lower than that of the Subantarctic zone (Figure 4), which is probably the result of ice melting during the summer (Gordon et al., 1977). Due to the low temperatures (Figure 3), the oxygen solubility in this area is higher than that in the Subantarctic. This results in an increase in dissolved oxygen in the AAW (Figure 5). The phosphate, nitrate and silicate content in the AAW are relatively high. Surface values above 1.4 µmol/l in phosphate, 18 µmol/l in nitrate and 15 µmol/l in silicate are observed (Figures 6 to 8).

4.4 Equatorial Subsurface Water

Within the study area, the core of the ESSW is characterized by a salinity maximum, an oxygen minimum, a nutrient maximum and a sigma-θ of 26.84. The sigma-θ surface is deeper along the coast and in the northern portion of the study area (Figure 10). It slopes gently upward toward the South, intersecting the sea surface at about 58° S.

The potential temperature on the 26.84 isopycnal varies from 6° C to 8° C, with its maximum values off Chiloe Island (≈ 43° S) (Figure 11). Temperature inversions of the order of 0.1° C above the ESSW salinity maximum are present at stations P-48 and P-49; similar inversions have

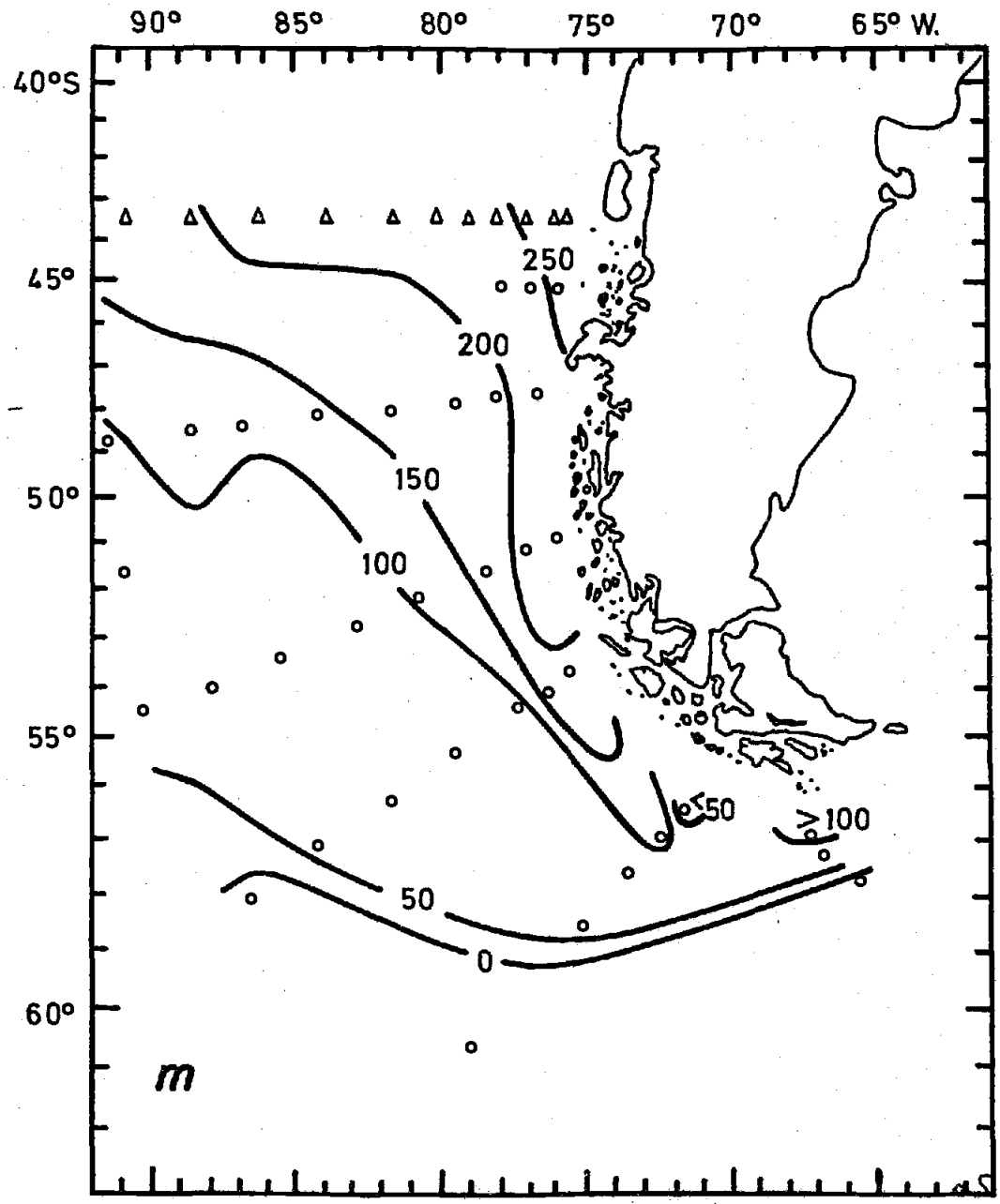

Figure 10. Bathymetry in meters of the 26.84 sigma-θ surface, from SCORPIO (Δ) 1967 and PIQUERO (∘) 1969 Expeditions.

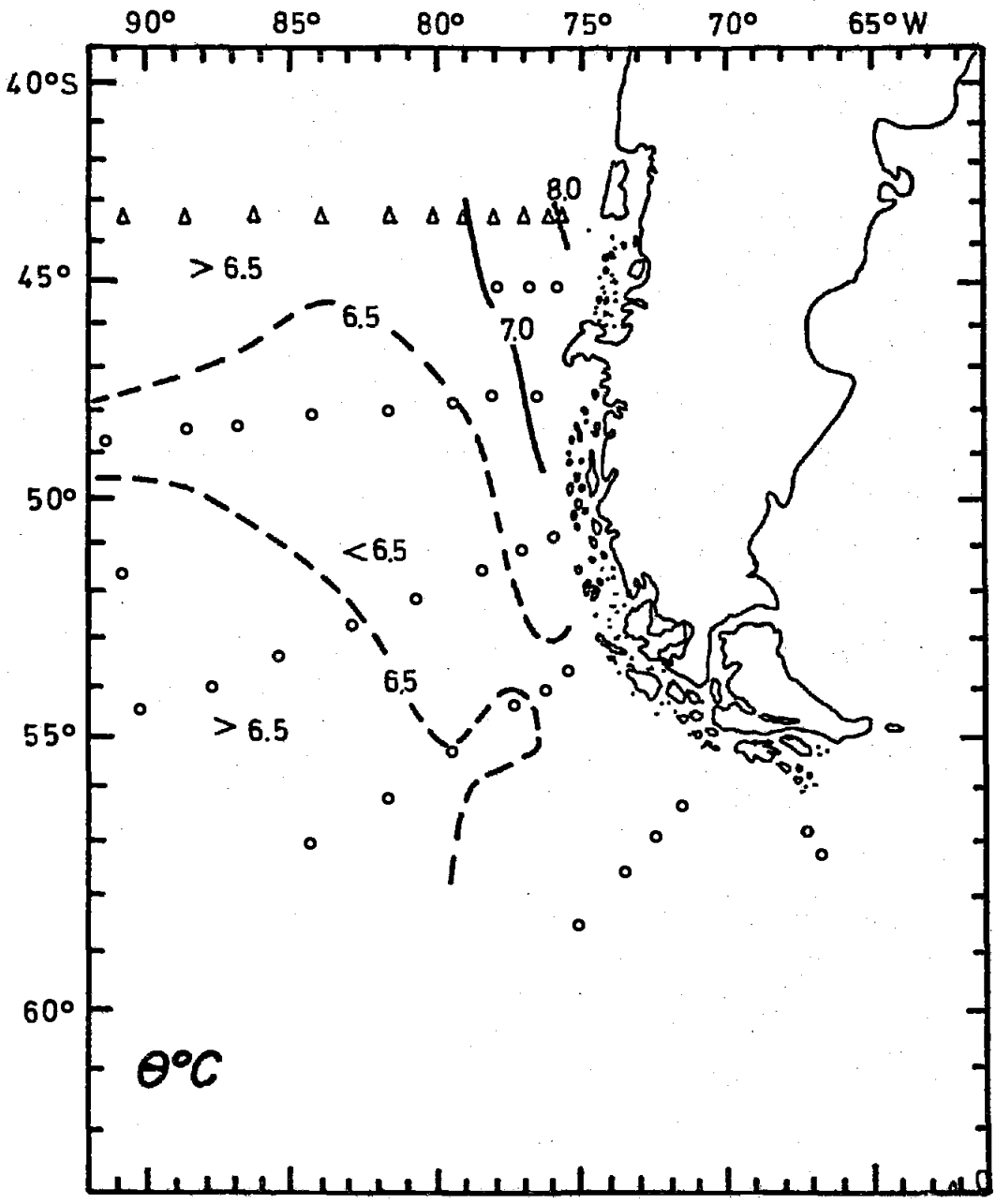

Figure 11. Potential temperature distribution on the 26.84 sigma-θ surface, from SCORPIO (Δ) 1967 and PIQUERO (∘) 1969 Expeditions.

been described for the ESSW north of 34° S by Silva and Sievers (1974) and Sievers and Silva (1975). The description of "warm water" as a characteristic of the ESSW was first given by Gunther (1936).

The salinity distribution on the 26.84 isopycnal shows a maximum in the NE portion of the region (Figure 12). The salinity decreases towards the south due to mixing with the less saline SAAW and AAIW. South of 50° S the ESSW salinity maximum can not be identified.

The oxygen content shows a distribution similar to that of the salinity and temperature but exhibits a minimum instead of a maximum (Figure 13). The lowest values appear near the coast and in the northern portion of the study area. Values as low as 1.35 ml/l were present at 223 m (sigma-θ = 26.78) at station S-76. The low oxygen content (<5.0 ml/l) persist to 52° S; this is a little farther south than the salinity maximum.

The phosphate, nitrate and silicate content of the ESSW show relatively high values close to the coast and towards the north (Figures 14 to 16). Silva and Konow (1975) have shown that the ESSW nutrient content off the coast of Chile is characterized by a maximum only south of 25° S. This maximum content in the vertical structure originates because of the comparatively lower nutrient values of the SAAW above and the AAIW underneath the ESSW. Values of 1.8 µmol/l in phosphate and 25 µmol/l in nitrate in the maximum persist as far as 52° S. The low oxygen content, high salinity and nutrients are remnant features of the highly oxygen depleted and nutrient enriched waters brought to the south by the poleward Peru-Chile Undercurrent from the eastern tropical areas.

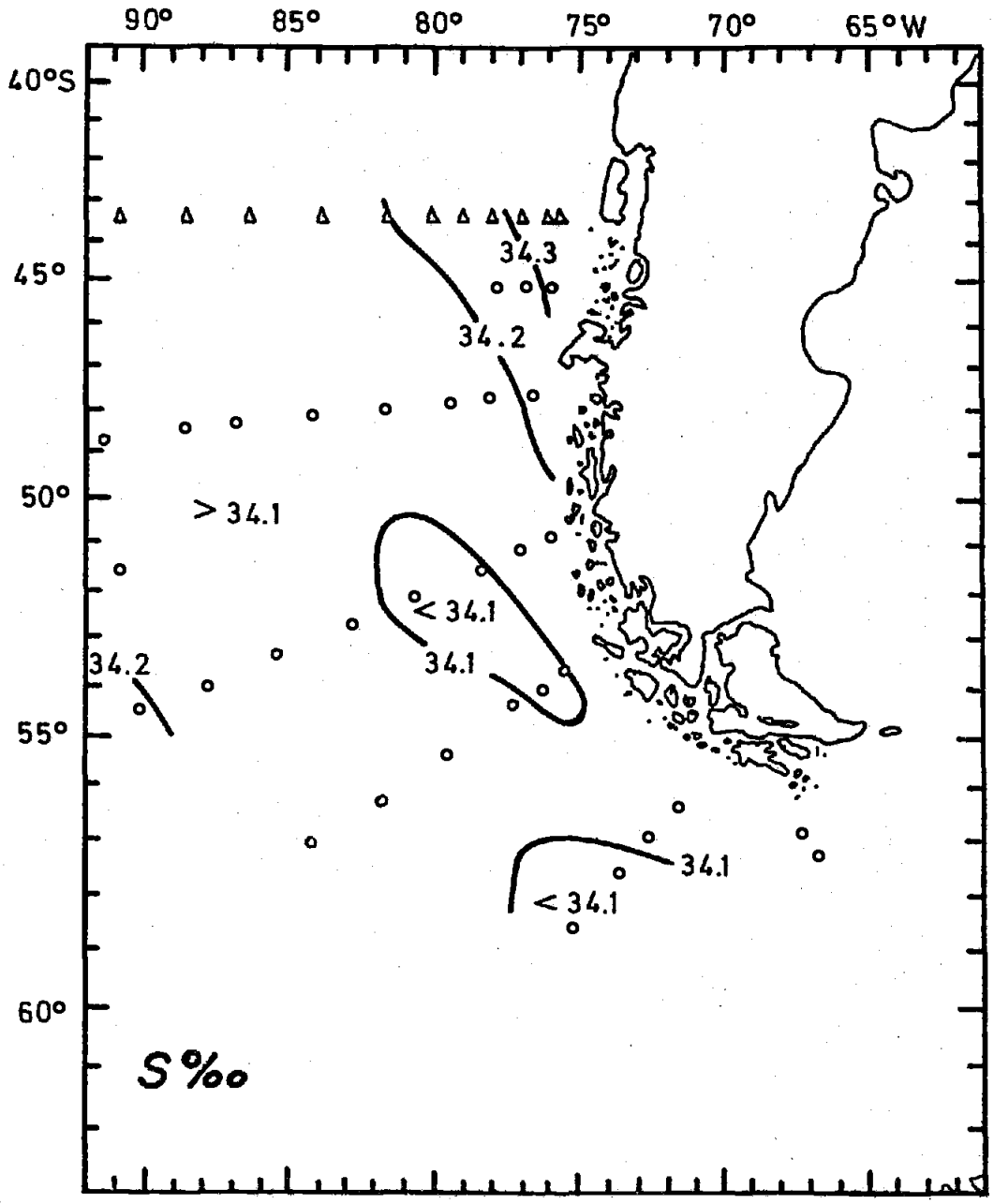

Figure 12. Salinity distribution on the 26.84 sigma-θ surface, from SCORPIO (Δ) 1967 and PIQUERO (o) 1969 Expeditions.

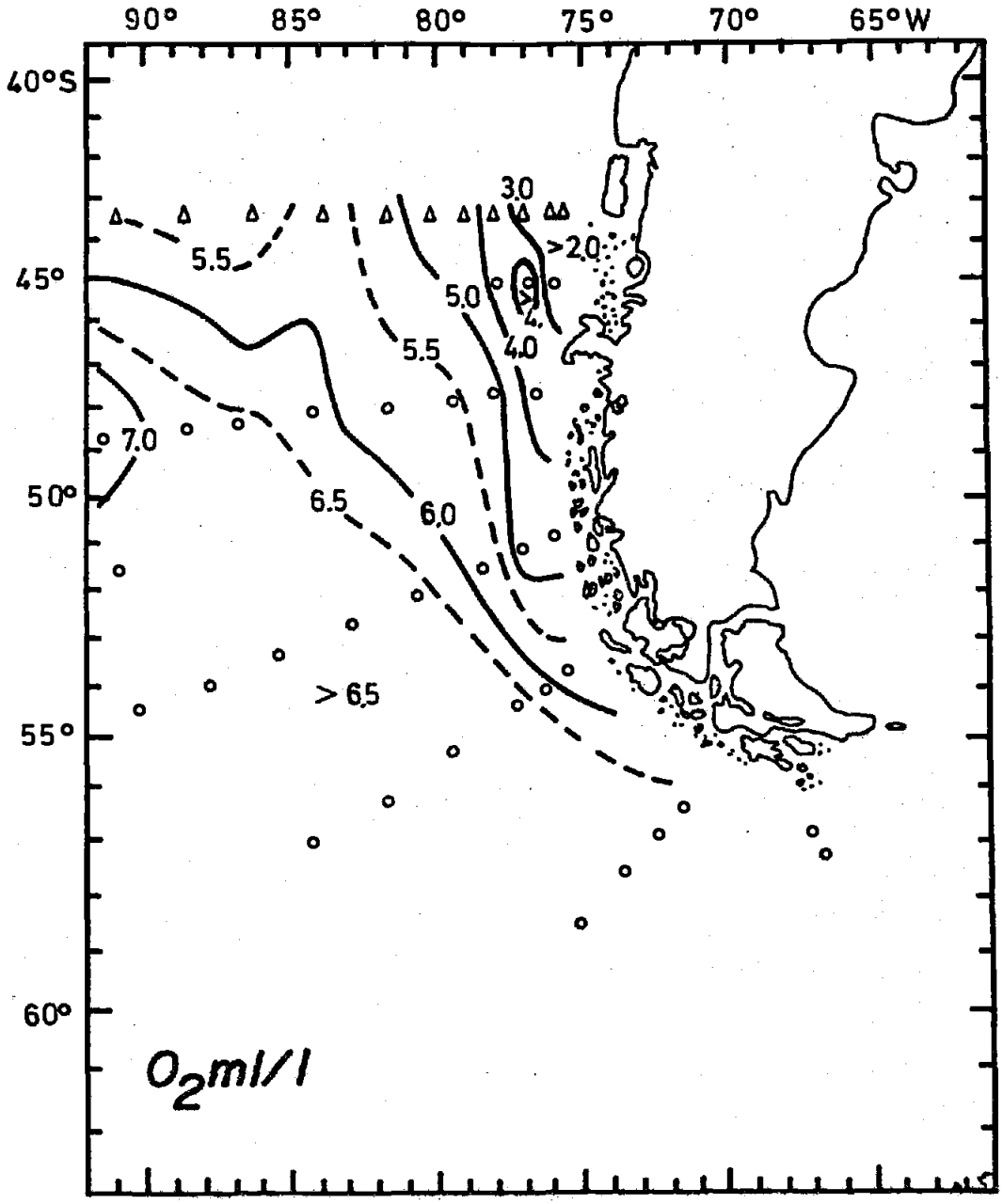

Figure 13. Dissolved oxygen distribution on the 26.84 sigma-θ surface, from SCORPIO (Δ) 1967 and PIQUERO (∘) 1969 Expeditions.

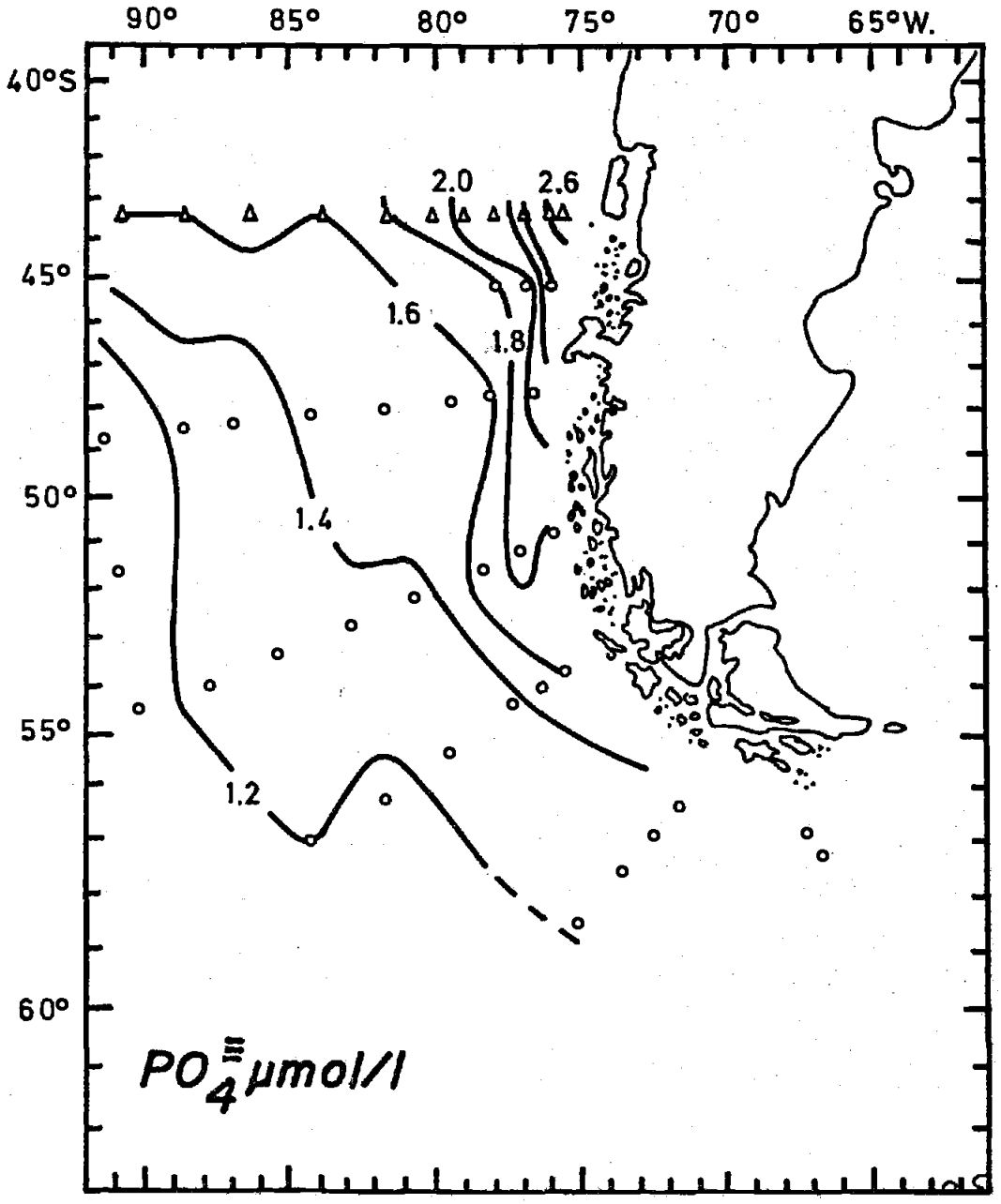

Figure 14. Phosphate distribution on the 26.84 sigma-θ surface, from SCORPIO (Δ) 1967 and PIQUERO (∘) 1969 Expeditions.

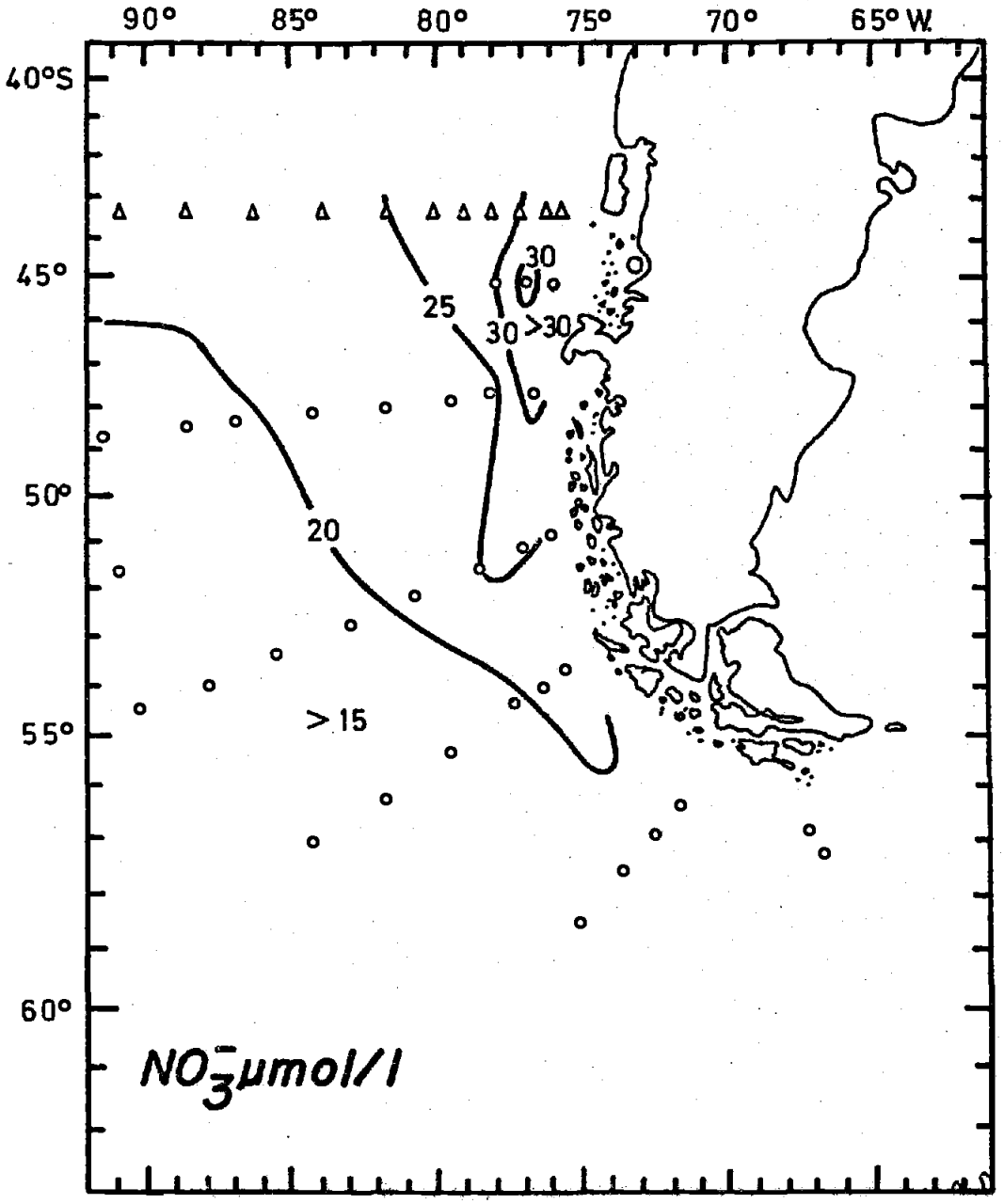

Figure 15. Nitrate distribution on the 26.84 sigma-θ surface, from SCORPIO (Δ) 1967 and PIQUERO (∘) 1969 Expeditions.

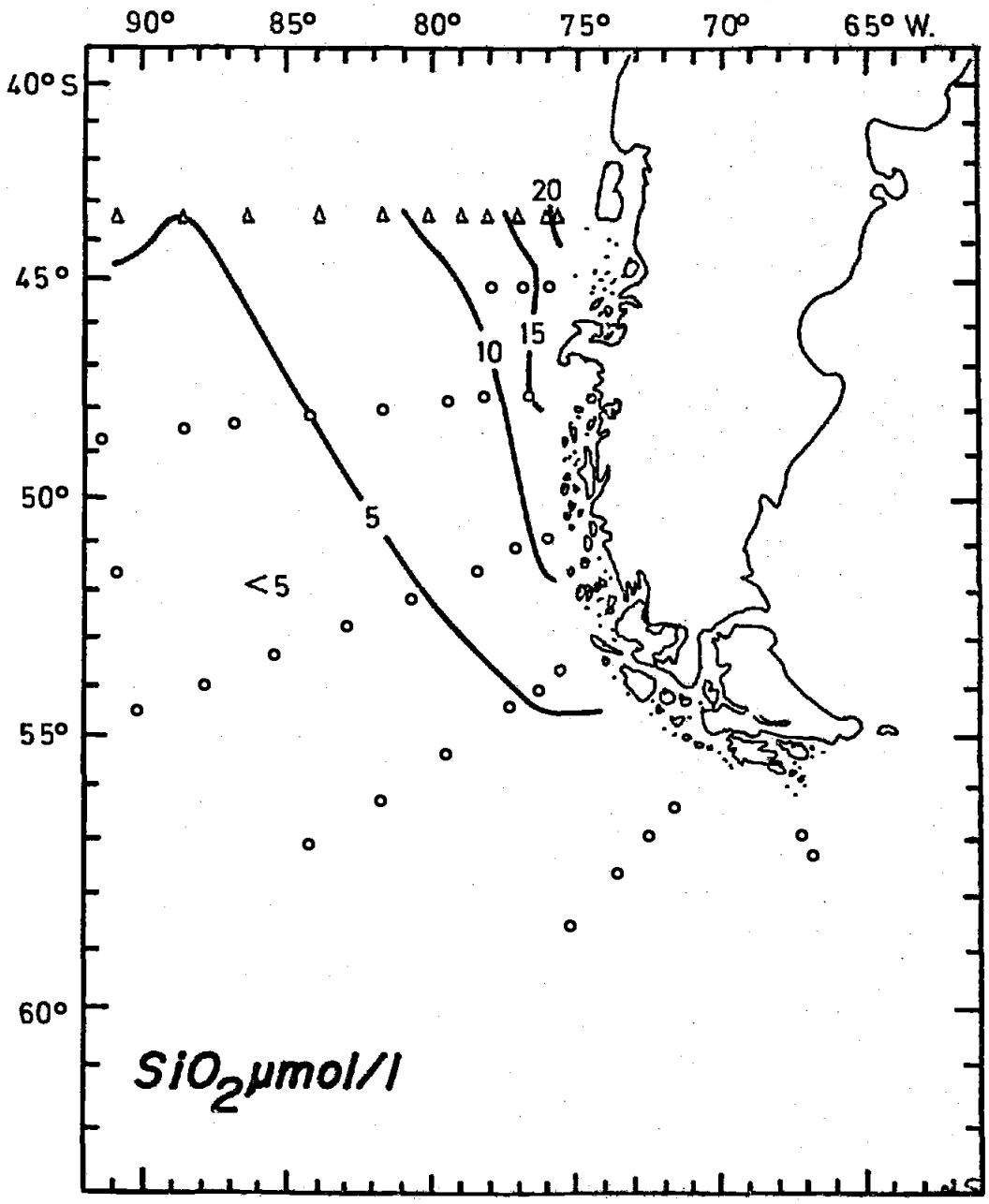

Figure 16. Silicate distribution on the 26.84 sigma-θ surface, from SCORPIO (Δ) 1967 and PIQUERO (∘) 1969 Expeditions.

4.5 Western Pacific Subsurface Water

From the θ-S diagrams of stations S-66 and S-76 (Figure 2), it can be seen that the small subsurface salinity maximum in station S-66 is a remnant of the major one present in S-76. A superposition of θ-S diagrams from S-76 towards S-66 (not shown) indicates that this subsurface maximum decreases in intensity westward. This would indicate a westward extension of the ESSW. However, some characteristics of the ESSW such as the low oxygen content do not seem to support this interpretation. A plot of the oxygen content vs. subsurface salinity maximum, for those stations north of 55° S, shows that the O_2-S pairs tend to form two groups (Figure 17). One group is associated with a high oxygen content (>4 ml/l) and the other with lower oxygen content (<4 ml/l). The existence of these distinct of clusters in the O_2 vs. S_{max} plot indicates the presence of two different water masses.

A superposition of θ-S diagrams taken from the SCORPIO Expedition (section at 43° S) (S.I.O., 1969) from S-30 (169° W) to S-75 (76° W) shows that a subsurface salinity maximum can be traced as far as S-70 at 82° W. It is proposed that this water mass, which is characterized by a subsurface salinity maximum not associated with an oxygen minimum, originates in the southern portion of the Western South Pacific.

As the waters located around 170° W move towards the east, surface salinity decreases, probably due to AAW transport across the Polar Front Zone (i.e. ring formation; Joyce and Patterson, 1977) and/or runoff from Southern Chile (Pickard, 1971). This decrease in the surface salinity combined with the presence of low salinity AAIW at intermediate depths causes the formation of a subsurface maximum (Figure 18). This maximum

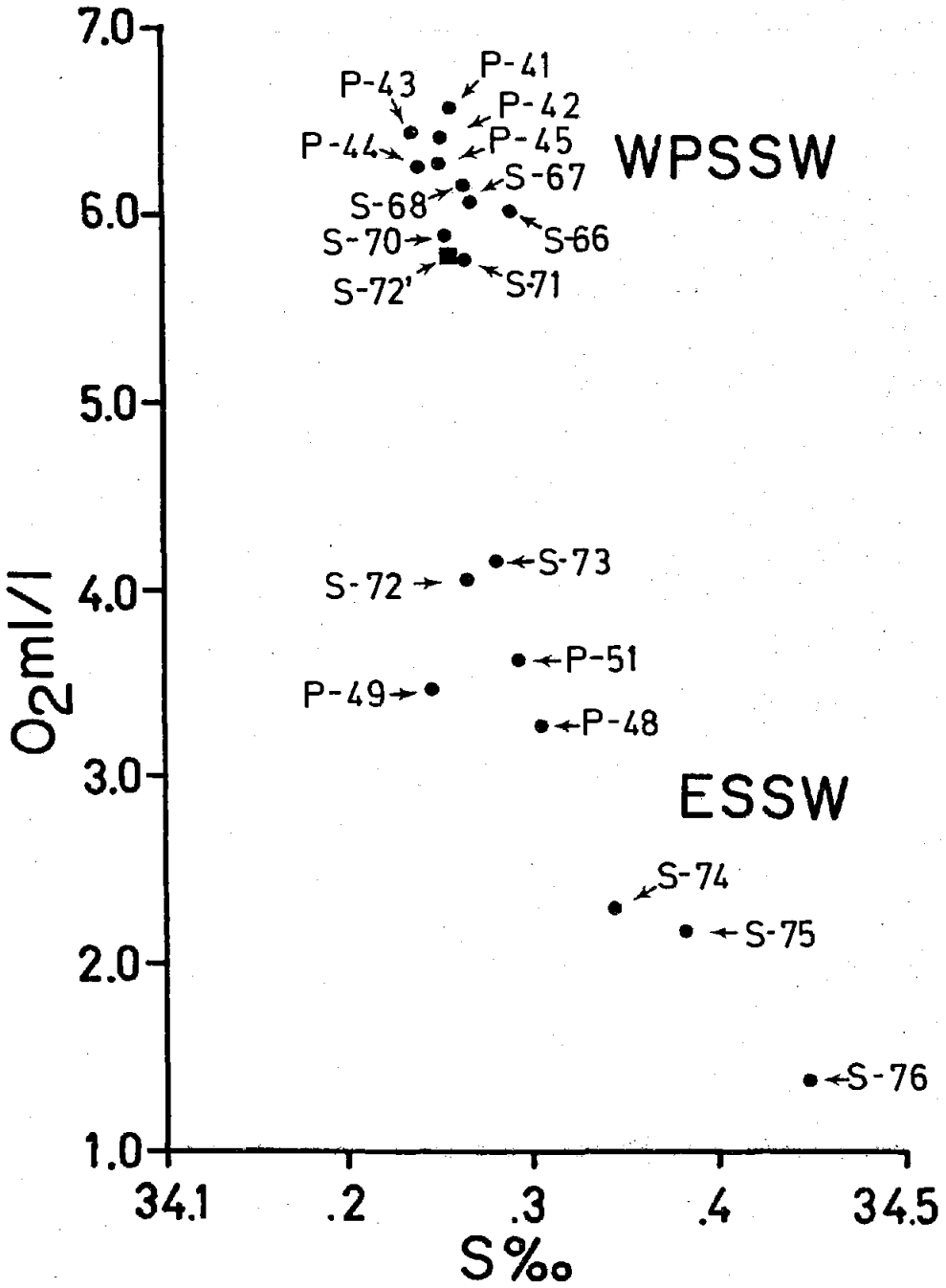

Figure 17. Dissolved oxygen vs. subsurface salinity maximum showing the separate groups of O_2-S_{max} pairs corresponding to two different water masses, from stations north of 55° S of the SCORPIO (S) 1967 and PIQUERO (P) 1969 Expeditions.

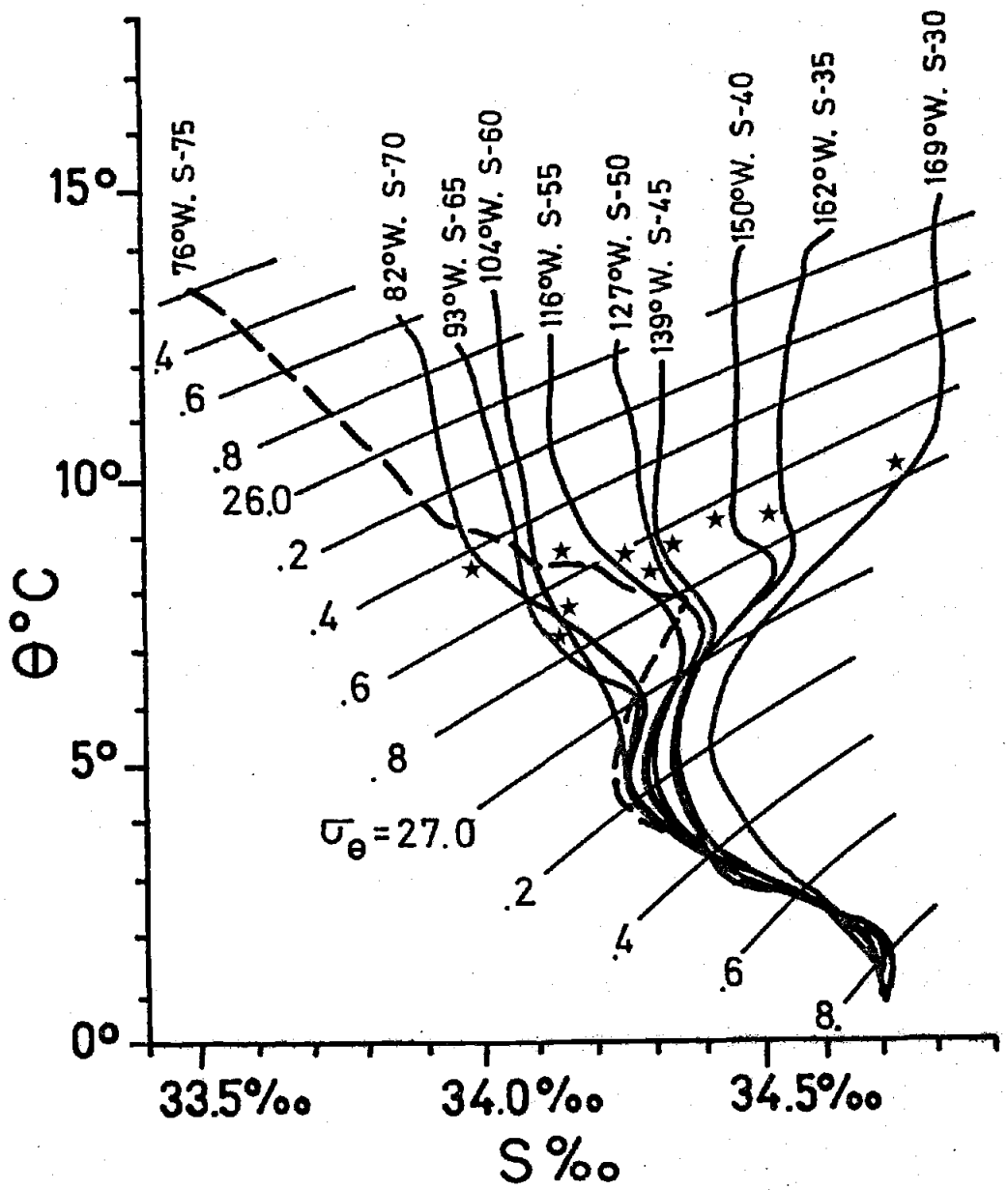

Figure 18. Superposition of θ-S diagrams along 43° S from 169° W to the Chilean Coast from selected stations of SCORPIO 1967. Stars indicate the depth of the base of the seasonal thermocline.

decreases in intensity eastward due to mixing with the less saline waters located above and below it. Even though the salinity maximum decreases eastward, the core of the WPSSW increases in density due to temperature decrease. The name of Western Pacific Subsurface Water (WPSSW) is given to this water mass which in the study area has a mean potential density of 27.06.

One notes in Figure 18 that the θ-S diagrams for station S-75 (dashed line) departs markedly from the trend of the salinity maximum between station S-30 and S-70, showing an increase in salinity and a decrease in density. This change is attributed to the presence of the ESSW.

A more exhaustive analysis on the properties of the WPSSW is beyond the objectives of this study because of the area involved. Therefore, the WPSSW nutrient characterization as well as its spatial extension is work to be accomplished in the future.

4.6 Antarctic Intermediate Water

North of 55° S the bathymetry of the 27.12 sigma-θ, where the AAIW is located, presents rather constant depths of around 600 m (Figure 19). South of 55° S it slopes upwards reaching the sea surface south of the Polar Front Zone.

The potential temperature has a relatively homogeneous distribution along the 27.12 isopycnal. Close to the Polar Front Zone, as this water mass shoals, the potential temperature drops rapidly at the rate of about 3° C in 100 km (Figure 20).

The salinity of the AAIW in the study area is also fairly uniform, with values between 34.20 and 34.25°/$_{oo}$ north of 55° S (Figure 21). The

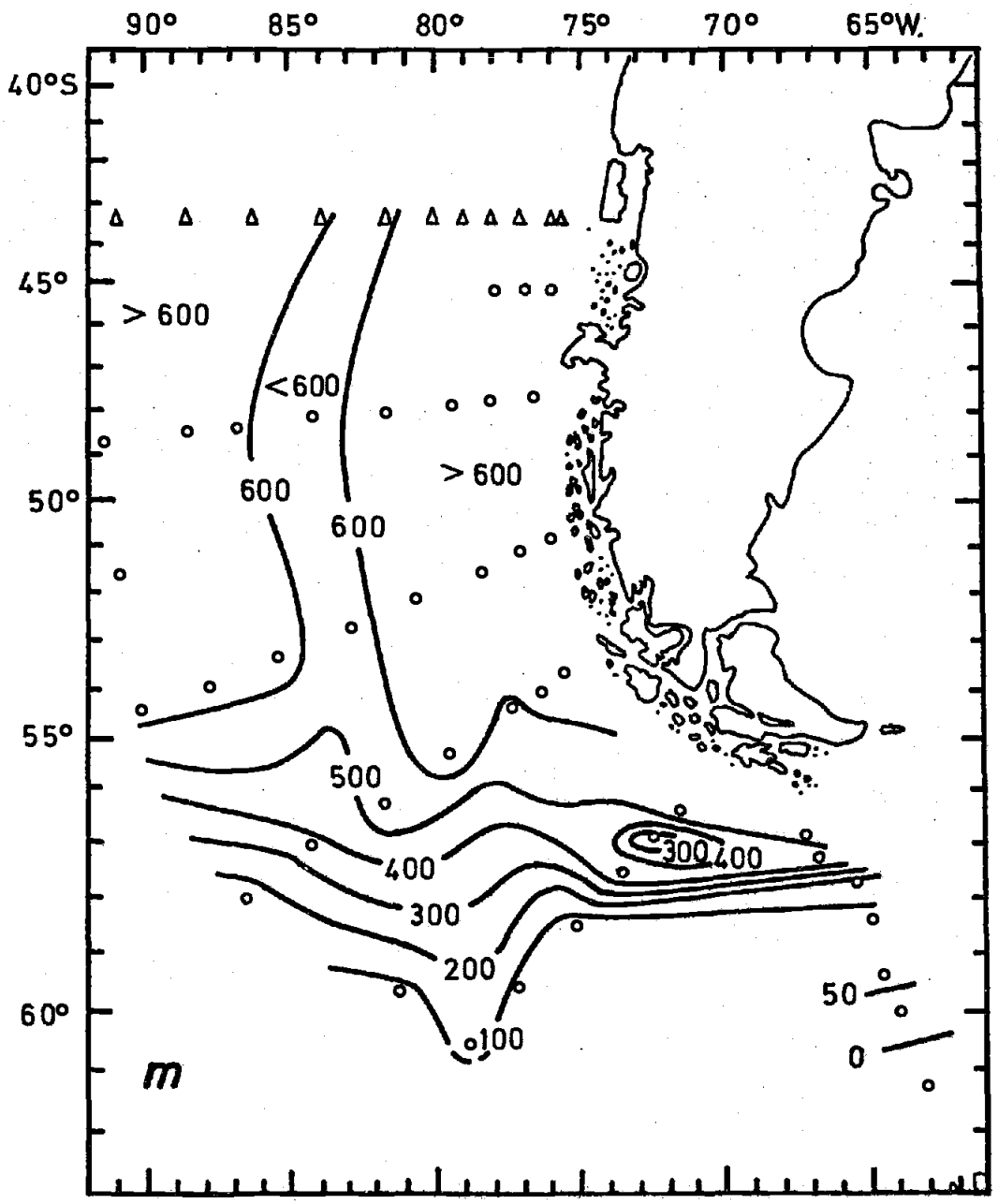

Figure 19. Bathymetry in meters of the 27.12 sigma-θ surface, from the SCORPIO (Δ) 1967 and PIQUERO (∘) 1969 Expeditions.

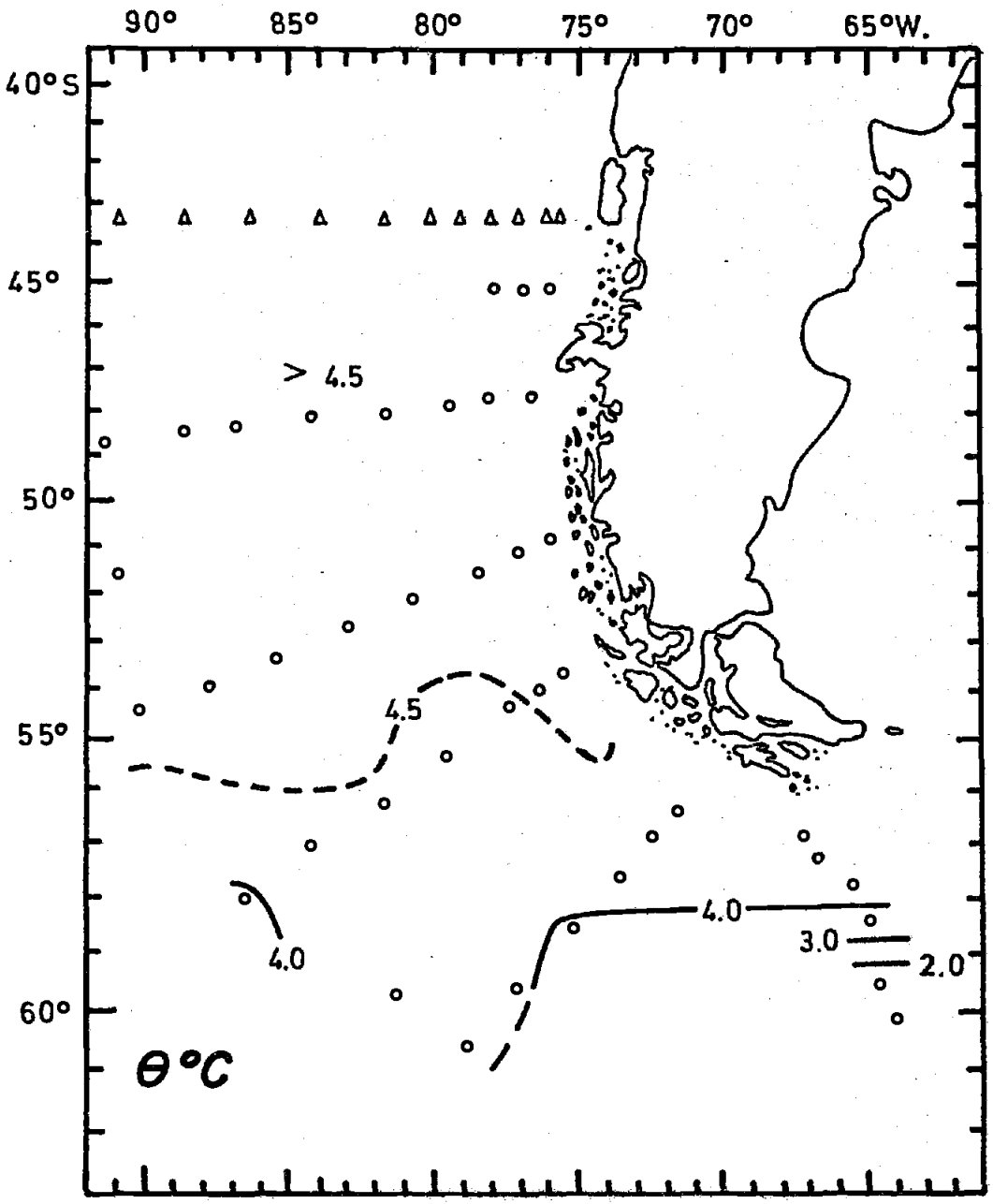

Figure 20. Potential temperature distribution on the 27.12 sigma-θ surface, from the SCORPIO (Δ) 1967 and PIQUERO (∘) 1969 Expeditions.

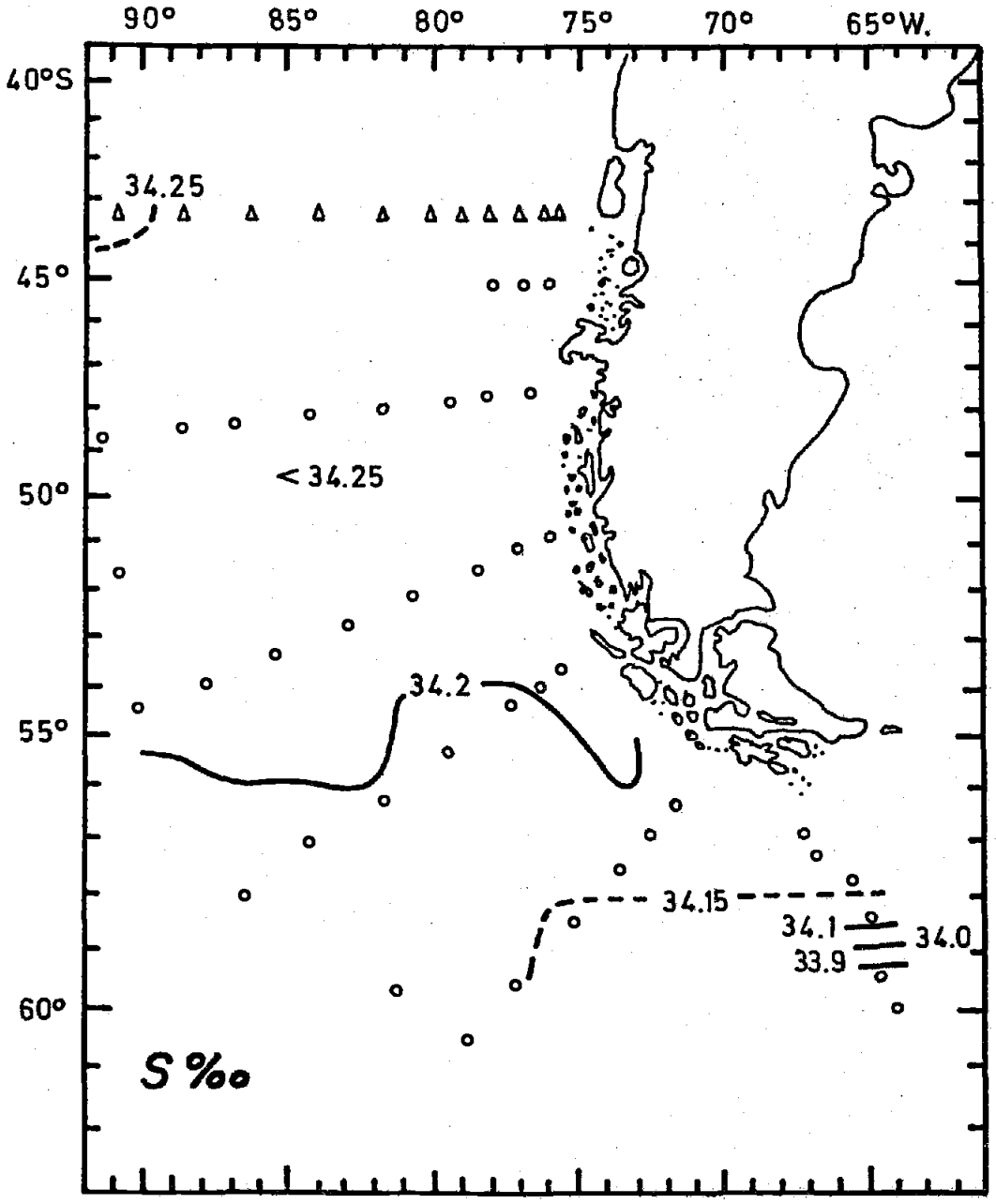

Figure 21. Salinity distribution on the 27.12 sigma-θ surface, from the SCORPIO (Δ) 1967 and PIQUERO (∘) 1969 Expeditions.

salinity vertical distributions in the three northernmost oceanographic sections A, B and C (not shown), comprise a layer of relatively homogeneous salinity with values between 34.20 and 34.30°/₀₀. This nearly homogeneous layer, located between 200 and 900 m, contains the characteristic AAIW salinity minimum and becomes shallower and less saline as it approaches the Polar Front Zone.

As in the case of potential temperature and salinity, the dissolved oxygen is also fairly uniform (Figure 22). Oxygen increases poleward mainly because the water on the 27.12 sigma-θ surface is cooler and fresher, increasing oxygen solubility. Close to the Chilean coast and between the oxygen poor ESSW above and PDW below, the AAIW shows a maximum oxygen content. Beyond the area where the ESSW oxygen minimum is present, the AAIW does not show a relative maximum in dissolved oxygen.

Phosphate and nitrate in the AAIW along the 27.12 isopycnal, exhibit nearly homogeneous distributions (Figure 23 and 24). The silicate distribution on the 27.12 sigma-θ is rather different from that of phosphate and nitrate, even though north of 55° S it is also nearly homogeneous (Figure 25). Closer to the Polar Front Zone, silicate diminishes to a minimum (<5 µmol/l) at the Polar Front Zone, increasing again southward. This situation is the result of the use of a fixed mean isentropic surface to describe the AAIW distribution. The 27.12 sigma-θ surface represents the core of AAIW in most of the area, but close to the Polar Front Zone it reaches depths lower than 100 m and this is where the SAAW or AAW is located. Therefore, the minimum in silicate on sigma-θ 27.12 near the Polar Front Zone can be explained by the presence of low silicate SAAW, while the increase to the south of the Polar Front

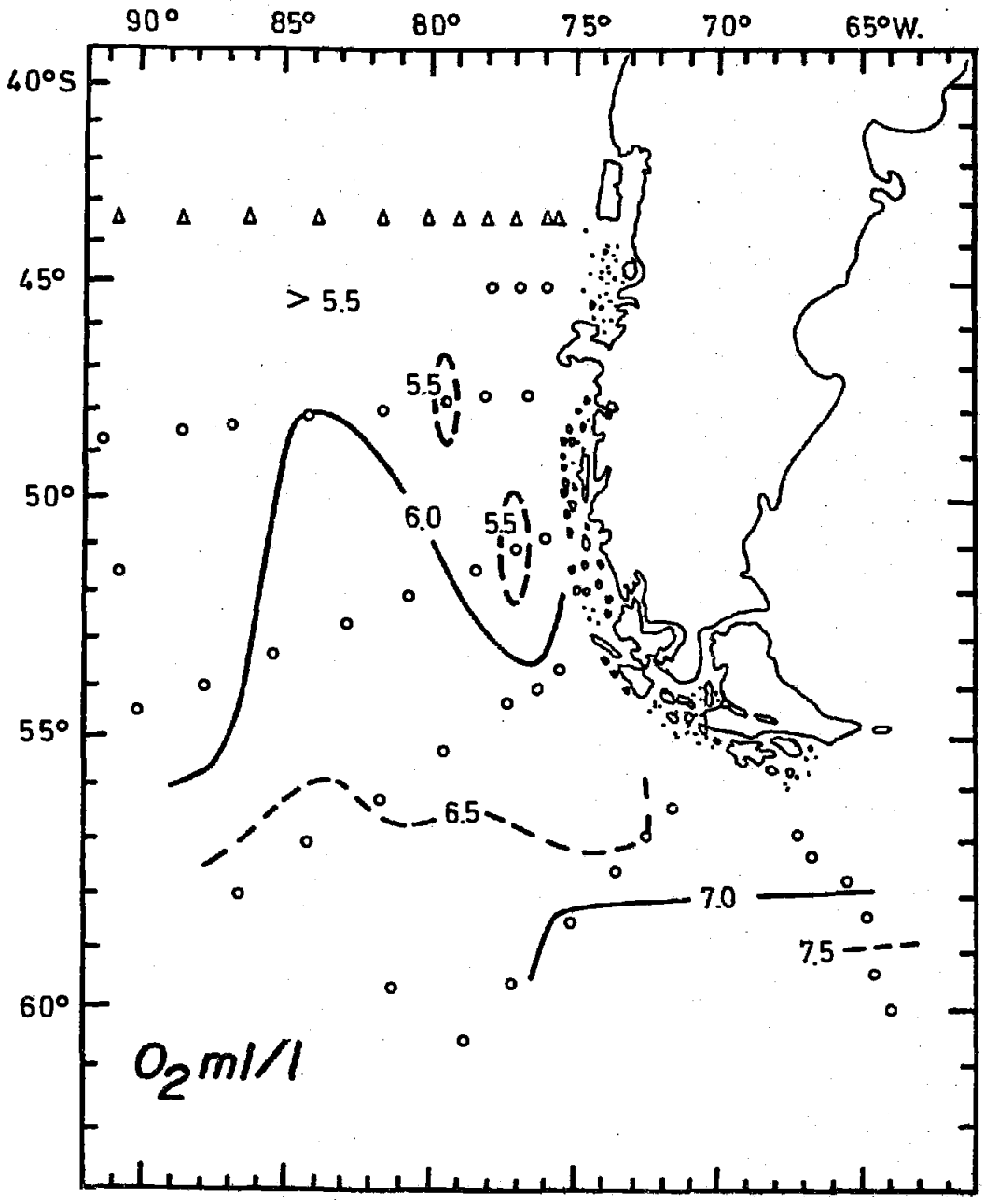

Figure 22. Dissolved oxygen distribution on the 27.12 sigma-θ surface, from the SCORPIO (Δ) 1967 and PIQUERO (∘) 1969 Expeditions.

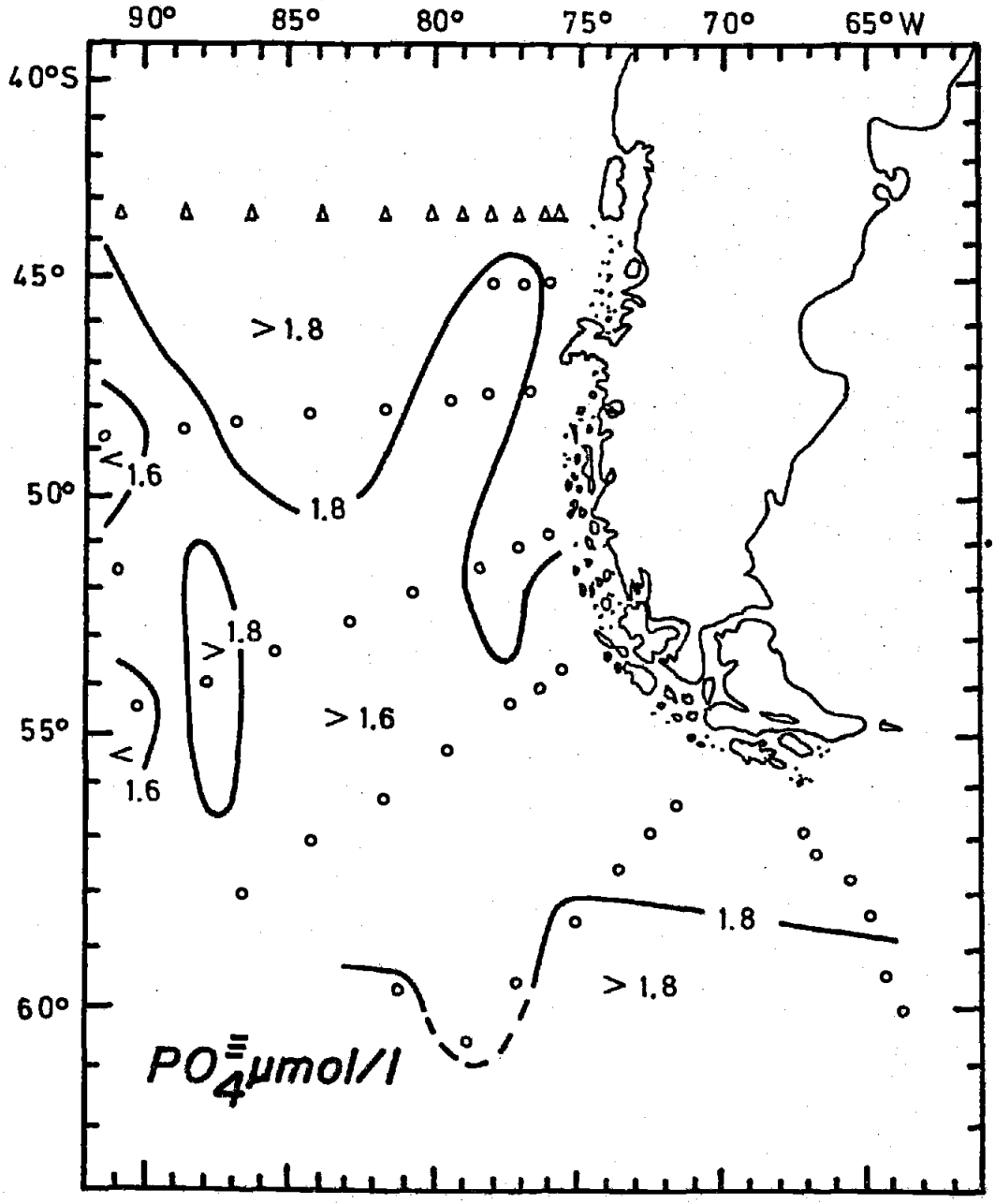

Figure 23. Phosphate distribution on the 27.12 sigma-θ surface, from the SCORPIO (Δ) 1967 and PIQUERO (∘) 1969 Expeditions.

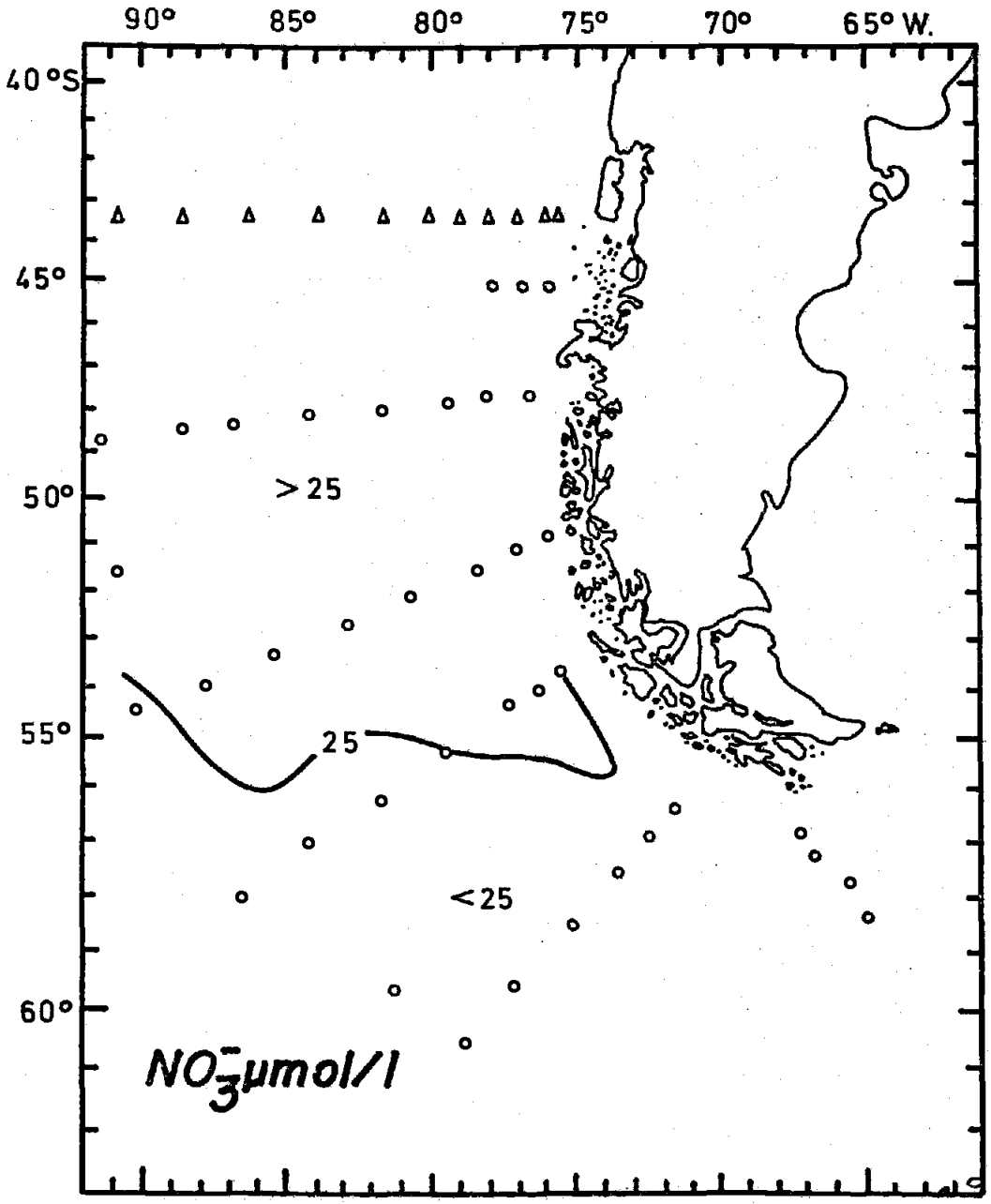

Figure 24. Nitrate distribution on the 27.12 sigma-θ surface, from the SCORPIO (Δ) 1967 and PIQUERO (∘) 1969 Expeditions.

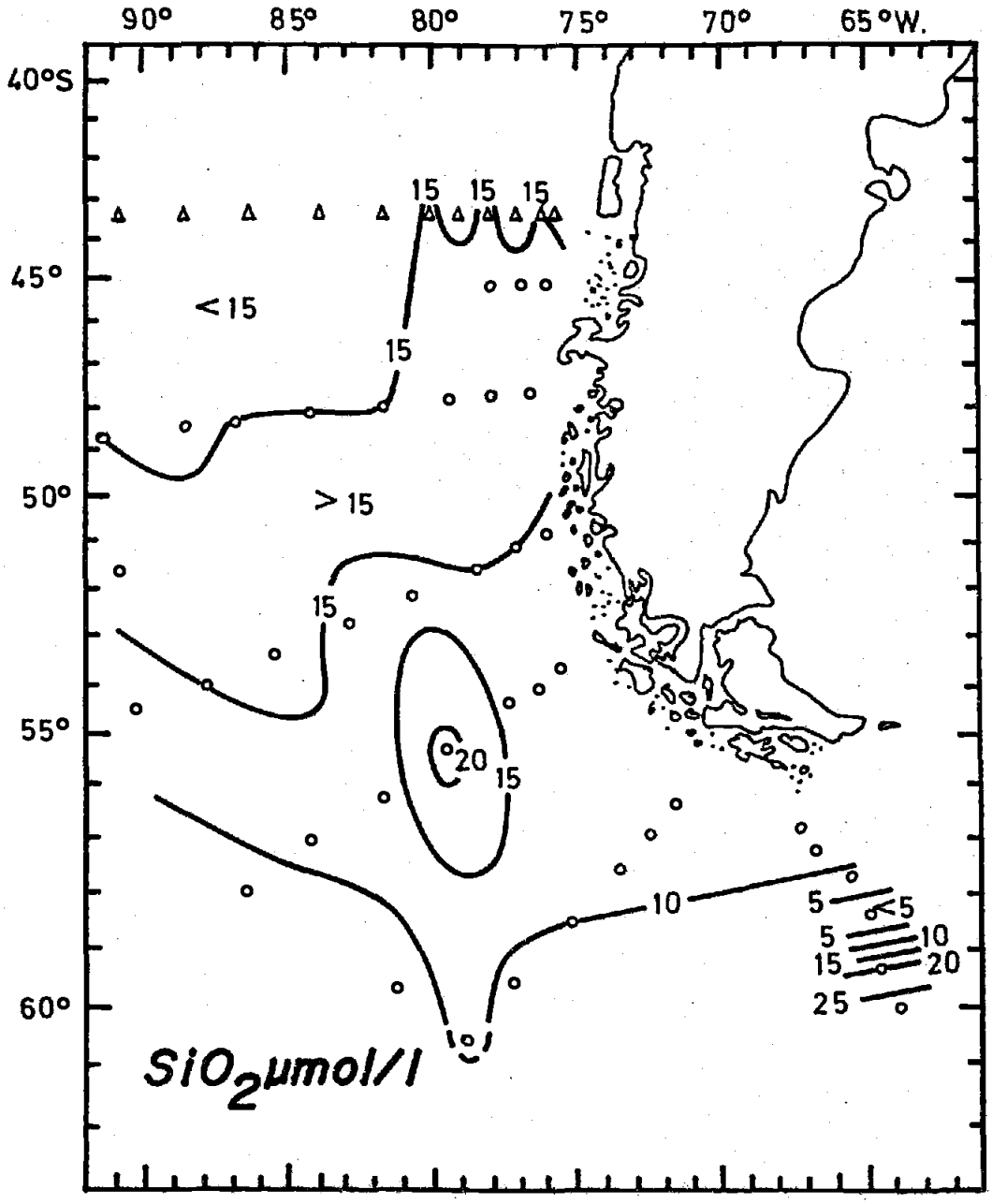

Figure 25. Silicate distribution on the 27.12 sigma-θ surface, from the SCORPIO (Δ) 1967 and PIQUERO (◦) 1969 Expeditions.

Zone is explained by the presence of high silicate AAW. This situation was not evident in the phosphate and nitrate distributions because of the relatively high values of these properties in SAAW in contrast to the silicate.

In a similar fashion to oxygen but in an opposite sense, nutrients in the AAIW show a minimum concentration in the vertical structure where the ESSW is present. Reid (1973a) points out that although the nutrients exhibit minima in the vertical, the actual concentrations in the AAIW are high, as might be expected from waters of a high latitude origin. These high concentrations define minima only because of the relative higher concentrations of the overlying ESSW carried poleward from the eastern tropical areas (Reid, 1973a) and the high concentrations of the PDW beneath.

V. WATER MASS STRUCTURE TYPES

5.1 General considerations

When for a given area the temperatures and corresponding salinities of the water column are plotted against each other, the points fall on a characteristic curve showing the structure of the salinity-temperature relationship. This well defined curve is the end result of the vertical mixing processes that different original water masses have experienced during their movement toward the given area. The grouping of similar θ-S curves and the division of the study area into regions with similar types of curves will give important information bearing upon features observed in the circulation patterns.

5.2 Water structures present in the region

The PIQUERO-SCORPIO θ-S diagrams of the water column sampled north of the Polar Front Zone, from the seasonal thermocline to the bottom, can be grouped into four different types, each with a more or less characteristic structure. θ-S diagrams representative of each of these structures are shown in Figures 26 to 29. A geographic distribution of stations classified according to these structures is shown in Figure 30. The water masses present in these structures are given in Table I.

TABLE I. Water mass constituents of θ-S structures present in the area north of the Polar Front Zone.

Structure	Water Masses
I	SAAW - ESSW - AAIW - PDW
II	SAAW - WPSSW - AAIW - PDW - AABW*
III	SAAW - AAIW - PDW - AABW*
IV	SAAW - AAW - PDW - AABW

*May not be present in some stations showing this characteristic structure.

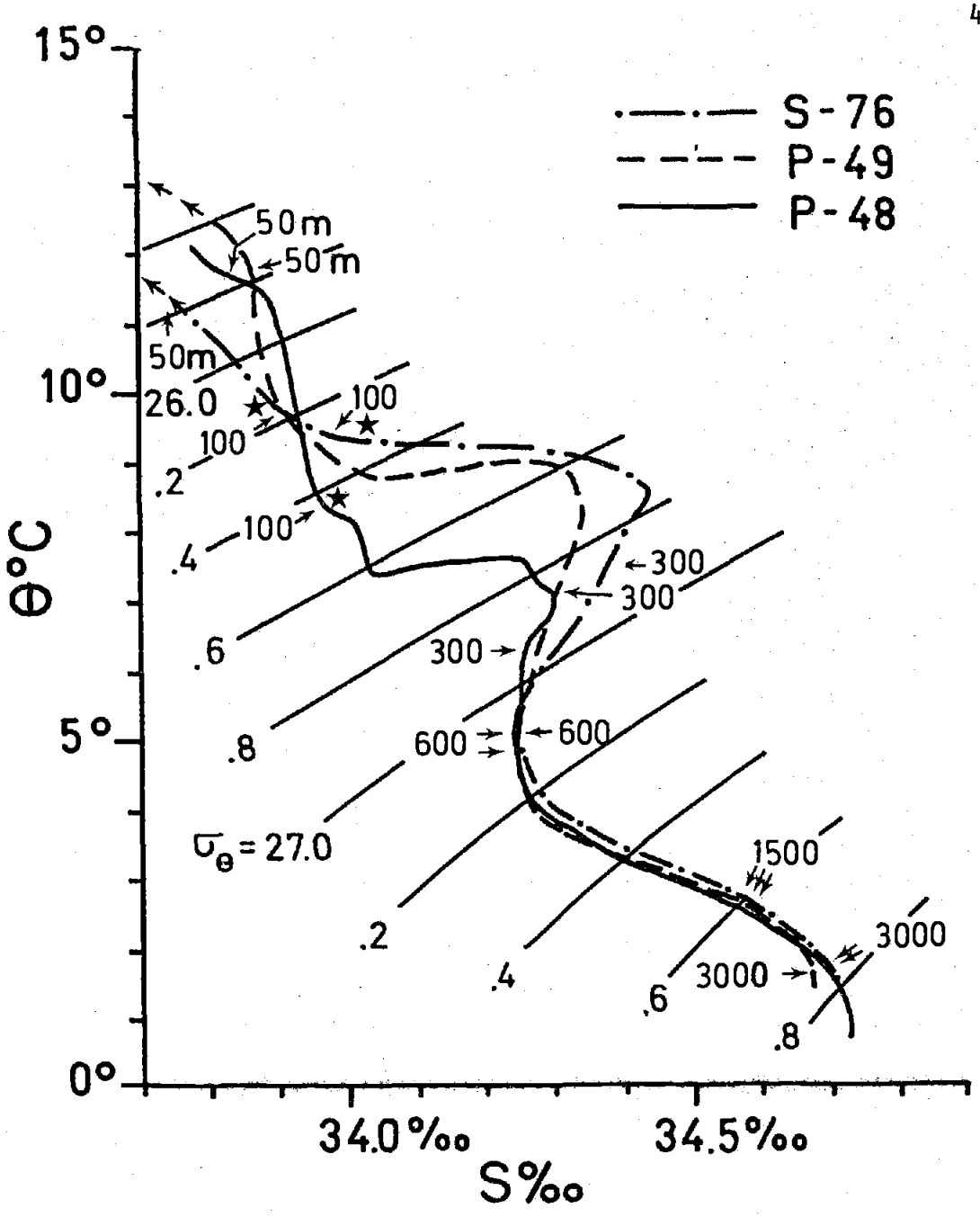

Figure 26. Representative stations showing Structure Type I from the SCORPIO (S) 1967 and PIQUERO (P) 1969 Expeditions. Stars indicate depths of the base of the seasonal thermocline.

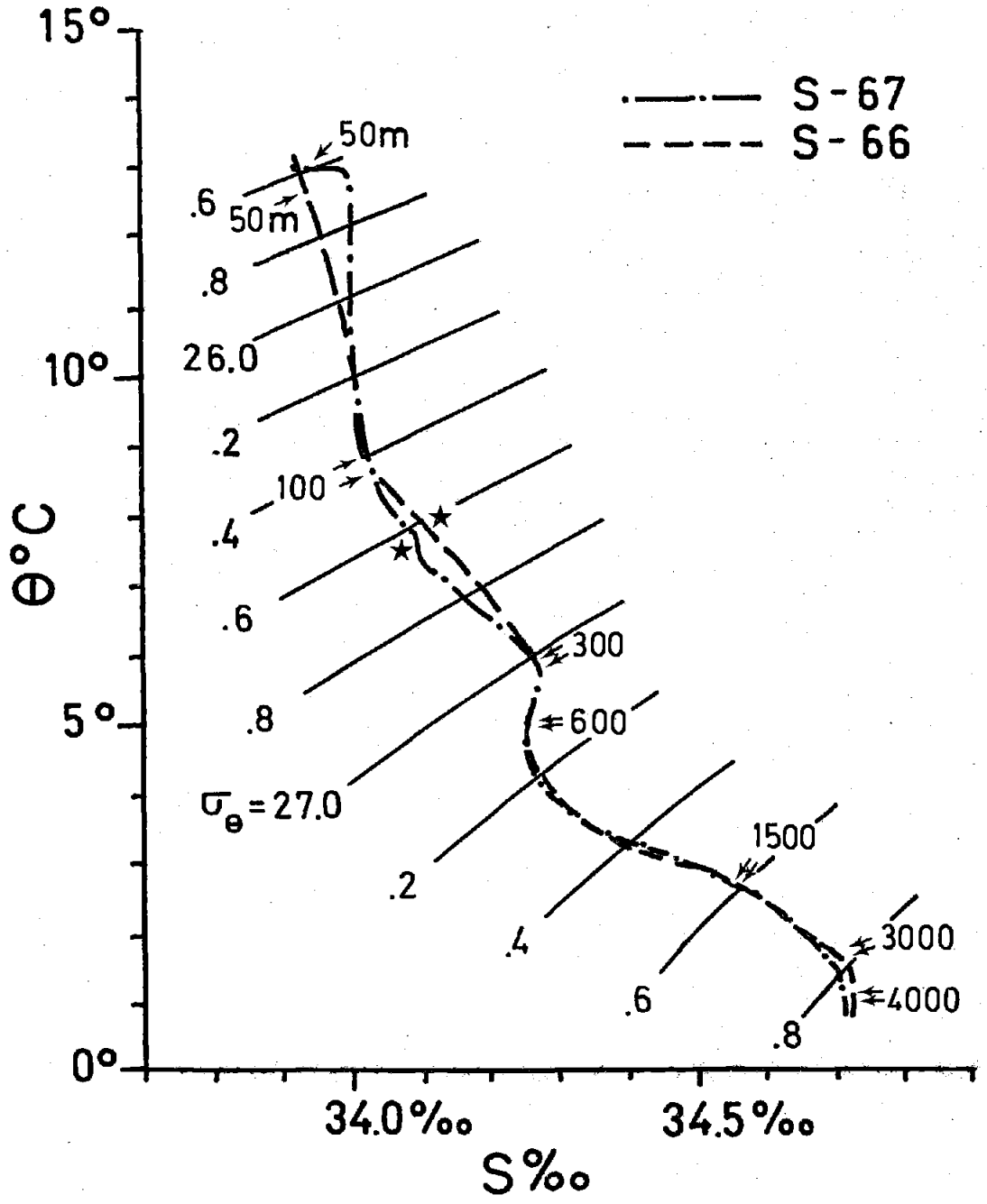

Figure 27. Representative stations showing Structure Type II from the SCORPIO (S) 1967 Expedition. Stars indicate depth of the base of the seasonal thermocline.

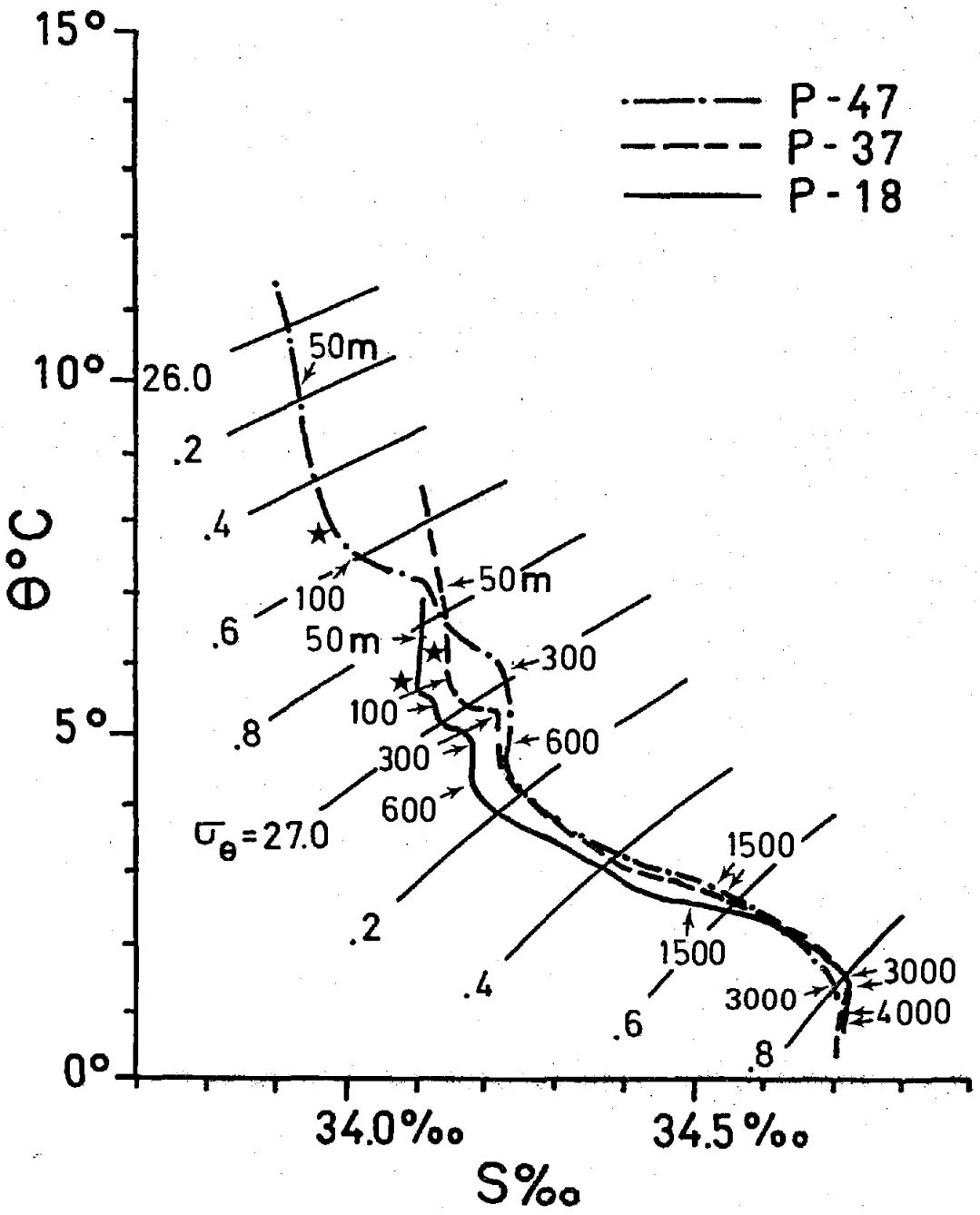

Figure 28. Representative stations showing Structure Type III from the PIQUERO (P) 1969 Expedition. Stars indicate depth of the base of the seasonal thermocline.

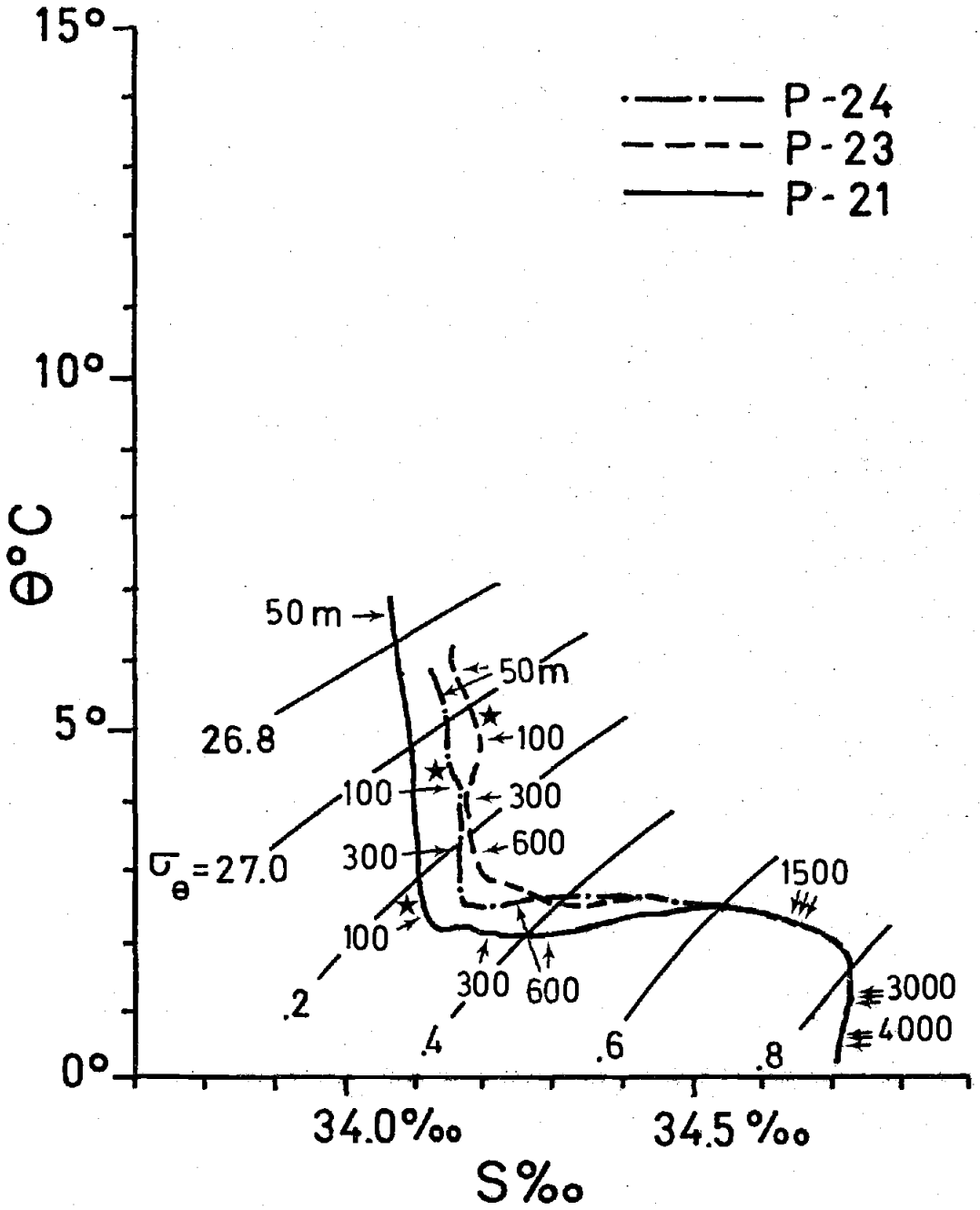

Figure 29. Representative stations showing Structure Type IV from the PIQUERO (P) 1969 Expedition. Stars indicate depth of the base of the seasonal thermocline.

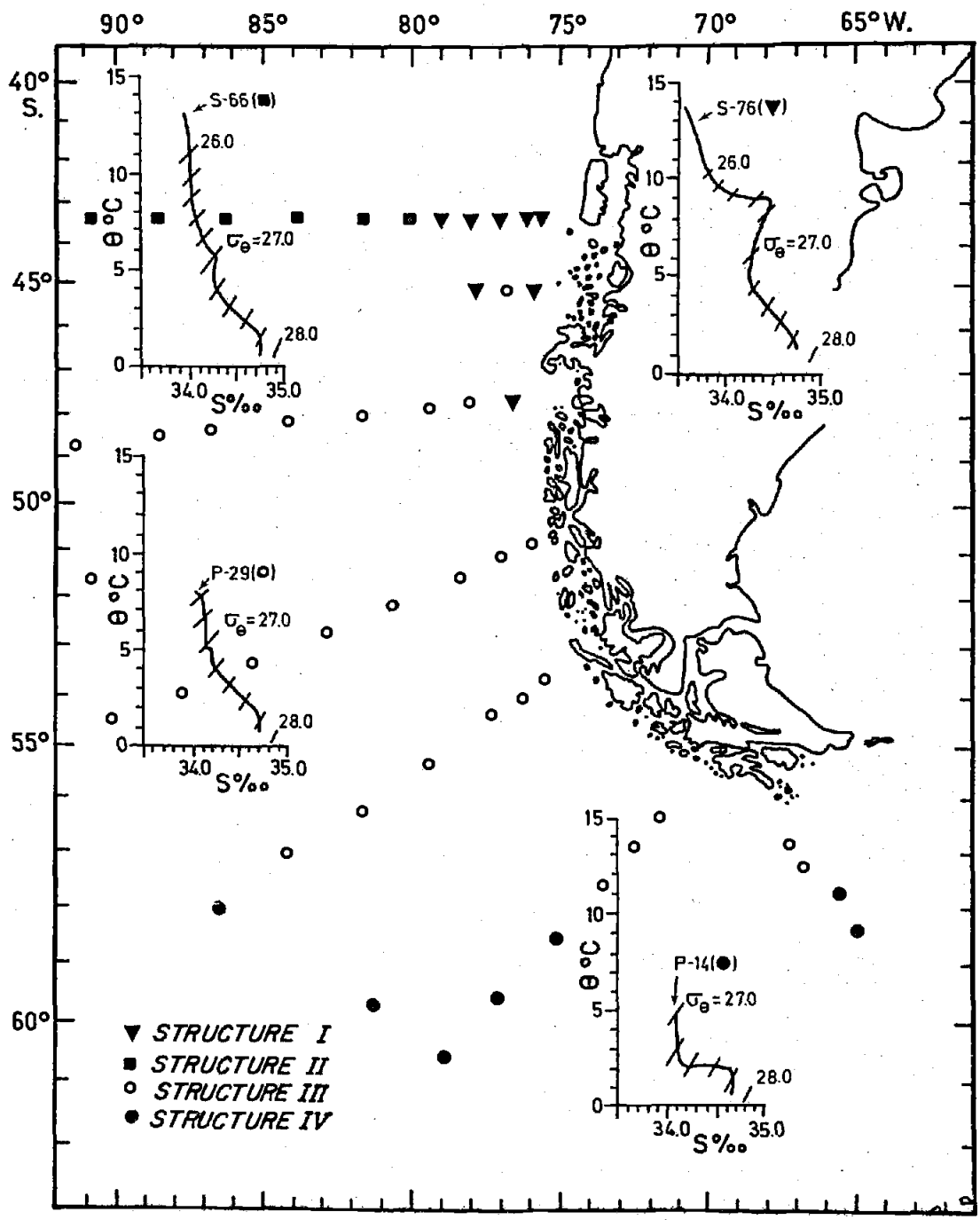

Figure 30. Distribution of θ-S structure types north of the Polar Front Zone for the SCORPIO 1967 and PIQUERO 1969 stations in the study area.

Some coastal stations are under the influence of the adjacent estuarine system, showing low surface salinity values (Figure 4). This low surface salinity produces a shallow halocline, which has not been considered in the water mass structure analysis.

Mamayev (1973) has performed an analysis of T-S structures of the upper 2500 m in the Eastern South Pacific based on data taken by the R/V Professor DERYUGIN in 1968. His work included the area between 30° and 53° S, 200 nautical miles off Chile and 110° W. Therefore, there is a region where Mamayev's (1973) study overlaps this study. For this common region, Mamayev (1973) described a T-S structure named Subantarctic type I, which corresponds to structure III of this work. He also described a transient type V, 100 - 150 km farther to the NW of the study area. This transient type V, structure II in this work, is still present in the study area even though its WPSSW component is very weak. Mamayev (1973) showed that the transient type V extended westward as far as 102°W. Farther to the west he described a transient type IV which does not show the maximum and minimum salinity content of the WPSSW and AAIW, showing instead a nearly homogeneous salinity layer between 300 and 1000 m. The superposition of θ-S diagrams from SCORPIO (Figure 18) shows that structure II [equivalent to Mamayev's (1973) transient type V] extends much farther to the west than 102° W. However, these diagrams do not show a nearly homogeneous salinity layer at subsurface and intermediate levels as shown by Mamayev's (1973) transient type IV west of 102° W. Structure II should be considered as extending westward to the point where the surface salinity minimum can not be considered as such.

Another study which includes the study region and which considers the water mass structure of the water column is that of Johnson (1972). He described two structures with three water masses in each. Those structures are the basis of his three point vertical mixing analysis. Neither of Johnson's (1972) structures includes the ESSW, even though he recognized the presence of the Peru-Chile Undercurrent and two of his working stations in this area are from SCORPIO Expedition (S-72 and S-76). Basically, Johnson's (1972) two structures correspond to structure III of this study, where the AABW was not included due to the maximum depth he considered (2500 m).

Since the ESSW has an important role in the upwelling off the central Chilean Coast (Brandhorst, 1971; and Silva, 1973) and its southernmost extension has not been clearly established, the geographic distribution of structure I will be discussed in detail. As can be observed from the water mass structure distribution chart (Figure 30), structure I extends as far south as 48° S with 79° W as its westernmost limit. Its distribution resembles a wedge, with its apex pointing toward the south. South of 50° S the ESSW salinity maximum can not be traced, because it has been completely dissipated due to vertical mixing with the less saline SAAW and AAIW. Toward the west a similar dissipation occurs, nevertheless a slight salinity maximum still persists in some of the remaining stations of sections A and B. This maximum is not a remnant of the ESSW from structure I, but rather it belongs to the WPSSW from structure II as has been discussed before. Station S-72, located at the western boundary of structure I, is a good example of such a situation, because of its slight double salinity maximum at 251 and

399 m (Figure 31). In addition to the differences in depth and density, the upper salinity maximum in S-72 is associated with a minimum in oxygen, while the lower one is not (See Figure 15, S-72 and S-72'). This situation can be interpreted as the result of the interleaving of structures I and II in the same oceanographic station.

From the above discussion it may be seen that the ESSW, carried southward by the Peru-Chile Undercurrent, spreads as far south as 48° S. This result complements that of Wooster and Gilmartin (1961), extending their proposed southernmost limit for the ESSW spreading by about 1000 km.

The distribution of structure II has been limited to the west of section A. Nevertheless, some of the stations in section B classified in structure III, could have been classified in structure II. This is because one structure transforms into another by slow mixing of some of the water mass components; therefore, transient or intermediate structures are often present.

Structure III is the prevailing structure found in the study area. It covers about 75% of the region studied. Structure IV, which includes AAW, is found in the neighborhood of the Polar Front.

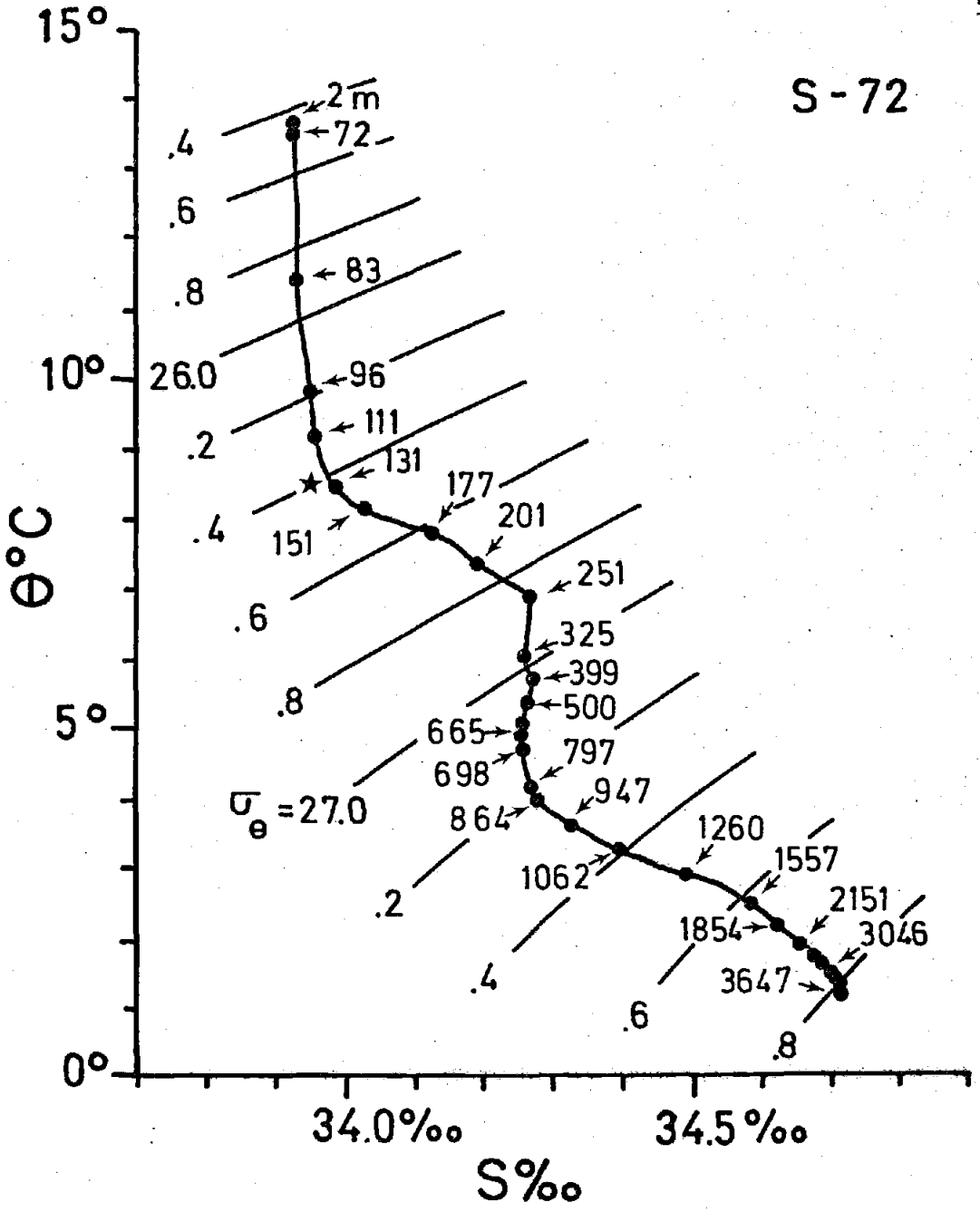

Figure 31. θ-S diagram of the SCORPIO station S-72 showing the presence of two weak subsurface salinity maxima at 251 and 399 m. The star marks the base of the seasonal thermocline.

VI. GEOSTROPHIC CIRCULATION

6.1 General considerations

Since most ocean currents satisfy geostrophic conditions and until recently direct current measurements have been scarce and difficult to obtain, most classical open ocean current studies are based on geostrophy. As it stated in the Introduction, the flow pattern in the study area is known only in its gross features. Therefore, the need exists for a more detailed study.

To improve knowledge of the flow pattern of the study area, this chapter will discuss the geostrophic flow on the sea surface and on the 26.84 and 27.12 isopycnals, all relative to 3000 db. Vertical geostrophic velocity sections relative to 3000 db will be used to complement the isentropic analysis. A short discussion on the θ-S structure relative to the geostrophic circulation will be also used to explain some of the flow features.

6.2 Flow on the sea surface

The sea surface can not be represented by a single isopycnal; therefore, it is not possible to apply isentropic analysis to it. Geostrophic flow at the sea surface must be interpreted from a dynamic height topography map.

The sea surface dynamic topography relative to 3000 db (Figure 32) shows a general flow toward the south in the southern half of the study area. This flow corresponds to the southern branch of the WWD, after its division off South America north of the area of study (Silva and Neshyba, 1977). The coastal part of this poleward flow corresponds to

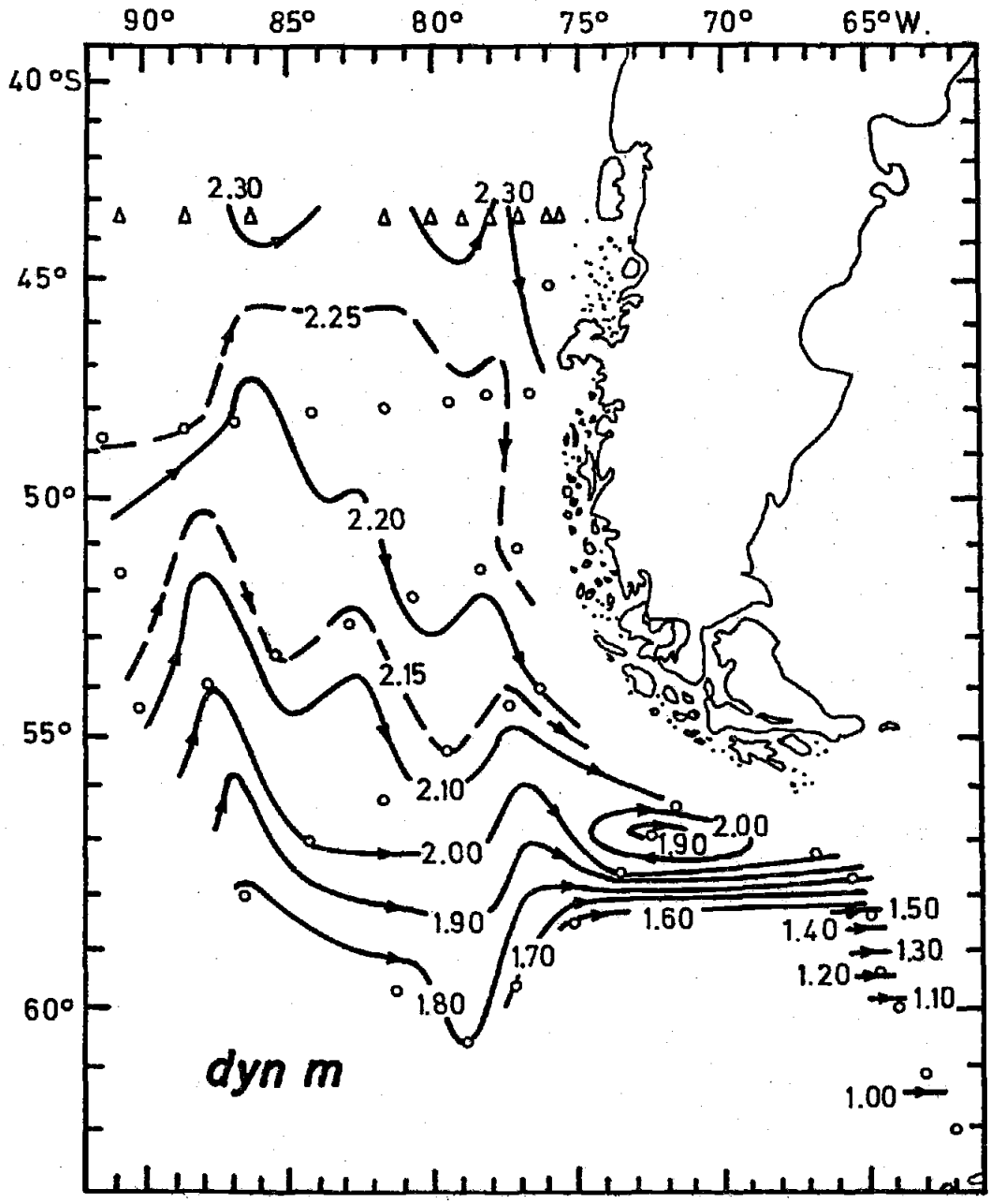

Figure 32. Dynamic topography of the sea surface relative to 3000 db, from SCORPIO (Δ) 1967 and PIQUERO (∘) 1969 Expeditions.

the Cape Horn Current, which also carries southward the less saline and comparatively lower nutrient estuarine water along the coast of Chile.

South of 55° S the general surface flow pattern is toward the East with much larger velocities than those of the northern part. This eastward flow is in agreement with generally recognized Antarctic Circumpolar Circulation in this part of the ocean (Sverdrup et al., 1942; Gordon, 1967; and Gordon and Bye, 1972).

The main geostrophic flow across the Drake Passage is concentrated north of 58° S, with maximum velocities greater than 30 cm/sec. South of 58° S the geostrophic velocity decreases toward the pole which is in agreement with previous reports of Ostapoff (1961), Gordon (1967), and Reid and Nowlin (1971).

6.3 Flow on the 26.84 sigma-θ surface (ESSW)

The thermosteric anomaly at the core of the ESSW has been shown by Wooster and Gilmartin (1961) to decrease from 160 cl/ton (sigma-t = 26.44) off Peru, to less than 140 cl/ton (sigma-t = 26.65) off central Chile. They suggested that this density increase arises from mixing with water of lower temperature.

If one analyzes the meridional sections of salinity off the Peru and Chile coast, prepared by Gunther (1936) or Wooster and Gilmartin (1961) or Silva and Konow (1975), it can be observed that the ESSW core diminishes in salinity and deepens as it moves southward. This could be explained in terms of a more active erosion of the ESSW core due to a stronger vertical mixing at its upper boundary (with SAAW), than at its lower boundary (with AAIW). The reason for this difference in upper and lower boundary mixing rate can be the relatively higher shear

in the former compared to that in the latter (see for example, Figure 35).

Because of the change in density of the ESSW core as it moves southward along the Chilean Coast, this core can not be represented by a single isopycnal, but by a family of them. The isopycnal of 26.84 represents the mean potential density where the ESSW core is located off southern Chile.

Geostrophic flow on this isopycnal (Figure 33) can be divided into two parts as was done with the sea surface flow. The southern part, south of 50° S, has a relatively fast geostrophic flow pointing toward the east. This is the continuation at subsurface levels of the Antarctic Circumpolar Current. In the northern part, mainly north of 50° S, the geostrophic flow is significantly slower. The eastern portion of the northern area shows a southward flow, while the western portion the general flow is to the north.

The poleward flow close to the coast of Chile can be interpreted as a remnant of the Peru-Chile Undercurrent. Nevertheless, a more rigorous explanation of the origin of this poleward flow can be based on an acceleration potential chart which includes a much larger extension to the north of the study area. Reid's (1965) acceleration potential relative to 1000 db on the 125 cl/ton isanostere, which is close to 26.84 sigma-θ, shows a poleward flow off Peru and Chile which is not defined south of 36° S. A farther southward extension of this poleward flow may be reasonable, since the available data at that time in this region was very scarce. It is reasonable to connect the poleward flow from Reid's (1965) chart with this study area, thus inferring that the

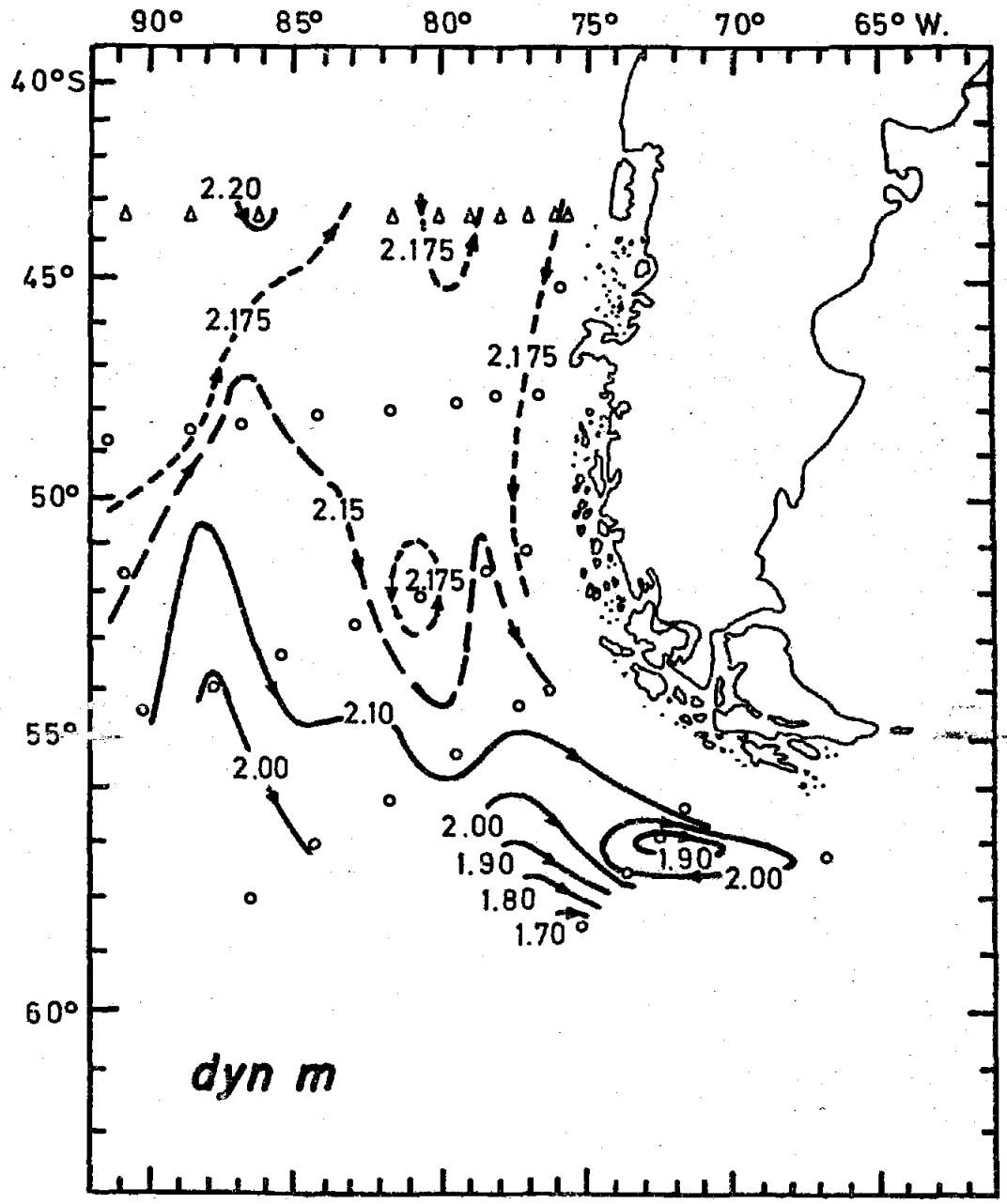

Figure 33. Acceleration potential on the 26.84 sigma-θ surface relative to 3000 db, from SCORPIO (Δ) 1967 and PIQUERO (◦) 1969 Expeditions.

Peru-Chile Undercurrent is present at this high latitude. Nevertheless, further evidence is required and will be presented later.

6.4 Flow on the 27.12 sigma-θ surface (AAIW)

The general circulation on the 27.12 isopycnal (Figure 34) is very similar to that present on the 26.84 sigma-θ surface. Again, main characteristics are the relatively slow flow in the northern portion of the area and a much faster flow in the southern part.

North of 55° S the flow direction is not very well defined, but a northward movement can be accepted as the general trend. Reid's (1965) acceleration potential map on 80 cl/ton isanostere (sigma-θ = 27.29), which he selected as the AAIW representative, does not show any detail in this area probably due to the scarcity of data. The acceleration potential map on the 27.10 sigma-t surface prepared by Johnson (1972) shows the flow in this region, north of 55° S, with a general northward direction. Nevertheless, the data used by Johnson (1972) for this region is also sparse (8 stations located mainly on the periphery of the study area).

South of 55° S the flow is well defined toward the east, with relatively high velocites. Again, this flow corresponds to the presence of the Antarctic Circumpolar Current at this level.

Since the flow on the 27.12 isopycnal in the vicinity of the Polar Front is directed mainly toward the east, the AAIW formed in the PIQUERO-SCORPIO area will be carried eastward. Therefore, this area will act mainly as a source region for Pacific AAIW to the Atlantic Ocean.

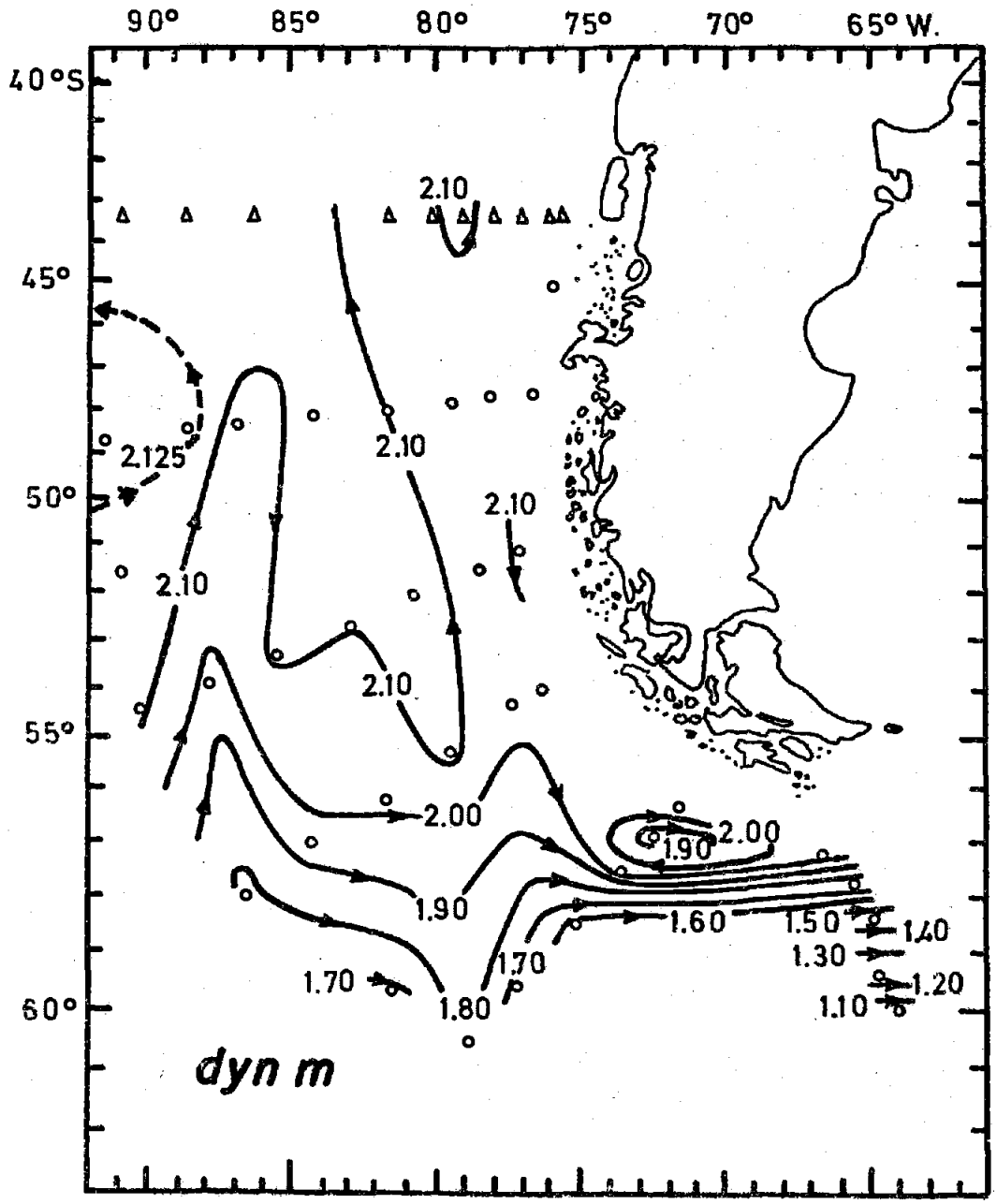

Figure 34. Acceleration potential on the 27.12 sigma-θ surface relative to 3000 db, from SCORPIO (Δ) 1967 and PIQUERO (∘) 1969 Expeditions.

6.5 Flow across vertical sections

Vertical sections of geostrophic velocity relative to 3000 db are shown in Figures 35 to 40. These vertical sections complement the information given by the horizontal flow on selected isentropic surfaces, showing the geostrophic velocity in the water column across sections perpendicular to the coast (sections A to F in Figure 1).

6.5.1 The coastal flow

The coastal subsurface flow associated with the ESSW on the charts of acceleration potential on the 26.84 sigma-θ extends as far as 150 km off the coast at section A (43° S) (Figure 35). The flow shows a maximum of 5.9 cm/sec at 250 m depth, which is also the depth at which the salinity maximum of the ESSW is found.

In section B (48° S) (Figure 36), the coastal flow shows neither a subsurface maximum nor a decrease in the velocity shear in the subsurface layer associated with the ESSW. Nevertheless, the ESSW salinity maximum is found at station P-48 (see Figure 26) at a depth of 252 m. The maximum velocity of 4.0 cm/sec occurs at the surface at a distance of 140 km offshore; the poleward flow extends to about 400 km offshore.

In section C (51° S) (Figure 37), the maximum velocity of the coastal poleward flow is again found at the surface (30 m depth) but at a value of 6.7 cm/sec. In this section, the flow extends some 300 km offshore. From sections C through F the general trend of the coastal flow is to increase in velocity, varying in offshore extent to a maximum of about 560 km at section F.

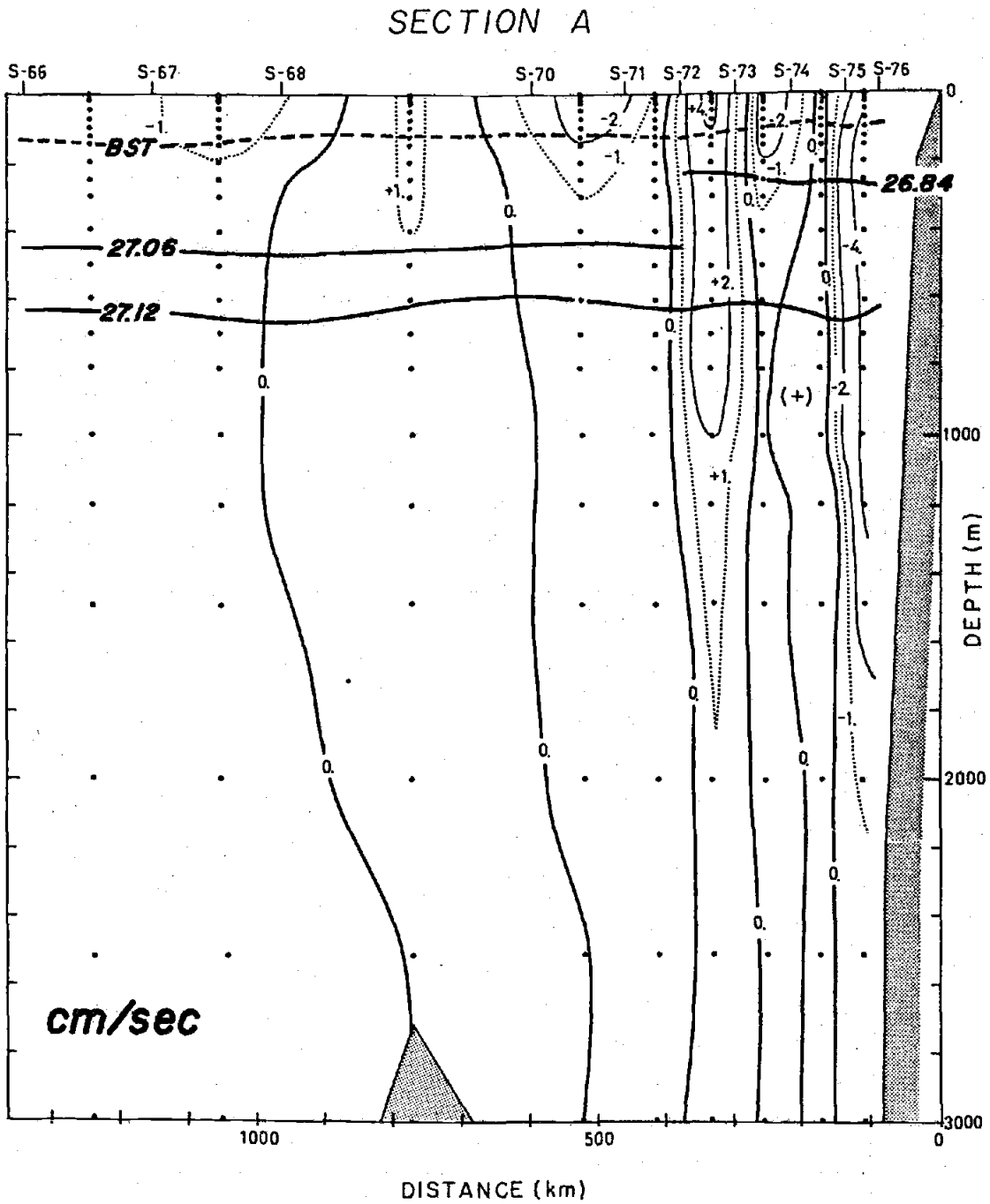

Figure 35. Geostrophic velocity relative to 3000 db at section A, from SCORPIO 1967 Expedition. Positive values indicate northward flow; negative values indicate southward flow. Solid horizontal lines represent the potential density at which the cores of ESSW (26.84), WPSSW (27.06) and AAIW (27.12) are found; dashed line is the base of the seasonal thermocline (BST).

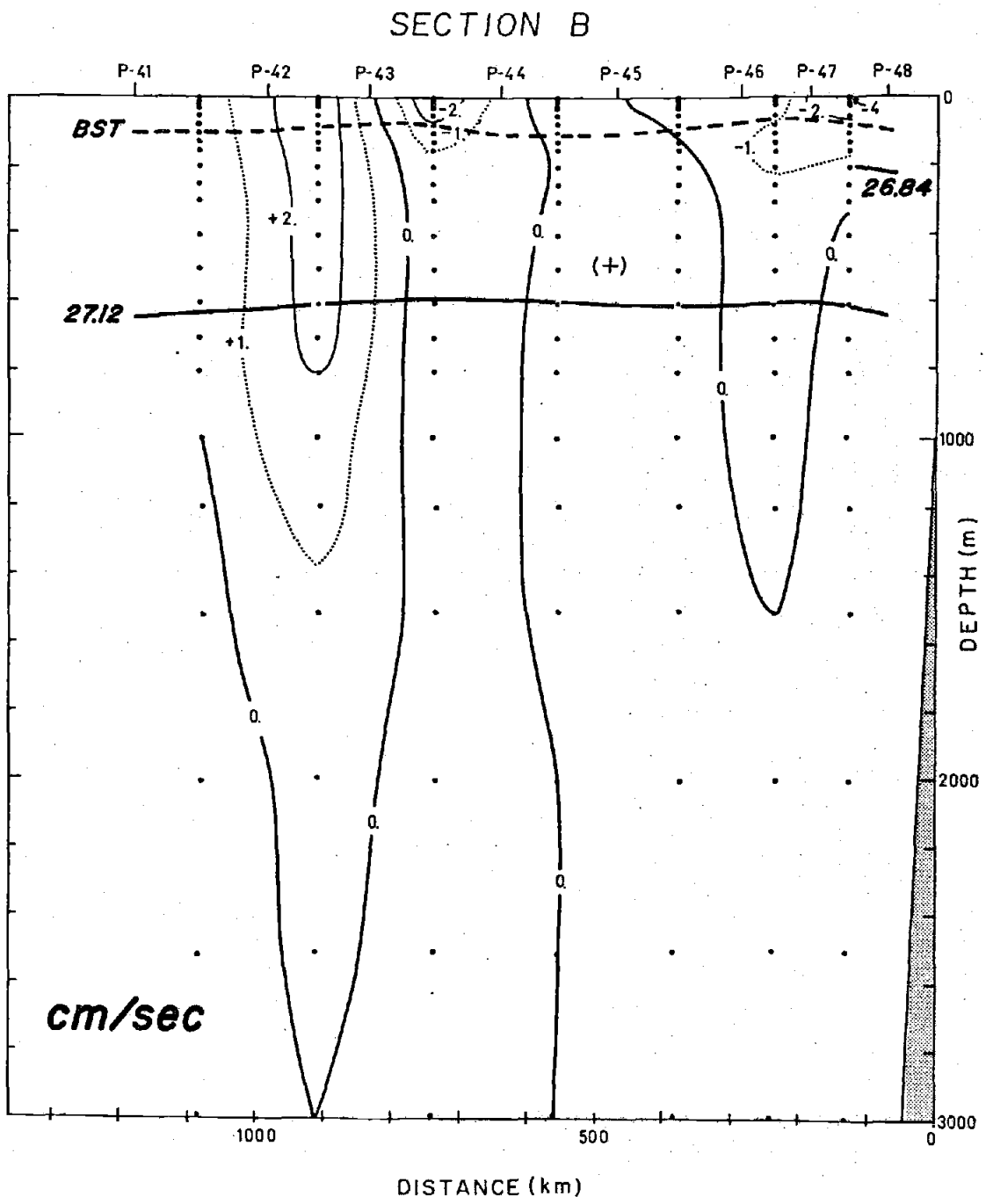

Figure 36. Geostrophic velocity relative to 3000 db at section B, from PIQUERO 1969 Expedition. Positive values indicate northward flow; negative values indicate southward flow. Solid horizontal lines represent the potential density at which the cores of ESSW (26.84) and AAIW (27.12) are found; dashed line is the base of the seasonal thermocline (BST).

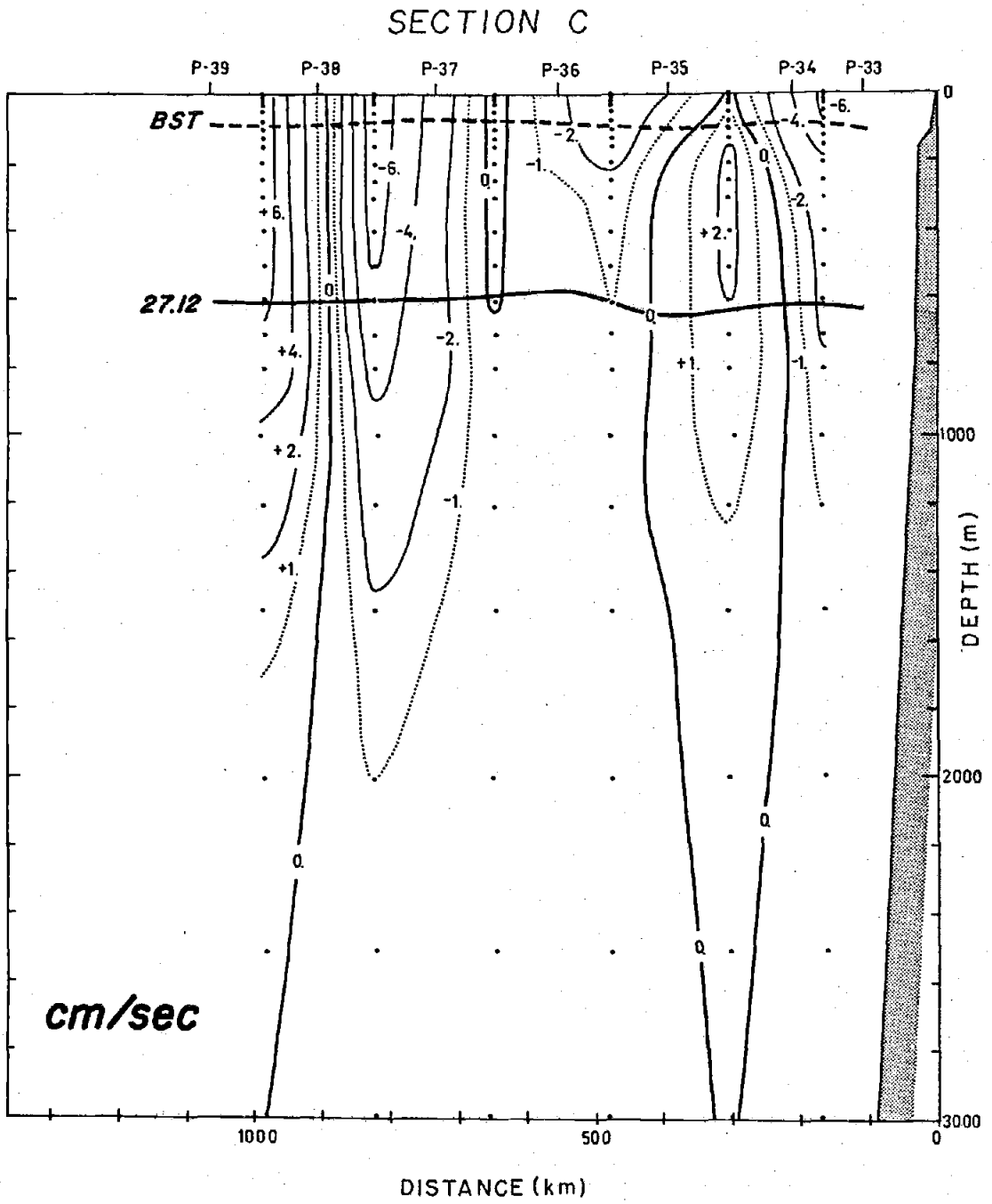

Figure 37. Geostrophic velocity relative to 3000 db at section C, from PIQUERO 1969 Expedition. Positive values indicate northward flow; negative values indicate southward flow. Solid horizontal lines represent the potential density at which the core of AAIW (27.12) is found; dashed line is the base of the seasonal thermocline (BST).

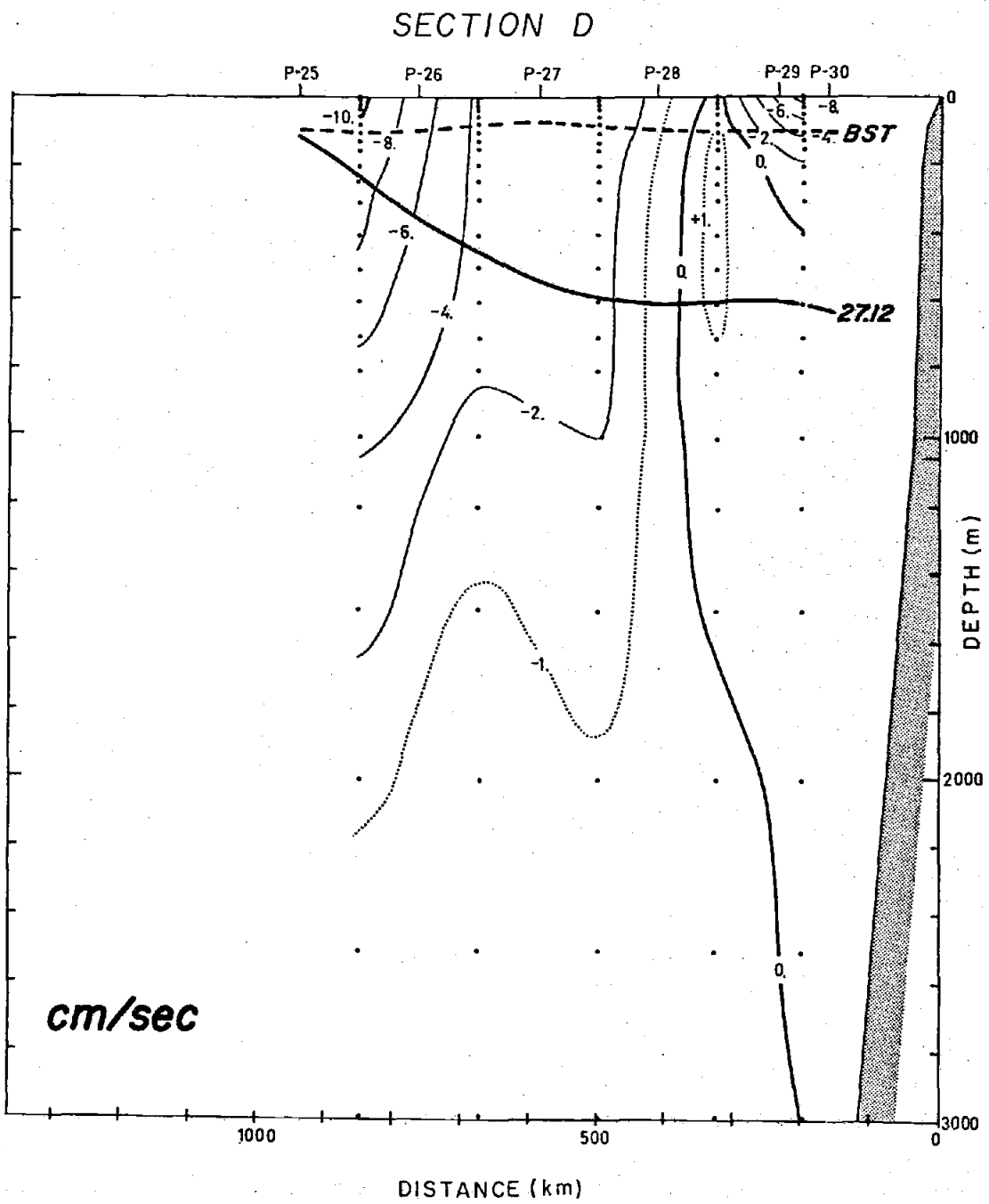

Figure 38. Geostrophic velocity relative to 3000 db at section D, from PIQUERO 1969 Expedition. Positive values indicate northward flow; negative values indicate southward flow. Solid horizontal lines represent the potential density at which the cores of ESSW (26.84) and AAIW (27.12) are found; dashed line is the base of the seasonal thermocline (BST).

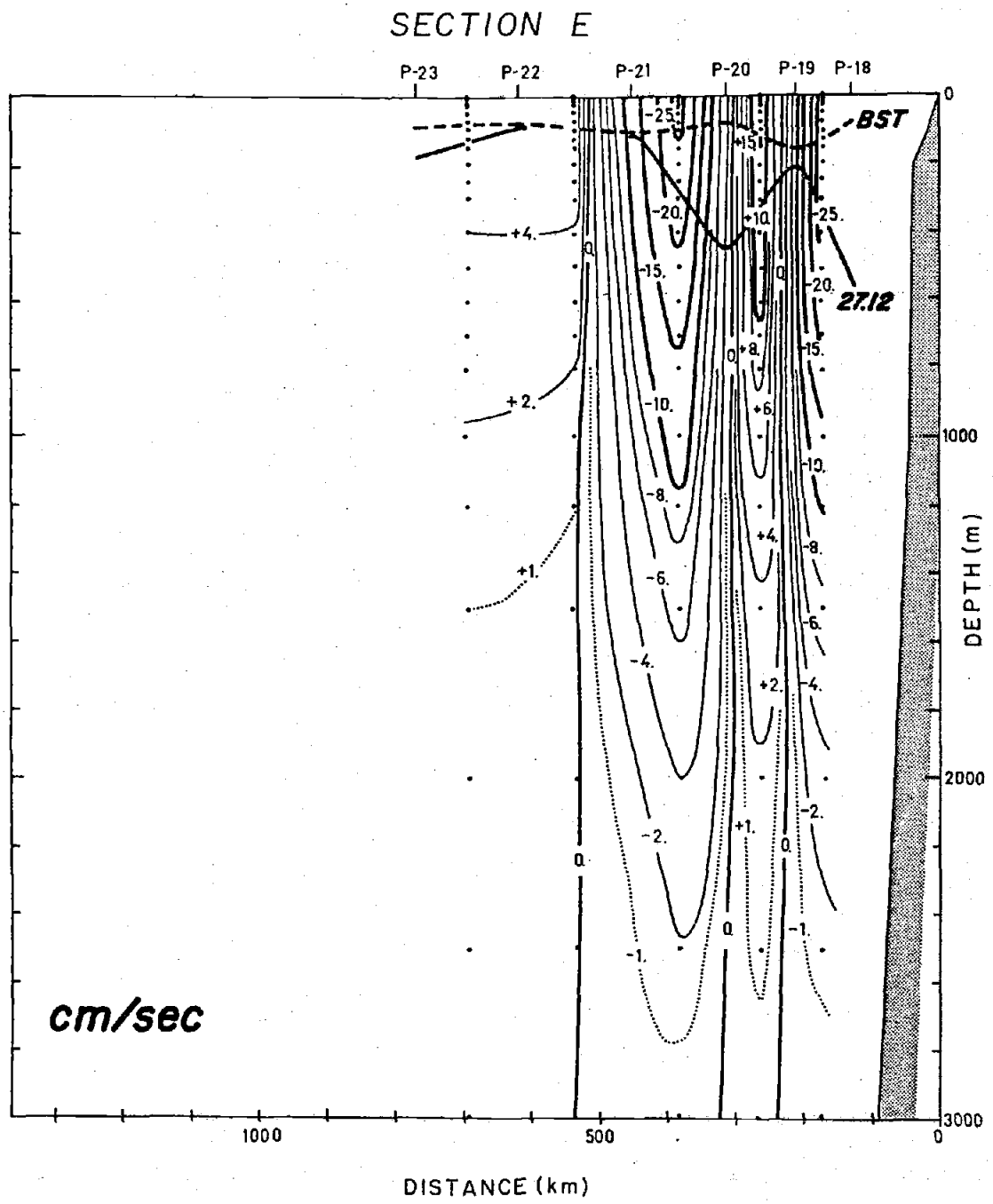

Figure 39. Geostrophic velocity relative to 3000 db at section E, from PIQUERO 1969 Expedition. Positive values indicate eastward flow; negative values indicate westward flow. Solid horizontal lines represent the potential density at which the cores of ESSW (26.84) and AAIW (27.12) are found; dashed line is the base of the seasonal thermocline (BST).

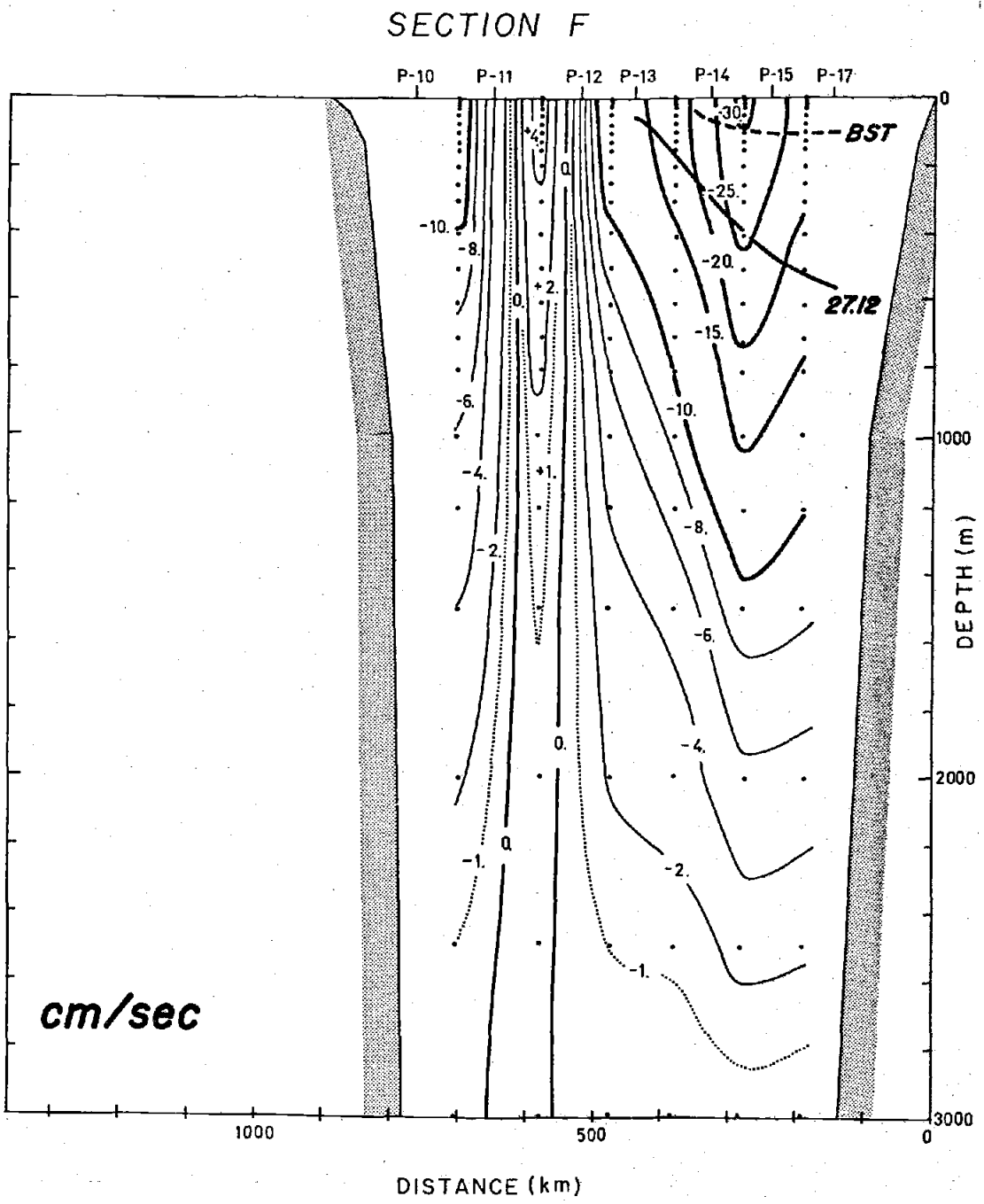

Figure 40. Geostrophic velocity relative to 3000 db at section F, from PIQUERO 1969 Expedition. Positive values indicate eastward flow; negative values indicate westward flow. Solid horizontal lines represent the potential density at which the cores of ESSW (26.84) and AAIW (27.12) are found; dashed line is the base of the seasonal thermocline (BST).

6.5.2 Identification of the subsurface coastal flow with the Peru-Chile Undercurrent

A central theme of this study is the question of the southernmost extension of the Peru-Chile Undercurrent. In this sense, the coastal flow described in the previous section may now be correlated with previously published data on the Undercurrent along the coasts of Peru and Chile as follows:

- From 6° to 24° S, STEP I Expedition (Wooster and Gilmartin, 1961); reference level 1000 db.
- From 24° to 28° S, MARCHILE VIII Expedition (Sievers and Silva, 1975); reference level 1000 db.
- At 35° S, geostrophic flow computed from stations 83 and 84 of section 35° S of the SCORPIO Expedition (S.I.O., 1969); reference level 2000 db.
- From 43° S to about 57° S, geostrophic flow computed for the study area using SCORPIO and PIQUERO data; reference level 3000 db.

Results from these expeditions and sources are combined in Figure 41. Arrows show the approximate position of the core of the Peru-Chile Undercurrent from 6° S to the northern limit of the study area using data from the first three of these sources.

Within the study area, the Undercurrent is clearly delineated through section A (43° S), as discussed in the previous section. At latitude 45° S, the PIQUERO Expedition yields a short, near coastal section consisting of three stations, P-49 through P-51 (see Figure 1). Geostrophic flow relative to 2500 db has been computed for this set of stations, and profiles are shown in Figure 42. The profile for flow between P-49 and P-50 shows two maxima above 300 m: the first occurs at the surface at a value of 5.7 cm/sec; a second, less pronounced maximum of 2.9 cm/sec occurs at 200 m. The latter is located within the subsur-

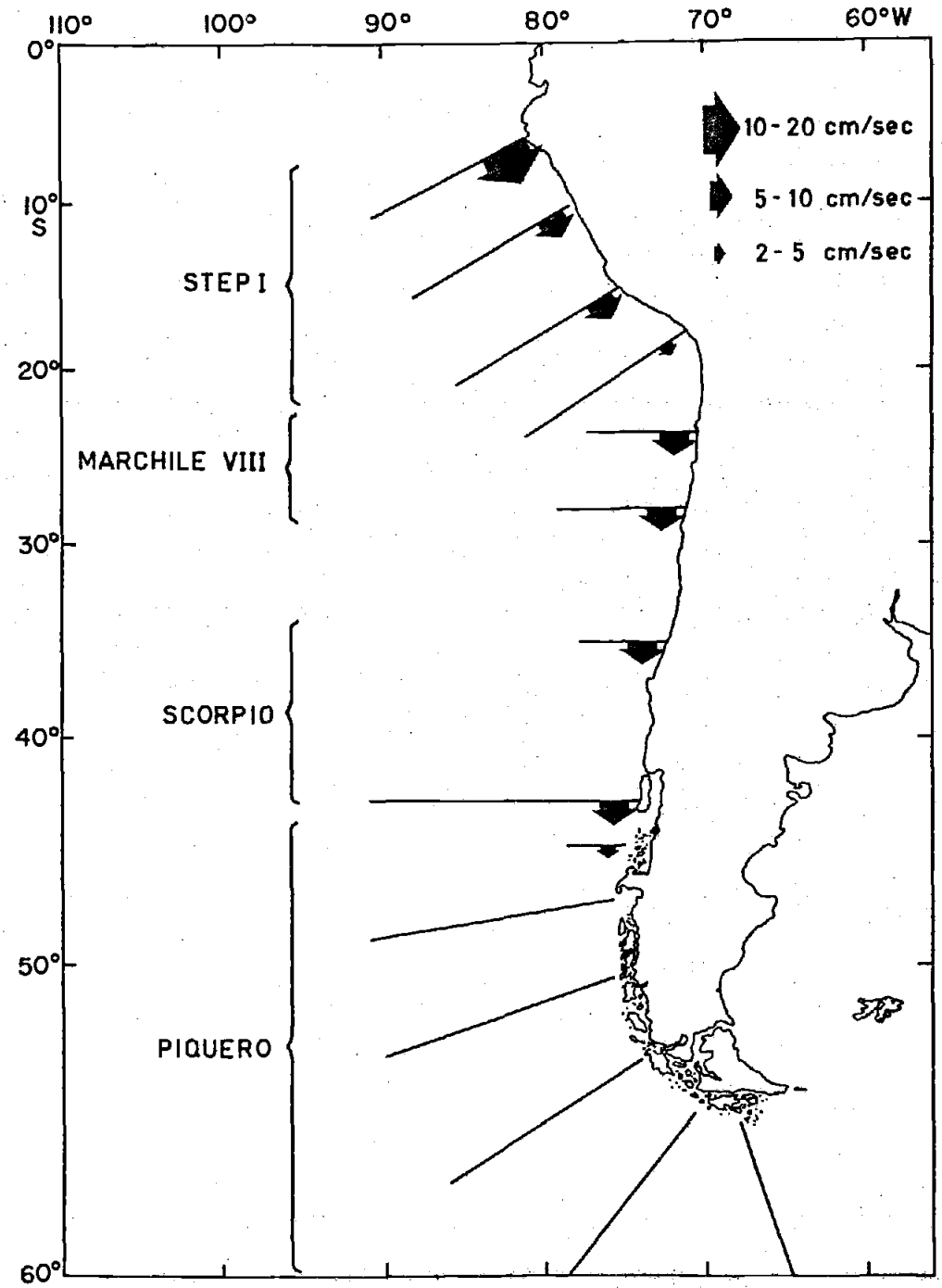

Figure 41. Composite of oceanographic sections showing approximate positions and geostrophic velocities of the core of the Peru-Chile Undercurrent based on STEP I 1960 (Wooster and Gilmartin, 1961), MARCHILE VIII 1972 (Sievers and Silva, 1975), SCORPIO 1967 (this study) and PIQUERO 1969 (this study) Expeditions. Respective reference levels are given in the text.

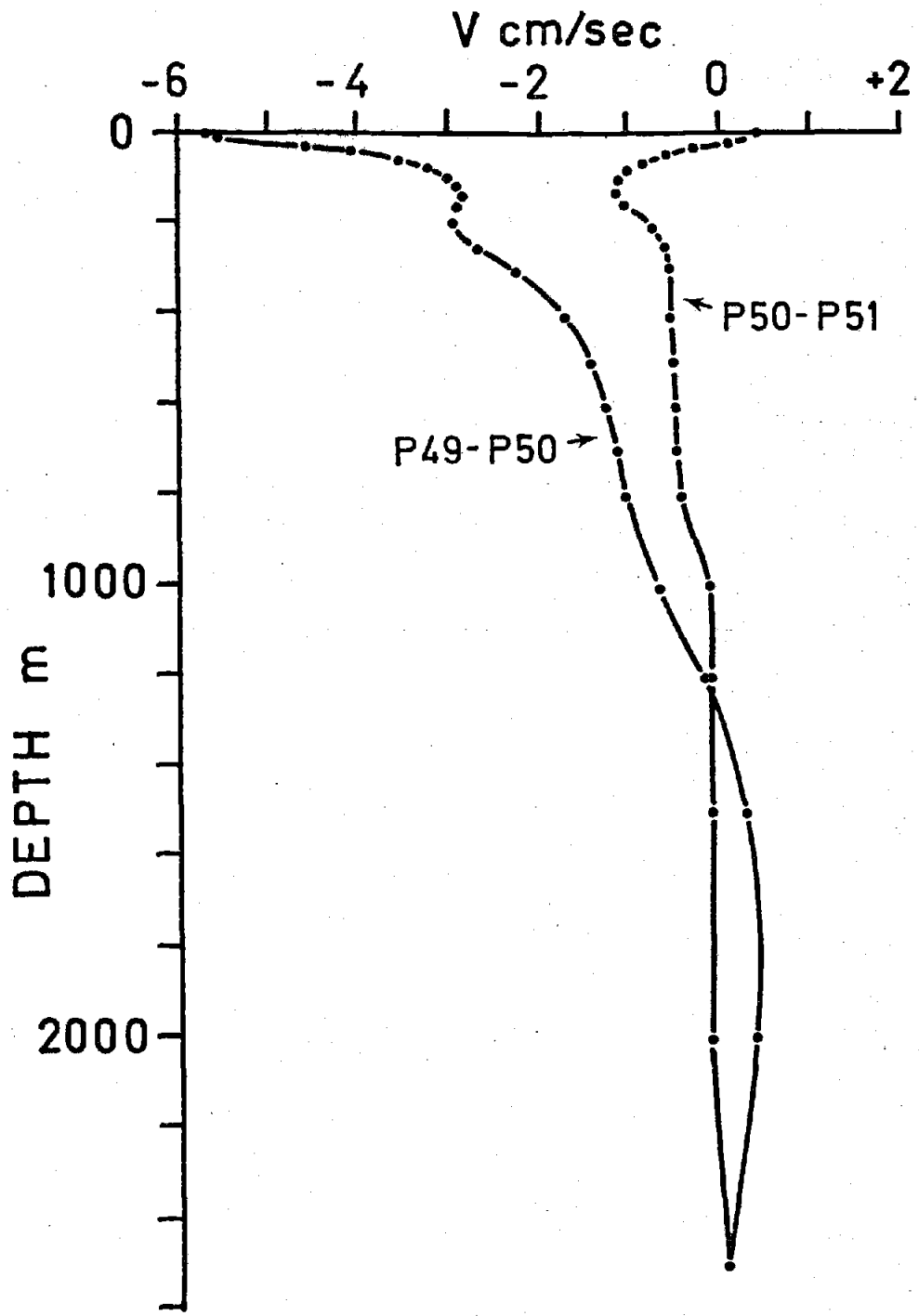

Figure 42. Geostrophic velocity profile relative to 2500 db for PIQUERO 1969 stations pairs P-49 - P-50 and P-50 - P-51. Positive values indicate northward flow, negative values indicate southward flow.

face salinity maximum of the ESSW. A similar subsurface maximum is found between stations P-50 and P-51. It is, therefore, reasonable to conclude that the Undercurrent still exists at this latitude, 45° S.

At 48° S, section B, the subsurface salinity maximum, oxygen minimum, and nutrient maximum which are characteristic of ESSW water are present at about 250 m depth. However, the geostrophic velocity regime (Figure 36) does not show a subsurface velocity maximum. At 51° S, section C, remnants of the low oxygen and high phosphate and nitrate still persist, but salinity and silicate do not show a maximum in the vertical distribution. Using the criteria of coincident subsurface velocity maxima and subsurface ESSW characteristics, one must conclude that the Peru-Chile Undercurrent loses its identity around 48° S. However, subsurface flow does exist at section B, as well as at sections further south, but can not be uniquely identified with the Peru-Chile Undercurrent characteristics.

The southernmost extension of the Peru-Chile Undercurrent is not absolutely established in this study. Further work must be done to answer some questions related to the Undercurrent in this area, such as: Does this southern extension undergo seasonal fluctuations? Does the latitude of the WWD impingement affect its southern and/or western extension? If the WWD impingement off Chile is under the influence of seasonal variations latitudinally, how will this affect the Undercurrent?

6.5.3 Geostrophic flow south of 48° S

The increase in the flow velocity in the surface coastal poleward flow or Cape Horn Current, may be the result of influx of runoff water

from the adjacent coast, elevating the sea level height and hence the flow velocity. The piling up effect due to the pressure exerted by the WWD against the coast may be important. The relatively high velocities present in sections E and F, is the result of the constriction effect of the Drake Passage to the zonal flow (Gordon and Bye, 1972).

The flow across the Drake Passage (Figure 40) follows the pattern described by Reid and Nowlin (1971), as would be expected since they also used PIQUERO data. Nevertheless, there is a difference between their geostrophic velocity values at the station pair P-15 to P-17 compared to those shown in section F (Figure 40). Even though Reid and Nowlin's (1971) velocity values at this station pair are referred to 3400 db, this can not account for a sea surface velocity difference of 13 cm/sec between the two studies. This difference seems to be the result of a computational error, since their surface value of 36.1 cm/sec could not be obtained by this writer from the corresponding station data set. As a result, the fastest geostrophic velocities are, in fact, located between the station P-14 and P-15, and not between P-15 and P-17 as shown by Reid and Nowlin (1961).

Direct current measurements near the bottom in the Drake Passage were reported by Reid and Nowlin (1971) to show mean daily speeds ranging from 0.5 to 14.7 cm/sec. These relatively high speeds at the bottom of the passage are further evidence of the absence of any given level of no motion for geostrophic computations in this area.

6.6 Geostrophic circulation and water mass structure

Since the geostrophic circulation is causally linked to the density field distribution, this type of circulation is directly related to the

θ-S structure present in a given area. At times, circulation features can be more easily explained in terms of θ-S or water mass structure.

The eastward flow south of 57° S (Figures 32 to 34), is dominated by structure IV (Figure 30). This eastward flow shows a sharp southward bend at station P-23. A detailed analysis of the θ-S structure present at P-23 indicates a transient structure between structures III and IV. This means that the water column in this station still shows remnants of structure III, even though it can be classified as structure IV. Therefore, remnants of characteristics of a northern station are present in the south, giving as a result the observed bend in the flow lines.

The clockwise eddy at station P-19 (Figures 32 and 34) seems also to be produced by a transient structure between III and IV (Figure 43). In this station, the θ-S structure between 714 and 1535 m resembles more closely structure IV than III. This could be the result of the presence of water which contains a major fraction of cold AAW in its composition. Joyce and Patterson (1977), in describing a clockwise ring formation at the Polar Front Zone, stated that: "within the Polar Front Zone the minimum" (temperature) "deepens abruptly and erodes splitting into multiple extrema of interleaving Antarctic/Subantarctic waters." Since the waters south of the Polar Front Zone are associated with a comparatively lower dynamic height than that of those to the north, the presence of AAW north of the Polar Front Zone will produce a lesser dynamic height in comparison to that of surrounding waters. Dynamic topography charts of 0/500, 500/1000, 1000/2000 and 2000/3000 db (not shown), indicate the presence of this eddy at all these levels.

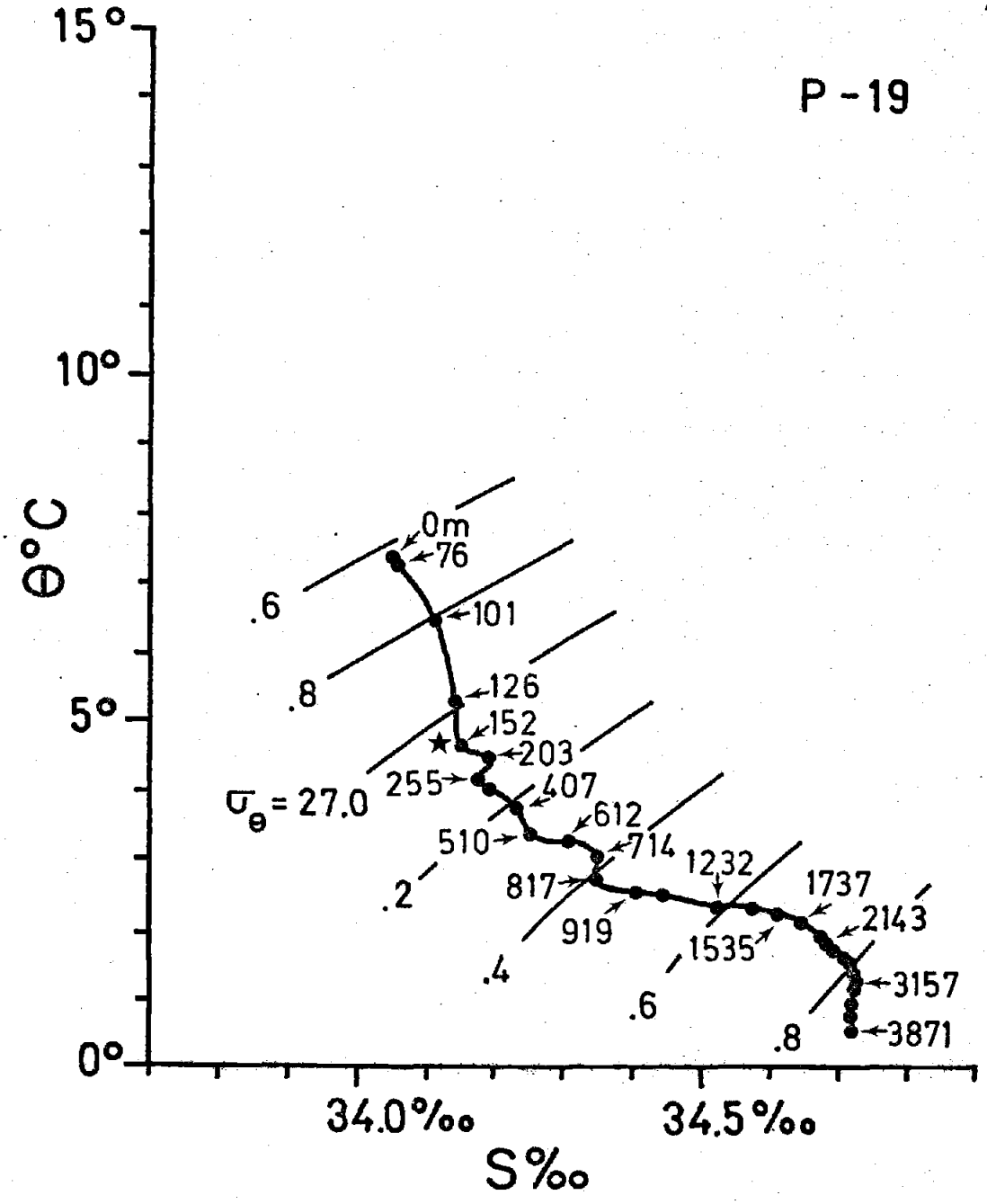

Figure 43. θ-S diagram of station P-19. The segment between 714 and 1535 m resembles a structure type IV, while the whole structure corresponds to structure type III. Star marks the base of the seasonal thermocline.

The highest dynamic difference between adjacent stations (≈ 10 dyn cm) is found in the 500/100 and 1000/2000 db zones which indicates that the segment 500 to 2000 m of the water column is the main contribution to the observed lower relative dynamic height of P-19.

On the other hand, counterclockwise flow east of the Drake Passage has been described by Gordon et al. (1977). They associated this flow with the presence of SAAW within the Polar Front Zone.

The poleward flow on the 26.84 isopycnal (Figure 33) is responsible for the presence of structure I off southern Chile. Nevertheless, this structure is also present westward of the core of this southward flow. This situation might be the result of horizontal diffusion rather than advection.

There is no evidence inside the study area of any relatively important flow carrying the WPSSW component of structure II eastward. Thus, the presence of structure II in this area may be interpreted as mainly due to a diffusive phenomenon. Nevertheless, Reid's (1965) acceleration potential maps on the 125 and 80 cl/ton isanosteres, show a general eastward flow between 40° and 50° S. This flow, which weakens eastward and turns northward around 90° S off Chile, may be responsible for the presence of structure II in this area.

VII. CONCLUDING REMARKS

To summarize this detailed analysis of the water mass structure and geostrophic circulation of the study area between 43° and 63° S, 91° W to the Chilean Coast, some concluding remarks can be made:

1. Previous studies of the high salinity, low oxygen poleward flow (Gunther, 1936; Wooster and Gilmartin, 1961) have placed its southernmost extension at 41° S. This study demonstrates clearly that this limit can be extended to at least as far as 48° S. South of this latitude the subsurface flow can not be definitely associated with the ESSW characteristics of the Peru-Chile Undercurrent.

Further study must be performed to establish whether or not the Peru-Chile Undercurrent's southernmost boundary is subject to seasonal variations. Questions to be answered by future work in the area are: (1) How does the latitude at which the WWD impinges the Chilean Coast affect the southern and/or western extension of the Peru-Chile Undercurrent? and (2) How does the probable seasonal fluctuation in the latitude of impingement of the WWD affect these same factors?

2. The presence of the WPSSW is proposed in this work as water carried from the extreme Southwestern Pacific Ocean into the study area below the surface low salinity water off southern Chile. This water mass is characterized by a subsurface salinity maximum, not associated with an oxygen minimum as is the ESSW. Further work has to be performed to establish its nutrient characteristics as well as its spatial distribution.

3. The low phosphate and nitrate contents of the surface coastal waters off southern Chile, seem to have their origins in the mixture of

ocean waters with estuarine waters of comparatively less rich nutrient content. Two point mixing explains around 60 - 70% of the nutrient variability of the waters in the study area where the salinity ranges between 33 - 34°/$_{oo}$. Biological and/or chemical processes may also be important causes of the relatively low nutrient concentrations of these coastal waters. More interdisciplinary work must be carried out in order to explain this feature.

4. The presence of seven water masses in the region of study were established from the θ-S diagrams below the seasonal thermocline: Subantarctic Water, Antarctic Water, Equatorial Subsurface Water, Western Pacific Subsurface Water, Antarctic Intermediate Water, Pacific Deep Water and Bottom Water.

5. Geostrophic flow in the study area can be divided in general into two regions. North of 55° S, where the circulation is relatively slow, with its eastern boundary flow toward the south along the Chilean Coast. South of 55° S, the circulation is much faster than in the northern portion. The flow has an eastward direction with high velocities characteristic of the Antarctic Circumpolar Current in this region.

BIBLIOGRAPHY

Brandhorst, W. 1971. Condiciones oceanograficas estivales frente a la costa de Chile. Rev. Biol. Mar., Valparaiso, 14(3): 45-84.

Cabrera-Muro, H. 1977. Precise North-South oceanographic transect in the Pacific Ocean. Master's Thesis. Corvallis, Oregon State University. 74 pp.

Callahan, J.E. 1972. The structure and circulation of the Deep Water in the Antarctic. Deep Sea Res., 19: 563-575.

CCS HUDSON. 1970. Data report of HUDSON-70 Expedition (MEDS Ref: 1810-69050). Marine Environment Data Service. Department of the Environment. Ottawa, Canada.

Defant, A. 1961. Physical Oceanography Vol. I. Pergamon Press, London. 285 pp.

Gordon, A.L. 1966. Potential temperature, oxygen and circulation of bottom water in the Southern Ocean. Deep Sea Res., 13: 1125-1138.

Gordon, A.L. 1967. Geostrophic transport through the Drake Passage. Science, 156: 1732-1734.

Gordon, A.L. and J.A.T. Bye. 1972. Surface dynamic topography of Antarctic Waters. J. Geophys. Res., 77(30): 5993-5999.

Gordon, A.L., D.T. Georgi and H.W. Taylor. 1977. Antarctic Polar Front Zone in the Western Scotia Sea - Summer 1975. J. Phys. Oceanogr., 7(3): 309-328.

Gunther, E.R. 1936. A report on the oceanographical investigations in the Peru coastal current. Discovery Rep., 13: 107-276.

Helland-Hansen, B. 1916. Nogen hydrografiske metoder. Skand. Naturforsker mote, 16: 357-359.

Johnson, R.E. 1972. Antarctic Intermediate Water in the South Pacific Ocean. Ph.D. Thesis. Corvallis, Oregon State University. 170 pp.

Joyce, T.M. and S.L. Patterson. 1977. Cyclonic ring formation at the Polar Front in the Drake Passage. Nature, 265: 131-133.

Mamayev, O.I. 1973. Water masses of the Southeast Pacific Ocean. In: Oceanography of the South Pacific 1972, comp. R. Fraser. New Zealand National Commission for UNESCO, Wellington: 1973., pp. 71-79.

Montgomery, R.B. 1937. A suggested method for representing gradient flow in isentropic surfaces. Bull. Amer. Meteor. Soc., 18: 210-212.

Neumann, G. 1968. Ocean currents. Elsevier Scientific Publishing Co. Amsterdam. 352 pp.

Ostapoff, F. 1961. On the mass transport through the Drake Passage. J. Geophys. Res., 65(9): 2861-2868.

Pickard, G.L. 1971. Some physical oceanographic features of inlets of Chile. J. Fish. Res. Bd. Canada, 28: 1077-1106.

Pickard, G.L. 1973. Water structure in Chilean fjords. In: Oceanography of the South Pacific 1972, comp. R. Fraser. New Zealand National Commission for UNESCO, Wellington: 1973. pp. 95-104.

Reid, J.L., Jr. 1961. On the geostrophic flow at the surface of the Pacific Ocean with respect to the 1,000 decibar surface. Tellus, 13(4): 489-502.

Reid, J.L., Jr. 1965. Intermediate waters of the Pacific Ocean. Johns Hopkins Oceanogr. Stud., No. 2, 85 pp.

Reid, J.L. 1969. Sea-surface temperature, salinity and density of the Pacific Ocean in summer and winter. Deep Sea Res., Supp. to Vol. 16: 215-224.

Reid, J.L. 1973a. Transpacific hydrographic sections at Lats. 43° S and 28° S: the SCORPIO Expedition - III. Upper water and a note on southward flow at mid-depth. Deep Sea Res., 20: 39-49.

Reid, J.L. 1973b. The shallow salinity minima of the Pacific Ocean. Deep Sea Res., 20: 51-68.

Reid, J.L. and W.D. Nowlin, Jr. 1971. Transport of water through the Drake Passage. Deep Sea Res., 18: 51-64.

Reid, J.L. and R.J. Lynn. 1971. On the influence of the Norwegian-Greenland and Weddell Seas upon the bottom waters of the Indian and Pacific Oceans. Deep Sea Res., 18: 1063-1088.

Reid, J.L. and R.S. Arthur. 1975. Interpretation of maps of geopotential anomaly for the deep Pacific Ocean. J. Mar. Res. Supp. Vol. 33: 37-52.

Robles, F., E. Alarcon and A. Ulloa. 1974. Water masses at the Northern Chilean Zone and their variations in a cold period (1967) and warm periods (1969, 1971-73). Presented at Reunion de Trabajo sobre el Fenomeno El Niño. Auspiciado por la Comision Oceanografica Intergubernamental. Guayaquil-Ecuador, 9-12 Diciembre 1974. 59 numbered pages.

Sandoval, E.T. 1971. The summer distribution of Tuna in relation to the general oceanographic condition off Chile and Peru. Far Seas Fisheries Res. Lab. Bull., 5: 23-88.

Scripps Institution of Oceanography. 1969. Physical and chemical data from SCORPIO Expedition in the South Pacific Ocean. USNS Eltanin Cruises 28 and 29. 12 March - 21 July 1967. SIO Reference 69-15. WHOI Reference 69-56. La Jolla, California. 89 pp.

Scripps Institution of Oceanography. 1974. Data Report. Physical and chemical data. PIQUERO Expedition, 16 December 1968 - 16 April 1969. SIO Reference 74-27. 59 pp.

Sievers C., H.A. and N. Silva S. 1975. Masas de agua y circulacion en el Oceano Pacifico Sudoriental. Latitudes 18° S - 33° S. (Operacion Oceanografica "MARCHILE VIII"). Cienc. y Tec. del Mar. Contrib. CONA No. 1: 7-67.

Silva S., N. 1973. Variaciones estacionales de temperatura, salinidad y contenido de oxigeno en la zona costera de Valparaiso (Septiembre de 1969 - Agosto de 1970). Inv. Mar., 4(3): 89-112.

Silva S., N. and H.A. Sievers S. 1974. Masas de agua, velocidad geostrofica y transporte de volumen entre Valparaiso e Isla Robinson Crusoe (Oceano Pacifico Sud Oriental). Pacifico Sur., No. 2: 102-120.

Silva S., N. and D. Konow H. 1975. Contribucion al conocimiento de las aguas en el Pacifico Sudoriental. Expedicion Krill. Crucero 3-4. Julio-Agosto 1974. Rev. Com. Perm. Pacifico Sur. 3: 63-75.

Silva S., N. and S. Neshyba. 1977. Corrientes superficiales frente a la costa austral de Chile. Cienc. y Tec. del Mar. Contrib. CONA No. 3: (in press).

Sverdrup, H.U., M.W. Johnson and R.J. Fleming. 1942. The oceans, their physics, chemistry and general biology. Prentice-Hall, New York, 1087 pp.

Taft, B.A. 1963. Distributions of salinity and dissolved oxygen on surfaces of uniform potential specific volume in the South Atlantic, South Pacific, and Indian Oceans. J. Mar. Res. 21(2): 129-146.

Warren, B.A. 1970. General circulation of the South Pacific. In: Scientific Exploration of the South Pacific. Warren S. Wooster (Ed.). pp. 33-49.

Wooster, W.S. and M. Gilmartin. 1961. The Peru-Chile Undercurrent. J. Mar. Res. 19(3): 97-112.

Wooster, W.S. and J.L. Reid, Jr. 1963. Eastern Boundary Currents. In: The Sea, Ideas and Observations on Progress in the Study of the Seas. Vol. 2. M.N.I. Hill (Ed.). Interscience Publishers. New York. pp. 253-280.

Wüst, G. 1935. Die Stratosphare des Atlantischen Ozeans, Inn: Wiss: Ergebn. Deutsche Atlant. Exped. "meteor," 1925-1927. Vol. 6, Pt. 1, Sect. 2: 109-288.

Wyrtki, K. 1963. The horizontal and vertical field of motion in the Peru Current. Bull. Scripps Inst. of Ocean., 8(4): 44-72.

Wyrtki, K. 1966. Oceanography of the Eastern Equatorial Pacific Ocean. Oceanogr. Mar. Biol. Ann. Rev., 4: 33-68.

Wyrtki, K. 1967. Circulation and water masses in the Eastern Equatorial Pacific Ocean. Int. J. Oceanol. and Limnol., 1(2): 117-147.

Wyrtki, K. 1975. Fluctuations of the dynamic topography in the Pacific Ocean. J. Phys. Oceanogr., 5: 450-459.

Zuta, S. and O. Guillen. 1970. Oceanografia de las aguas costeras del Peru. Bol. Inst. Mar. Peru-Callao, Vol. 2, No. 5, pp. 157-324.